RIGA TECHNICAL UNIVERSITY

Faculty of Power and Electrical Engineering

Institute of Power Engineering

Baiba OSE-ZAĻĀ

Student of Doctoral Study Program "Power and Electrical Engineering (Electrical Machines and Apparatus)"

DESIGN OPTIMIZATION OF CYLINDRICAL MAGNETIC COUPLER BASED ON CALCULATIONS OF MAGNETIC FIELD

Doctoral Thesis

Scientific supervisor

Dr. habil. sc. ing.

V. PUGAČEVS

Scientific advisor

Dr. habil. sc. ing.

J. DIRBA

Riga 2015

ANNOTATION

The doctoral thesis is made with intention to develop an optimization methodology for the cylindrical magnetic coupler (CMC) based on the calculations of its magnetic field.

The thesis is written in English and is 139 pages long. Its parts are introduction, 5 chapters, main conclusions, 8 appendices and bibliography with 190 reference sources. It has been illustrated by 72 figures and 15 tables.

Introduction. The topicality of the present doctoral thesis and the substantiation of the necessity for done researches are given, the aim of the research and from it consequent tasks are given, as well as the scientific novelty is given.

1st chapter. The terminology issues are described; the types and classification of CMCs are given. The main design parameters of CMC are overviewed, and the materials used in couplers are analyzed, as well as the main characteristic of CMC is analyzed.

2nd chapter. The influence of design parameters and of the materials used in permanent magnets on the active coupler main characteristic — maximum mechanical torque M_{max} — is researched and analyzed. A calculation methodology for the maximum mechanical torque acquisition is chosen and developed, based on the calculations of CMC magnetic field. Also the reactive CMC is researched, and it is compared with the active CMC.

3rd chapter. The main principles and methods of obtained data analysis are overviewed and analyzed, and the regression models/method is chosen. With the regression method the new objective function and control parameters models are acquired, from which the most suitable are chosen and tested.

4th chapter. The most commonly used optimization methods in electrical engineering are overviewed and analyzed, and the other popular optimization methods used in the last decade are given. An optimization tool is chosen, it is applied to the optimization of CMC design using the objective function models and the control parameters models. The made optimization allows developing of the optimization methodology for active CMC.

5th chapter. Two sets of CMC experiments are given: experiments of obtaining coupler mechanical torque curve and the experiment of obtaining the maximum mechanical torque for the new optimal design CMC. The recommendations of potential researches also are given for improvement of the coupler optimal design in future.

In the last part — main conclusions — the most important from all the conclusions made in the present thesis are given.

ANOTĀCIJA

Promocijas darbs ir veltīts cilindrisko magnētisko sajūgu (CMS) konstrukcijas optimizācijas metodoloģijas izstrādei, pamatojoties uz magnētisko lauku aprēķiniem.

Promocijas darbs ir rakstīts angļu valodā un satur 139 datorsalikuma lapas. Darbs sastāv no ievada, 5 nodaļām, galvenajiem secinājumiem, 8 pielikumiem un literatūras saraksta, kurā ir doti 190 informācijas avoti. Darbs ilustrēts ar 72 attēliem un 15 tabulām.

Ievadā ir pamatota darba aktualitāte, veikto pētījumu nepieciešamība, ir formulēts darba mērķis un no tā izrietošie darba uzdevumi, kā arī dota zinātniskā novitāte.

1. nodaļā ir aprakstīta terminoloģijas problemātika, magnētisko sajūgu veidi un klasifikācija. Ir apskatīti CMS galvenie konstrukcijas parametri, analizēti sajūgos izmantotiem materiāli un CMS galvenais raksturlielums — maksimālais mehāniskais moments M_{max}.

2. nodaļā pētīta un analizēta aktīvā CMS konstrukcijas parametru un pastāvīgajos magnētos izmantoto materiālu ietekme uz sajūga galveno raksturlielumu. Izvēlēta un izstrādāta aprēķinu metodoloģija maksimālā mehāniskā momenta noteikšanai, balstoties uz magnētiskā lauka aprēķiniem. Pētīts arī reaktīvais CMS un veikta tā salīdzināšana ar aktīvo sajūgu.

3. nodaļā apskatīti iegūto datu analīzes principi un pamatmetodes, no kurām izvēlēta viena — regresijas modeļi. Izmantojot regresijas modeļu metodi, iegūti jauni mērķfunkcijas un kontroles parametru modeļi, no kuriem izvēlēti atbilstošākie, un tie ir testēti.

4. nodaļā ir apskatītas un analizētas elektrotehnikā biežāk izmantotās optimizācijas metodes, kā arī dotas citas pēdējos gados populārākās optimizācijas metodes. Izvēlēts optimizācijas rīks, un veikta CMC konstrukcijas parametru optimizācija mērķfunkcijas modeļiem ar kontroles parametru ierobežojumiem.

5. nodaļā doti divi CMS eksperimentu komplekti: mehāniskā momenta līknes noteikšanai un maksimālā mehāniskā momenta noteikšana jaunajam, optimālās konstrukcijas sajūgam. Dotas rekomendācijas par potenciāli veicamajiem pētījumiem CMS optimālās konstrukcijas pilnveidošanā nākotnē.

Pēdējā daļā — galvenajos secinājumos — ir doti nozīmīgākie no visiem promocijas darba izstrādē veiktajiem secinājumiem.

CONTENTS

INTRODUCTION

Nowadays in different production and research areas such as chemistry, pharmacy, physics, biology, oil and gas industry, food processing industry etc., there are technological processes, where the transmission and handling of liquids occurs in aggressive environments and/or some parts of a device cannot be allowed to osculate with the liquid or gaseous substance [172–174, 178, 182, 185]. All types of torque transmission, e.g., from motor shaft to mixer blades, in general can be split in two categories: with contact and contactless. The torque transmission with contact is implemented using lever-actuated friction clutches [104–106], when it is technologically hard to ensure hermetic conditions. For contactless torque transmission electromagnetic clutches [24, 57, 98, 143, 157, 167] and magnetic couplers [84] are used. With the application of electromagnetic clutches the mechanical energy (torque) is transmitted in a sealed camera [6], thus insulating the working shaft from aggressive environment or ensuring the work of device in an especially clean environment. Also magnetic couplers (MCs) are widely used where the mechanical energy is transmitted using magnets interaction forces.

In a contactless way the torque can be transmitted using either motor, whose rotor and the rotary system are placed in a liquid [5, 8, 97, 103, 149], or intermediary, as magnetic coupler (MC) or electromagnetic clutch. For the first way contactless synchronous motors [37] and induction motors are used, besides that the induction motors are used more often because of their simple design and high reliability and robustness [27, 175]. For the second way synchronous MCs are most often used. By applying the MCs the mechanical torque is transmitted almost without losses [176], additionally, hermetically sealed conditions can easily be ensured in the process.

So the MCs are widely used but only in the last two decades the enterprises in MCs production are using the high-energetic permanent magnets made of rare-earth alloys such as neodymium-iron-boron (NdFeB) [45] and cobalt-samarium (CoSm) [154], though in electrical machines production the use of these rare-earth alloy permanent magnets had already begun in the 1980s. First permanent magnets were made of aluminium-nickel-cobalt alloys and ferrites like barium-ferrite (BaFe) or strontium-ferrite (SrFe) were used in MCs [21, 47, 176, 186]. Thus it is important to consider which permanent magnet material should be used in a MC.

All over the world the enterprises that produce MCs have standardized models of them, and for the client the most suitable coupler from the given ones is suggested for their

equipment. Usually the permanent magnets are designed in rectangular form (e.g. [16]), but for the same size coupler, when the magnets are with rounded/circular edges, the torque is increased by more than 30 per cents [110]. Therefore, it is also very important for the shape of the permanent magnets to be taken into account.

Thus, the **objective/aim** of this work is: to develop a methodology for obtaining the most optimal cylindrical magnetic coupler (CMC) design parameters combination according to chosen boundary values of variables and so that the CMC has the highest effectiveness.

Consequently, the **tasks** are:

1) Overview the latest research about CMC design and its optimization;
2) Choose the main CMC characteristic and its influencing design parameters;
3) Choose the base design of CMC, for which the optimization will be made, and the boundary values of independent variables;
4) Develop a calculation methodology and choose the application software for obtaining the basic characteristics;
5) Define the objective function, synthesize the necessary formulas that will be used in optimization;
6) Analyze the optimization algorithms, choose the optimization tool, and obtain the most optimal CMC design parameters;
7) Make a CMC sample and make its experimental testing;
8) Compare experimental results with data, obtained with developed calculation methodology and with the new mathematical model/formula.

The following investigation methods are used in this research:

- Qualitative:
  - Interviews;
  - Grounded theory.
- Quantitative:
  - For mathematical model development — *AutoCad*, *QuickField* (based on finite element analysis/method) and *SIMCA* (multivariate data analysis and optimization tool);
  - Experiment planning;
  - For formula synthesis — program tool (based on regression models).

The used methods and made research allowed to achieve following **scientific novelties**:

- The chosen software tools (*AutoCad*, *QuickField*) allowed to develop the methodology of acquisition of CMC physical parameters (of interest such as mechanical torque, its maximum value, and magnetic flux density, its maximum values in the yokes) based on the calculations of coupler magnetic field;
- The provided transfer from rectangular permanent magnets to rounded ones increases the value of maximum mechanical torque for more than 30 % (publication [110]);
- The transfer from disc form MC to cylindrical MC in the water counters allowed to avert the external influence from strong permanent magnets on the counting system of consumed water (V. Pugačevs, A. Ivanovs, B. Tarancevs, B. Ose. Ūdens patēriņa skaitītājs. LV 14434, 17.08.2011.);
- The new design reactive MC is developed that increases the value of maximum mechanical torque comparing to the same dimension analogous reactive couplers (Latvian [134] and European [133] patents and publication [113]);
- The new previously nonexistent mathematical models/formulas of active CMC are synthesized for certain boundaries of the chosen variables, thus allowing to forecast the values of maximum mechanical torque, maximum mechanical torque per volume, and the maximum values of magnetic flux densities (publication [109]);
- The optimization of CMC is made (in chosen tool *SIMCA*) by synthesized new models/formulas, which allowed developing the optimization methodology for CMC. The optimum design of CMC (with rounded permanent magnets) is manufactured and tested, the experiments proved the expected results.

The made research and given scientific novelties are scientifically approbated in publications, conference reports, and Latvian and European patents, and practically are approbated in the CMCs' manufacturing at the Latvian enterprise "Environment, Bioenergetics and Biotechnology Competence Centre" (shortly named also BTC) where the couplers are implemented in mixers, and these mixers are sent to Germany for use in the laboratory equipments.

1. CYLINDRICAL MAGNETIC COUPLER

Definition. *Magnetic coupler* is a machine [136] used to transfer mechanical torque between two or more parts without direct contact using permanent magnets' (PM) interaction forces. The MCs are produced with a sealed screen between the half couplings (Fig. 1.1).

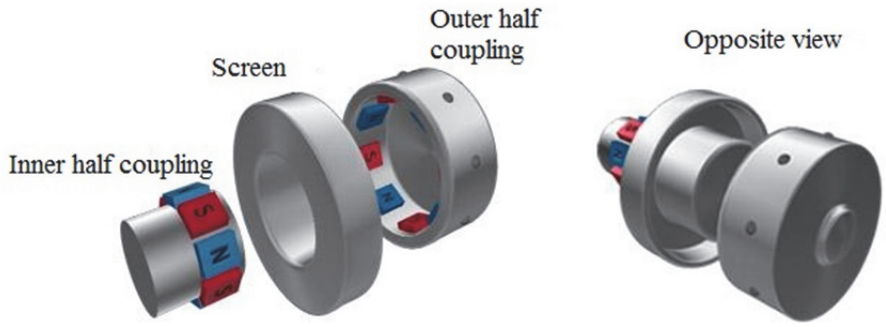

Fig. 1.1 Magnetic coupler

The magnetic coupler (most often) **works this way:** an engine through its shaft rotates the inner half coupling, and because of the attraction and repulsion forces of the PMs between the both half couplings also the outer half coupling starts to rotate [110, 84]. These interaction forces work equally in both ways — when the inner half coupling is driven, the outer half coupling follows, and when the outer half coupling is driven, the inner half coupling follows.

The name for magnetic coupler must be clarified. With the given definition of how the device works, in Eastern-European (Russia and many former Soviet countries) such a device is called a *magnetic clutch* [29, 59–72, 92, 93, 100, 120, 188]. In Western countries (the USA, Canada, Germany) *magnetic clutch* means either the *clutch* or *switch* with magnetic system [18, 25, 31, 136], the abbreviation of either an *electromagnetic clutch/brake* [18, 54, 96], or a *magnetic powder/fluid clutch* [159, 160], but the device itself is quite often called a *magnetic coupling* [16, 17, 85–90]. It is not correct to use *magnetic coupling* for the overviewed device according to terminology [77, 82] because in scientific literature a *magnetic link* is understood by this term [10, 46, 48, 49, 74, 80, 99].

The *half couplings* are also variously called: *inner*/*internal* and *outer*/*external coupling* (as one of two linking parts)/ *rotor* (as both parts are rotating; there is no stator)/ *half coupling* (as two parts of one magnetic circuit). All these terms are equally common, but in this work the *inner* and *outer half couplings* are chosen to be used.

MC is an exception — the other types of coupling devices are called *clutches* [77]: electromagnetic clutch, electro-mechanical clutch, friction clutch etc.

Application. Magnetic couplers are used in different pumps (e.g. centrifugal, gear pump), compressors, liquid (or gaseous/solid substance) mixers, agitators, fans, blowers and autoclaves (usually the reactive MCs). Some application examples are given in Appendix 1.

1.1. Magnetic couplers' classification

The rotation of both half couplings for the MC under investigation is synchronous [50], so this synchronous clutch can be considered as a type of contact-less electrical machine (Fig. 1.2) [79].

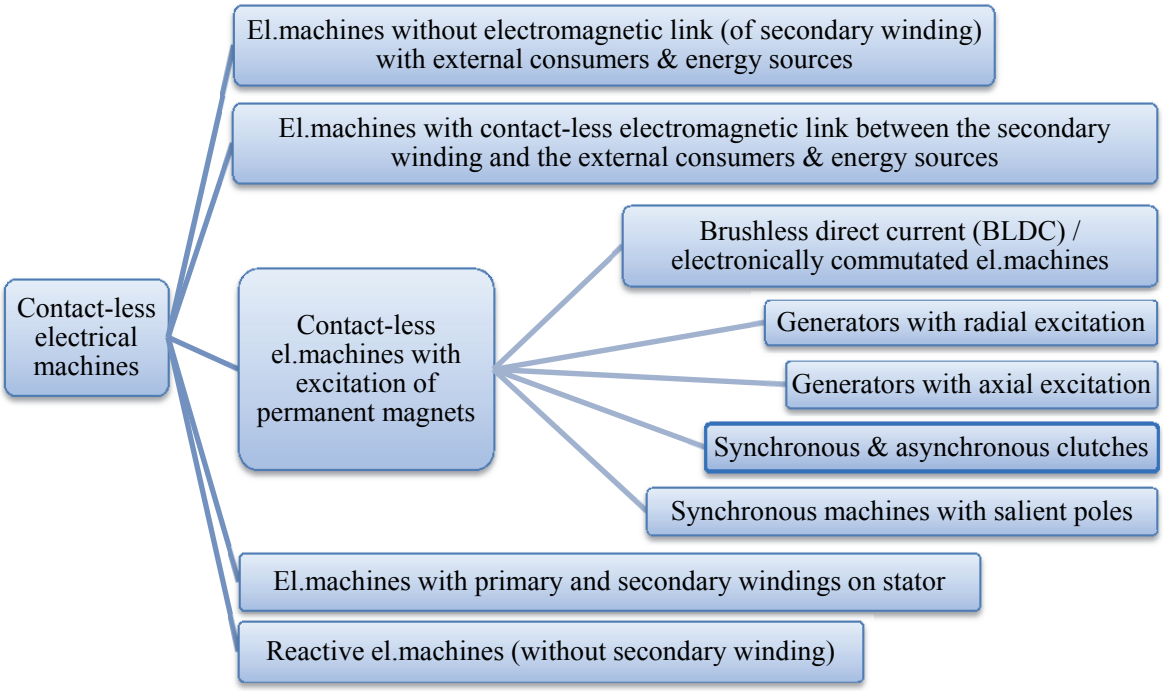

Fig. 1.2 Contact-less electrical machines' classification by design

The synchronous and asynchronous clutches can be divided into three main groups (Fig. 1.3) [172, 173, 176, 179–181, 183, 184, 189].

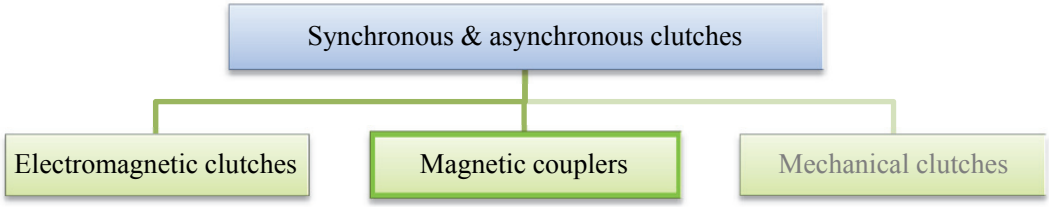

Fig. 1.3 Main groups of synchronous and asynchronous clutches

Magnetic couplers' classification by different categories is given in Fig. 1.4–Fig. 1.6. In this work an active, motion transferring and one-way motion (rotational) magnetic coupler with one working air gap is going to be investigated.

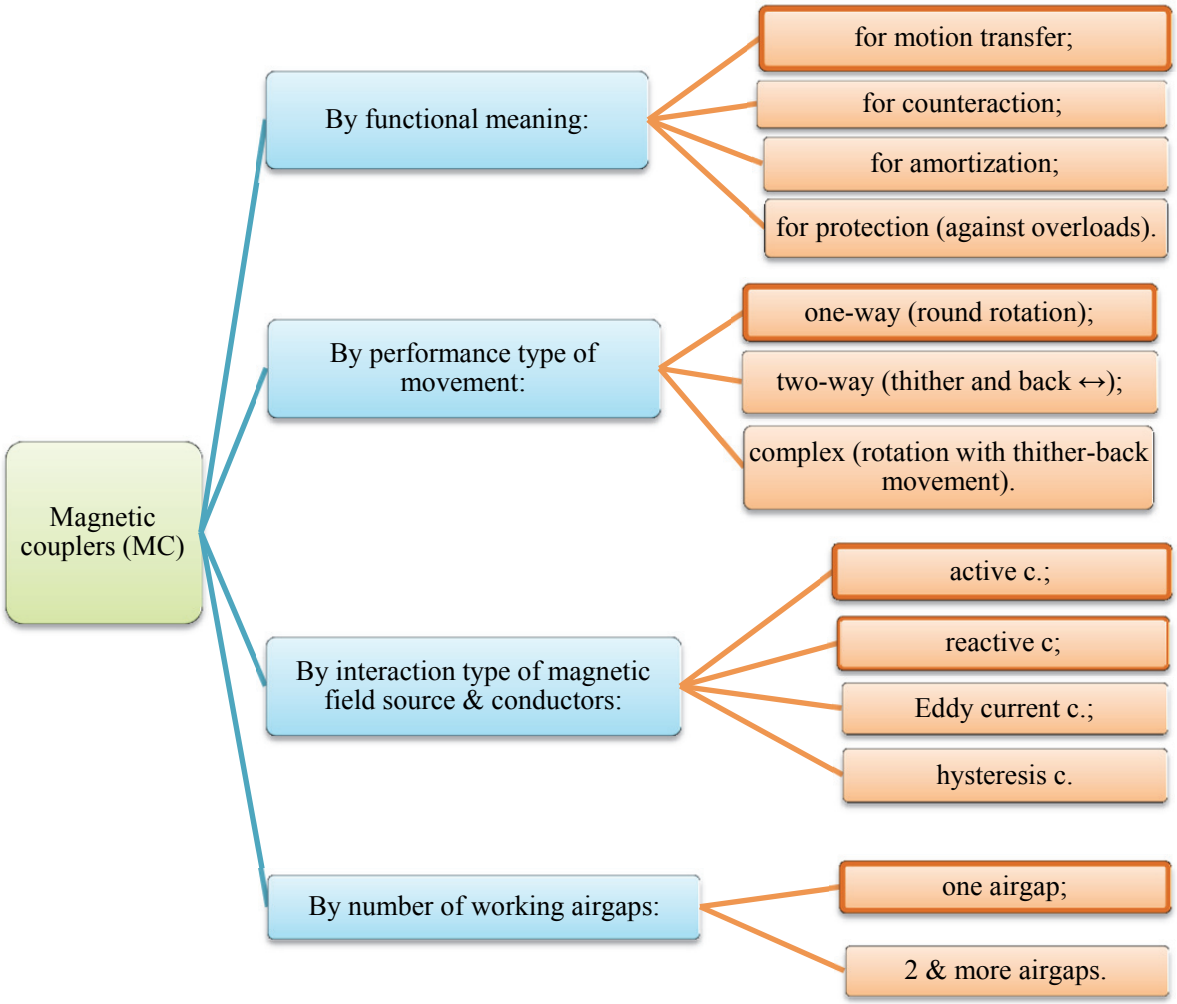

Fig. 1.4 Magnetic couplers' classification

The explanation and examples of active, reactive, Eddy current and hysteresis MCs are given in Appendix 2.

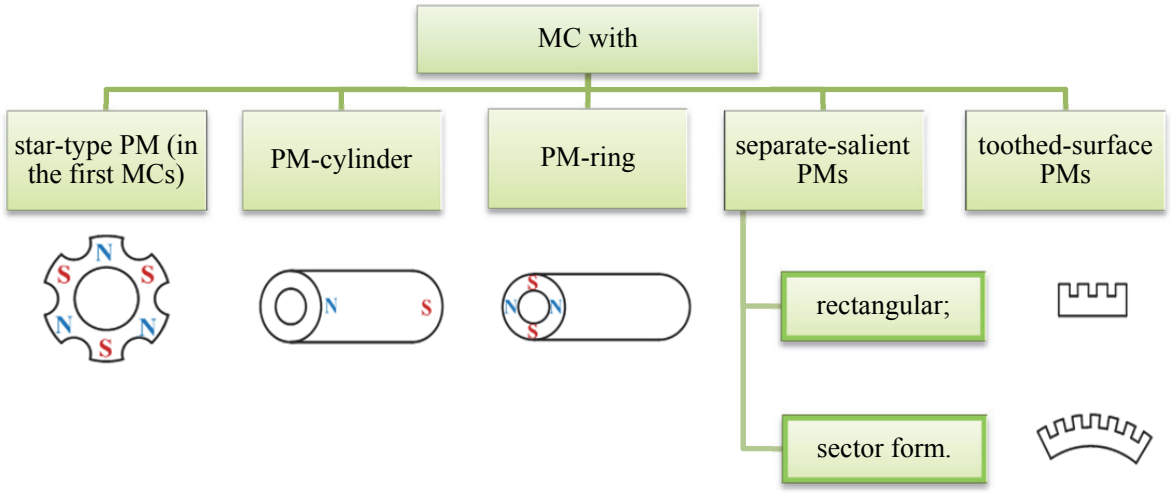

Fig. 1.5 PMs' forms for MCs

The MCs can be classified by the form of magnets' working-surface such: axial/disc form MCs, radial/cylindrical MCs and linear MCs (Fig. 6).

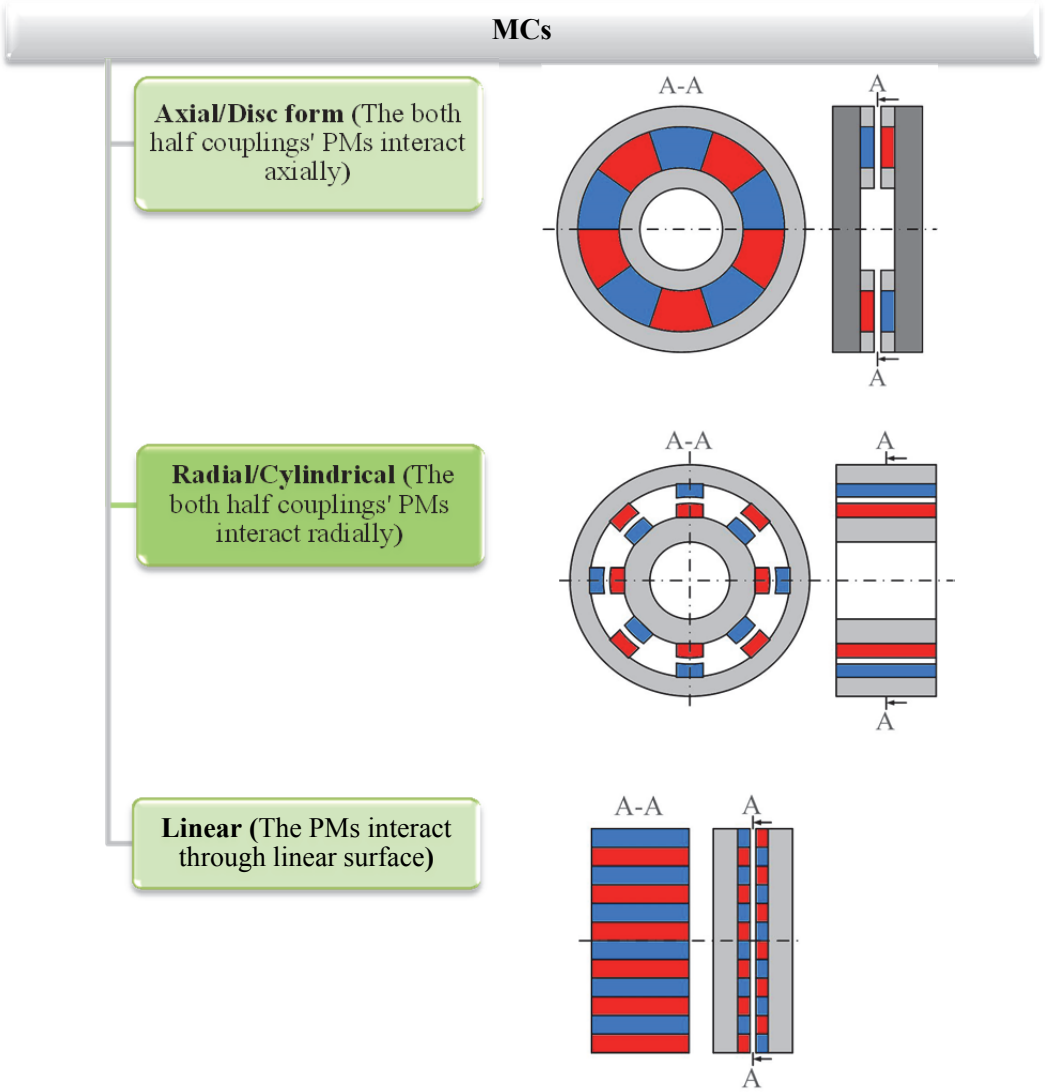

Fig. 1.6 MCs by form of PMs' interaction surface

A cylindrical magnetic coupler (CMC) is the object to be investigated in this research work. Some technical data of CMCs:

- A sealed screen suitable for sterile environment;
- Can be used for the processing of different substances such as liquids, gases and solid particles;
- Designed to operate at a wide range of power (< 2.5 kW);
- Able to operate at a wide range of pressure (< 4 MPa or 40 bar);
- Maintaining a high level of ability to work at a wide range of temperature (10–200 ºC, the upper limit of temperature depends on used PM material).

1.2. Main design parameters of CMC

The form of PMs used in MCs may differ, but most often the rectangular PMs are used in CMC [16, 17, 85–90, 176, 182, 184]. The main design parameters of a CMC are given in Fig. 1.7 and they are:

- Axial length of coupler — l;
- Inner radius — R_1;
- Inner half coupling PMs placement radius — R_2;
- Outer half coupling PMs placement radius — R_3;
- Outer radius — R_4;
- Air gap — δ;
- PMs' height — h_{PM};
- PMs' width — b_{PM};
- Outer half coupling yoke height — h_y.

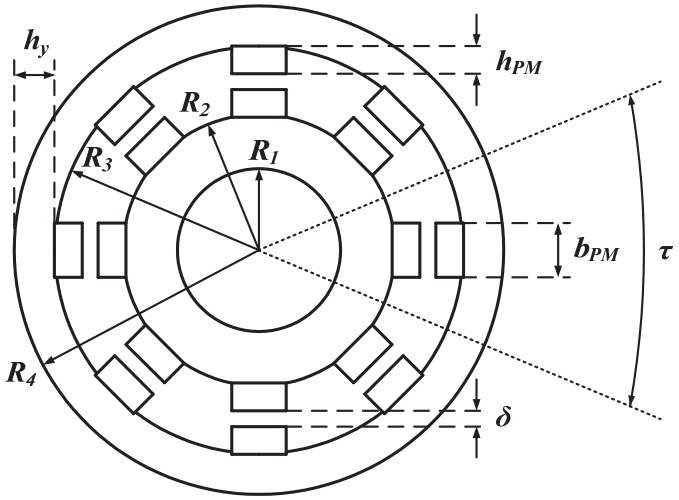

Fig. 1.7 Main design parameters of CMC in cross-section

In calculations the pole pair number p is used, where $2p$ is the number of PMs. In the given example (Fig. 1.7) the number of PMs is $2p = 8$ and the pole pair number is $p = 4$. PMs are counted up only in one half coupling, because the number is equal on both half couplings, and it is a very rare, specific case, when the numbers of PMs on both half couplings differ from each other.

Additionally to the given radiuses R_3 and R_4 the yoke height h_y is used, because it changes by (1.1) [177, 187] and depends on the number of PMs, the PMs' width, the material used in PMs, and the chosen value of magnetic flux density to be controlled in the yoke.

$$h_y = \frac{\pi R_3 \beta' B_r}{p\, 2\, B_{steel}}, \tag{1.1}$$

where h_y — yoke height in outer half coupling [m];

R_3 — outer half coupling PMs placement radius [m];

β' — coefficient that shows what part of a pole pitch τ is covered by PM width b_{PM} : $\beta' = \left(b_{PM}/\tau_{in} + b_{PM}/\tau_{out}\right)/2$;

B_r — PM residual induction [T];

p — pole pair number;

B_{steel} — monitored value of magnetic flux density in yoke [T], chosen B_{steel} = 1.8 T.

The PMs' material also influences the CMC design. In design calculations the PM magnetic permeability μ_{PM} is taken into account, acquired from magnet residual induction B_r and coercive force H_c, these values are given in catalogues. In this work the relative magnetic permeability of PMs μ_* (1.2) is used [176, 177].

$$\mu_* = \frac{B_r}{H_c \mu_0} = \frac{B_r}{H_c 4\pi 10^{-7}}, \tag{1.2}$$

where μ_* — PM relative magnetic permeability;

B_r — PM residual induction [T];

H_c — PM coercive force [A/m];

μ_0 — magnetic permeability of air and it is $\mu_0 = 4\pi 10^{-7}$ [H/m].

1.3. Materials used in CMC

Nowadays the choice of available materials is very wide. The choice mainly depends on the product manufacturer available funds. There are cheaper and more expensive materials and the latter usually provide higher quality, reliability, durability, and from these aspects also simpler or cheaper maintainability follows.

Such parts of CMC are overviewed — PMs, yokes and sealing screen — because their properties will be used in application software used in the modelling of magnetic field.

1.3.1. Permanent magnets

All materials can be divided into the magnetic (such materials have unpaired electrons) and the non-magnetic/*diamagnetic* ones (these materials have paired electrons), because the magnetic properties of materials result from the motions of electric charges within them [11, 53, 81, 135, 139, 145, 186]. The motions of either the rotation in element orbits or the spins about the axis of the charges induce the equivalent electric currents, thus the magnetic fields are produced. The field-producing effect of an orbit or spin is called its

magnetic moment. The magnetic materials are divided into following types: paramagnetic, ferromagnetic, antiferromagnetic, and ferrimagnetic. Often the difference between these materials is visualized with their atomic magnetic moment lines (Fig. 1.8).

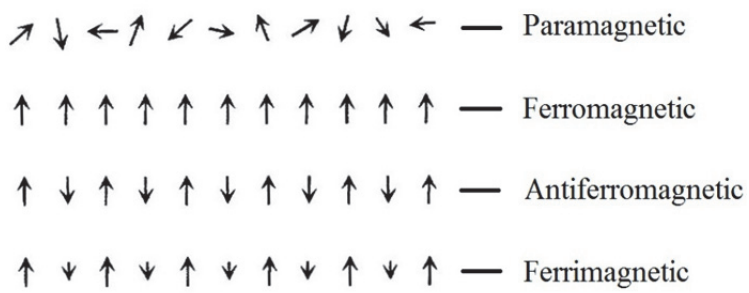

Fig. 1.8 Directions of magnetic moments for solid magnetic materials

Ferromagnetic materials (metals such as iron, cobalt, nickel) have a relative permeability greater than unity and generally it is very high. The permeability is not constant because it depends upon the degree of magnetization. These materials exhibit hysteresis — the relevance between the induction and the magnetizing force (Fig. 1.9). The induction corresponding to a given magnetization force depends upon the previous magnetic history. If the magnetizing force is increased indefinitely, the induction approaches a limiting/saturation value. The form of magnetization-demagnetization loop varies for different types of magnetic materials, as magnetically *soft*-, magnetically *hard*- and *highly energetic* materials. Soft magnetic materials have low values of residual induction and coercive force, and small maximum energy (BH_{max} area), furthermore, they can be easily demagnetized. Hard magnetic materials have high values of residual induction and coercive force, and their magnetization remains after the field is switched off. The permanent magnets belong to hard magnetic and highly energetic materials [11, 53, 81, 135, 139, 145, 186].

As it is seen (Fig. 1.9), with increasing magnetization force H from zero the induction B also increases, but non-linearly by OABC. This non-linearity is one of the characteristics for ferromagnetic materials and thus the PMs. If the increase of H is stopped at a point as B and then decreased, the induction does not retrace by the original curve in reverse order, but it lags behind the OAB curve — indicated by B, B_r, H_c and lower. This lag is called *magnetic hysteresis*. The point where the magnetizing force is equal to zero is called the *residual induction* B_r, but the negative magnetizing force, at which the induction becomes zero, is called the *coercive force* H_c. The closed curve starting from B through B_r, H_c, etc. back again to B is called a *hysteresis loop*. The ratio of B to H is called the *permeability* μ [139].

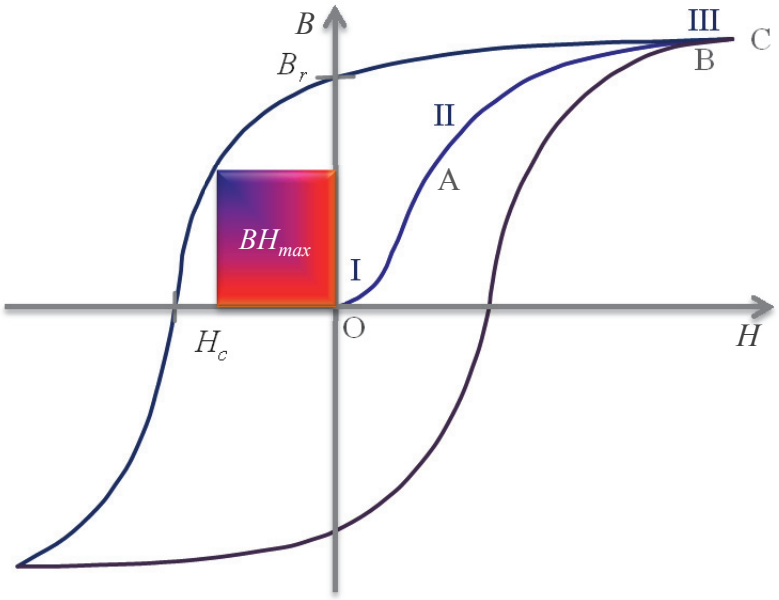

Fig. 1.9 Hysteresis loop

In stage I by increasing magnetizing force H the increase of induction B is comparatively small, but in stage II — a small increase of H produces a relatively large increase in B. The increase of B is again small in stage III, and in this stage the induction asymptotically approaches a limiting value which is called the *saturation induction* B_s. For this reason, stage III is also called the *saturation range* [139].

In the first magnetic couplers simple permanent magnets made of Ba-ferrite, Sr-ferrite, Co-ferrite, Ni-ferrite or aluminium-nickel-cobalt alloys (Alnico) were used [137, 139, 176, 186]. The *ferrites*, also known as *ceramic magnets*, are made as a composite of iron oxide and metal carbonate. Ferrites became widely used because of their availability since the 1950's. Most popular of ceramic magnets for many years were Ba-ferrites and Sr-ferrites. Ceramic magnets can be produced using pressing and sintering. By pressing the ceramic alloy powder is compressed, but in sintering the alloy powder is first compressed and then fused in heat into a solid material. Ceramic magnets are brittle and hard — required diamond wheels to grind and shape. Ceramic magnets' grades can be both isotropic (equal magnetic properties in all directions) and anisotropic (magnetized in one direction, by pressing). Anisotropic magnets have the highest energy (up to 32 kJ/m^3 or 4 MGOe (mega Gauss Oersteds; most often used magnetic units and their ratios are given in Appendix 3)) among ceramic magnets. Ceramic magnets have low cost (compared with other PMs), resistance to corrosion, and high heat tolerance (maximum working temperature is up to 400 °C), but low mechanical strength [11, 41, 53, 135, 137, 139, 145].

Alnico magnets are made of an alloy from aluminium (Al), nickel (Ni), cobalt (Co) — from here follows the abbreviated name *Alnico* — with a small amount of other additional elements, added to enhance the properties of the magnet. Alnico magnets can be produced using casting and sintering. Sintered Alnico magnets have higher energy product (up to 43.8 kJ/m^3) than casted ones. These magnets have good temperature stability (maximum working temperature for different material grades is 540 °C) and good resistance to corrosion. A drawback of Alnico magnets is that they are prone to demagnetization due to clash [11, 41, 135, 137, 139, 145].

Next popular PM material group is the rare-earth alloys. The first were SmCo magnets (produced since the end of 1960s and researched since the beginning of 1960s [42, 53, 153, 163]) and then followed the NdFeB magnets [11, 58, 94, 102, 137, 140, 141, 163]. First NdFeB alloy was patented in 1981 as one of the rare-earth alloy containing the lanthanide [42, 58]. The historic use of different material permanent magnets can be demonstrated by the graphic [53] of maximum product energy by years (Fig. 1.10).

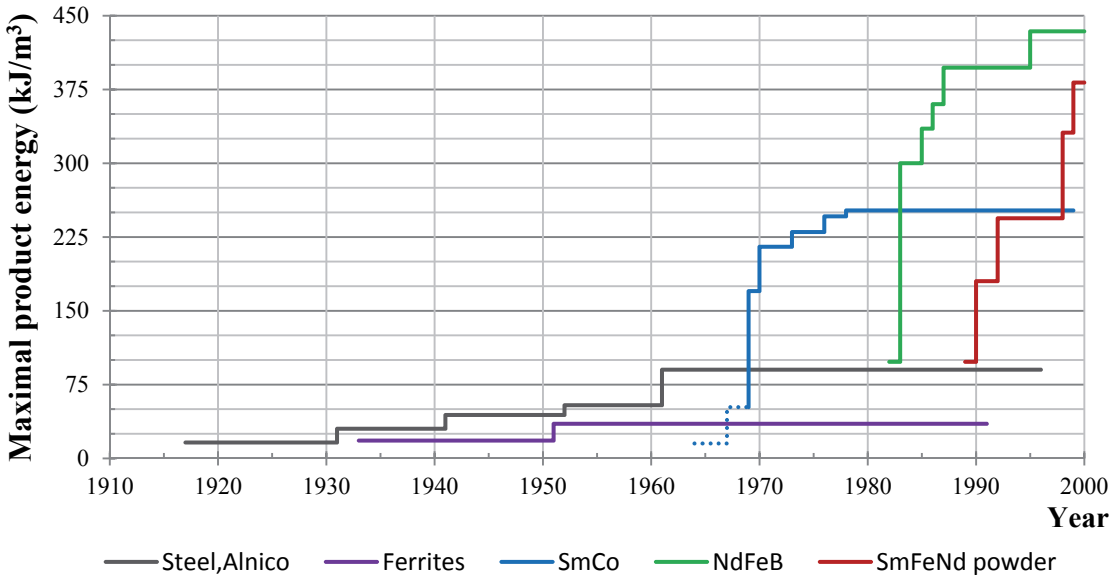

Fig. 1.10 Maximum product energy by year for different PM materials

The SmCo magnets are highly resistant to oxidation, have a lower maximum operating temperature than ceramic and Alnico magnets, but higher maximum operating temperature and better temperature resistance than NdFeB magnets. SmCo magnets are brittle and prone to cracking and exposed to thermal shock they may fracture. These magnets are most often applied in situations when the corrosion resistance is important due to the high cost of the material. There are two main SmCo magnet groups: $SmCo_5$ and Sm_2Co_{17}. The latter has the

highest maximum operating temperature and the other magnetic characteristics also are higher than to $SmCo_5$ [15, 53].

Nowadays NdFeB has become the most advanced commercialized PM material. These magnets have the highest energy products. When compared to SmCo magnets, NdFeB magnets are mechanically stronger, temperature less resistant and easily oxidized, thus there have been developed surface treatments from different materials (nickel, zinc and tin plating, copper, silver, gold and epoxy resin coating) [53, 95].

The comparison of the main PM materials is given in table 1.1 [11, 15, 53, 139, 117]. The values are (where possible) rounded because they vary in different sources.

The permanent magnets have a feature that they lose all magnetic properties at a certain temperature and this temperature is called Curie temperature t_C. This temperature affects the maximum possible temperature at which the magnets can be operated $t_{op\ max}$ (table 1.1). PMs are suggested to be used in temperature above 0 °C till allowed maximum operating temperature. Exception is the Ba-ferrite magnets because only they can be also operated below 0 °C (till −40 °C) [11, 53, 139].

When a magnet is used in temperature that is above the given maximum operating temperature and below the Curie temperature, some percentage of magnetization is irreversibly lost. In such a situation bringing the magnet back down to room temperature (20 °C) will leave it with magnetic properties, but the magnet strength will definitely be weaker [11, 53].

Table 1.1

Comparison of PM materials

PM material type	Maximum value (counting all grades) for:				
	Maximum product energy BH_{max} (kJ/m^3)	Residual induction B_r (T)	Coercive force H_c (kA/m)	Operating temperature $t_{op\ max}$ (°C)	Curie temperature t_C (°C)
Ceramic	32	0.4	240	200	450
Alnico	36	1.15	130	540	860
SmCo	250	1.00	1200	350	800
NdFeB	430	1.2	1350	200	350

All the magnetic parameters are given in intervals and the intervals vary for different grades of each PM material type, e.g. table 1.2 [117]. The N, N_SH and N_EH (given as examples, there are more) are the grades, but the given numbers (30, 35, ..., 50) mean the

highest value of maximum energy product (in mega gauss Oersteds; N40, than $BH_{max} \leq$ 40 MGOe or 318 kJ/m^3) and it depends on the magnetization.

Table 1.2

Parameters for NdFeB magnets (some material grades)

Material type	Residual induction B_r (T)	Coercive force H_c (kA/m)	Maximum product energy BH_{max} (kJ/m^3)	Maximum operating temperature $t_{op\ max}$(°C)	Curie temperature t_C (°C)
N35	1.17–1.21	>875	263–279	80	310
N40	1.26–1.29	>875	302–318		
N45	1.33–1.37	>875	342–358		
N50	1.41–1.45	>875	382–398		
N30SH	1.08–1.12	>803	223–239	150	340
N35SH	1.17–1.21	>859	263–279		
N40SH	1.26–1.29	>907	302–318		
N45SH	1.33–1.37	>907	342–358		
N30EH	1.08–1.12	>803	223–239	200	350
N35EH	1.17–1.21	>859	263–279		

The PM manufacturers usually give the demagnetization curves (Fig. 1.11), from which it is suggested to choose the magnets. In this graph the marks for permeance coefficient k_p too are given, also called *load line*, *operating slope* or *B/H of magnet*. The permeance means the ability to conduct the magnetic flux [136, 139] and it is a reciprocal to permeability. The permeance coefficient must be taken into account by choosing the most suitable PM material, because in its calculation (provided by manufacturers) the shape of PM and the surrounding environment of PM is represented (by which the way of PM placement in magnetic circuit is understood) (Fig. 1.12). So, first, the shape of PM must be chosen, then, the dimensions of PM must be given, after that the permeance coefficient is calculated. Knowing the permeance coefficient k_p, the load line must be drawn — from the origin point ($B = 0$, $H = 0$) to an appropriate mark of k_p (the green line in Fig. 1.11). For every *intrinsic* curve of a temperature set (as the orange line in Fig. 1.11) there corresponds a certain *normal* curve (as the blue line in Fig. 1.11). It is an *operating point*, where the load line intersects the normal curve (as the red point in Fig. 1.11). The normal curves have the *knees*, where the line brakes and goes down almost vertically. In this example the maximum operating temperature

$t_{op\ max}$ is 100 °C, because the intersection point between the load line and normal curve must be right at the knee.

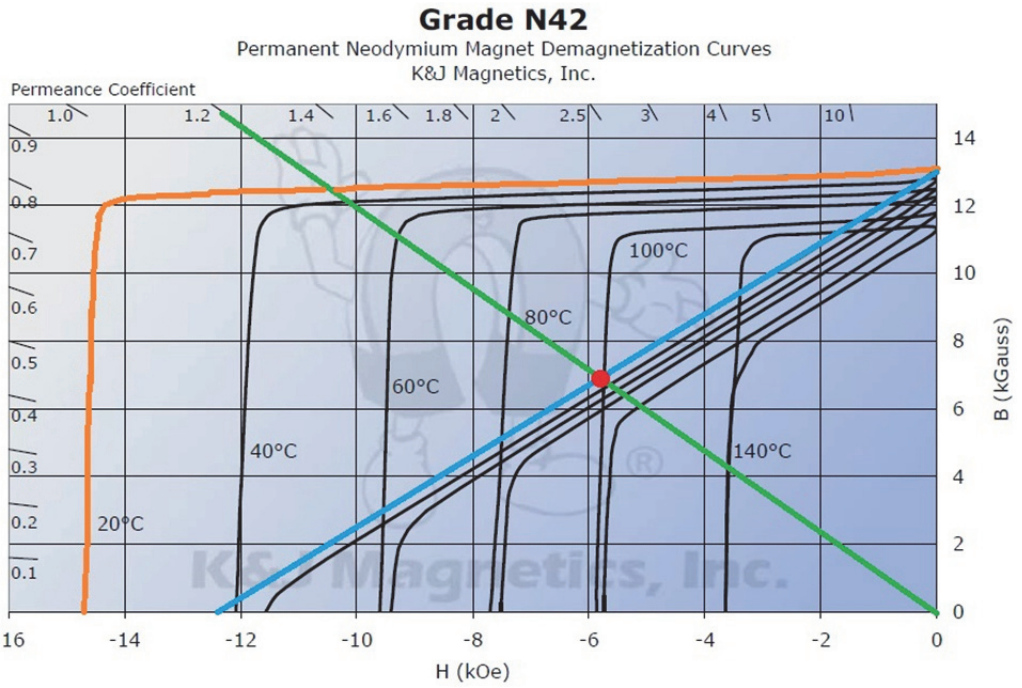

Fig. 1.11 Demagnetization curves for NdFeB magnet grade N42

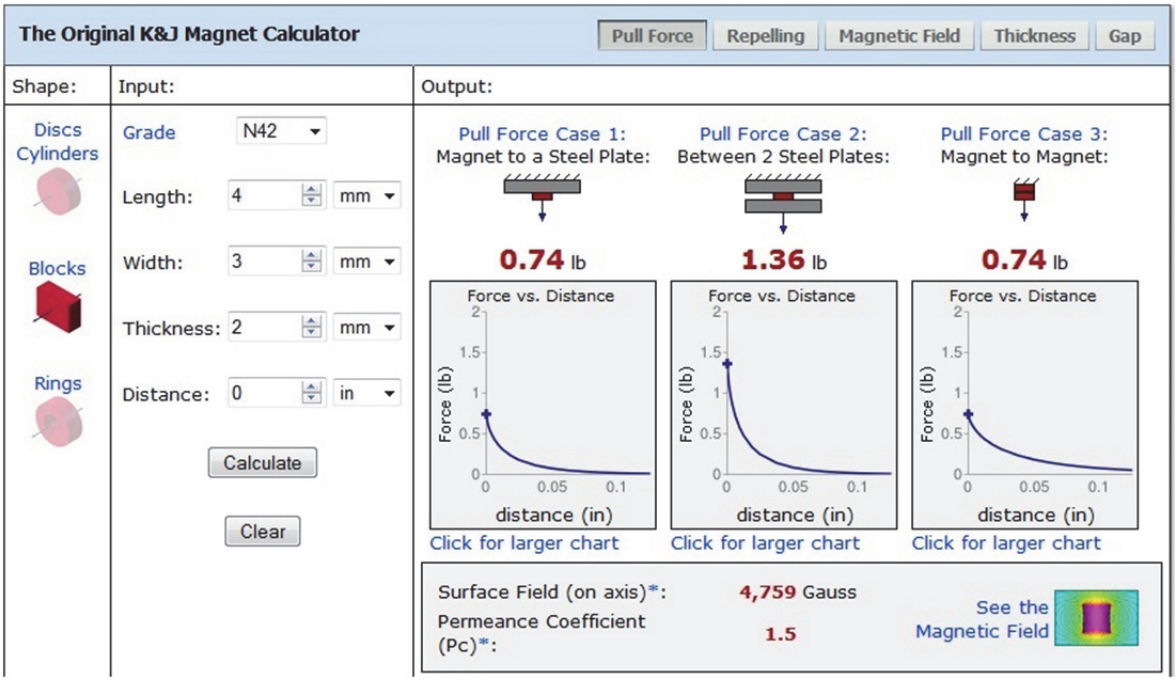

Fig. 1.12 Example of calculator for permeance coefficient k_p

So in general PMs are characterized by a hysteresis loop (Fig. 1.9) and its corresponding physical parameters:

a) Magnets maximum energy BH_{max} [J/m^3];

b) Residual induction B_r [T];

c) Coercive magnetization force H_c [A/m];

d) Maximum operating temperature $t_{op\ max}$ [°C]

On laboratory equipment named Hystograph with its connected software named MAG-Expert an experiment was made (Appendix 4) acquiring the demagnetization curve. The two sample PMs are made of NdFeB. The results show that the real physical parameters of PMs may vary from those given in catalogues, though usually they are located in the given interval.

1.3.2. Yokes

The MC yokes are made of magnetically soft steel. Steel is a type of metal alloys (Fig. 1.13) [151, 152]. The steels can be classified by their composition (Fig. 1.14) [151].

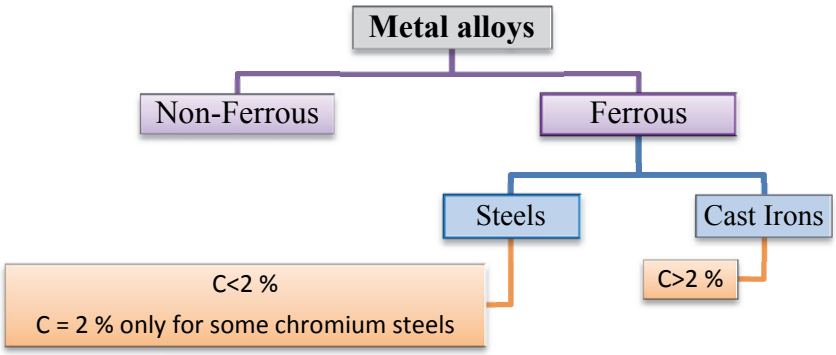

Fig. 1.13 Basic classification of metal alloys

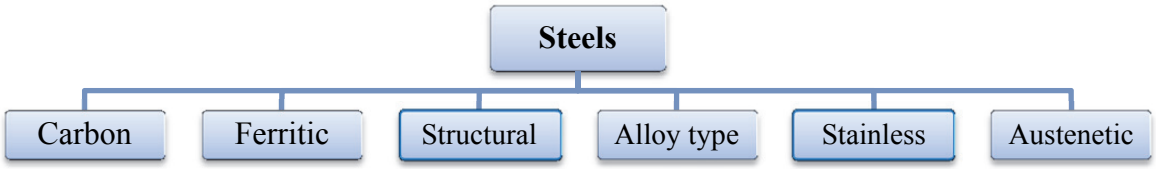

Fig. 1.14 Steels classified by their composition

Steels (alloy, stainless etc.) that are used in tools are also named *tool steels* and their classification [2, 3, 151, 152] is given in Fig. 1.15.

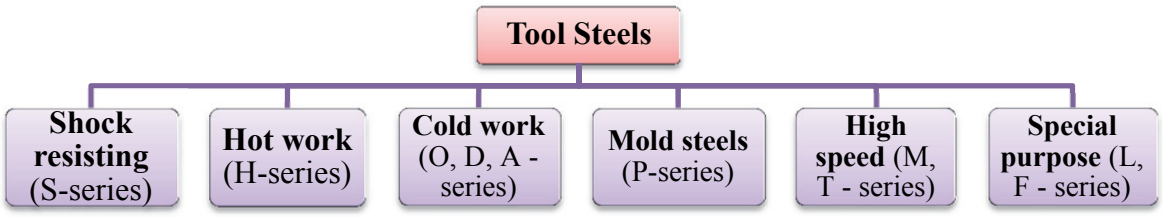

Fig. 1.15 Tool steels classification

The classification of steels given in European Union standard EN 10020:2000 "Definition and classification of grades of steel" is made by chemical composition and main qualities (Fig. 1.16). One type of the *alloy quality steels* are the iron-silicon alloys, from which most known is *electrical steel* (used in electrical machines and apparatus, transformers) also named *silicon steel*, *silicon electrical steel*, *transformer steel* or *lamination steel*; some electrical steel grades go also under *non-alloy quality* steels [2, 3, 152].

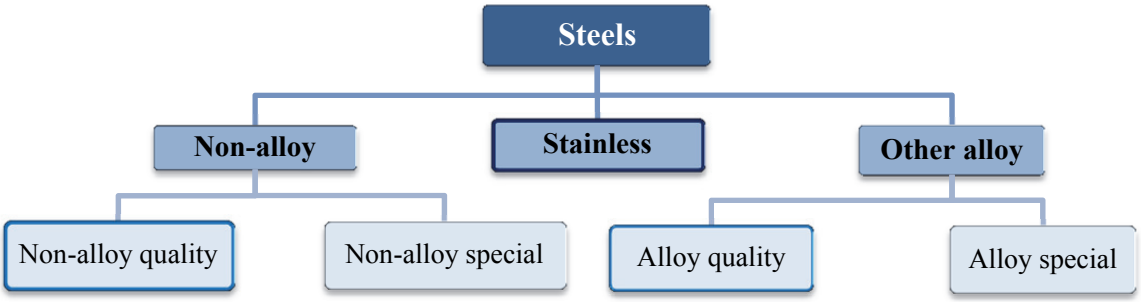

Fig. 1.16 Steels classified by standard EN 10020:2000

Electrical steels are divided into *oriented* and *non-oriented* electrical steel (Fig. 1.17). The *oriented* steel is electrical steel where the crystals' cube edges are aligned nearby parallel to the direction in which the steel is rolled. Oriented electrical steels have low core losses and high magnetic permeability that leads to efficient and economical use [2, 13, 151].

The *non-oriented* electrical steels have such magnetic properties that are practically the same in any direction in the plane of the material. Non-oriented electrical steels have good uniformity and with a special processing they have also high permeability even at high magnetic flux densities [2, 12, 14, 151].

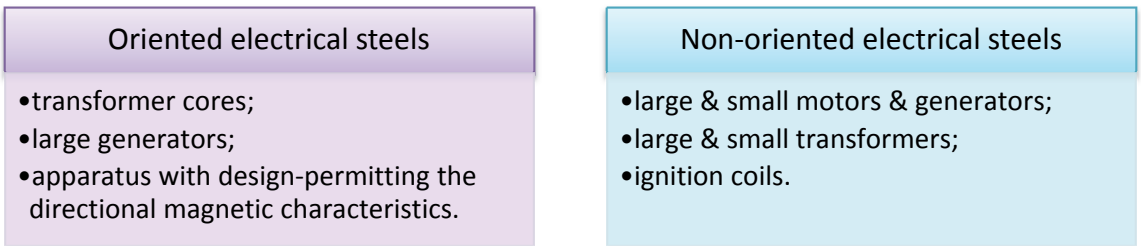

Fig. 1.17 Electrical steels' types and their popular applications

The magnetic properties of electrical steels depend on heat treatment [151]. The fully processed electrical steels are usually layered with insulating coating [12–14, 151, 152].

In this research for magnetic couplers' yokes the *structural* steel Ст3 (in Russia) is used, and it is classified under the *non-alloy quality* steels (Fig. 1.16) because of its chemical content though it also is often used in electrical machines (e.g., in housing) and apparatus. Its equivalent or very similar steel grades are SS330 (in Japan), RSt37-2 (in Germany, according

to DIN 17100), 40B (in the UK), A 284 Gr. D (in the USA, according to ASTM [120]), E 24-2 (in France, according to NFA 35-501), Fe360B (in Italy), Q235 (in China) and 13-12-00 or t312-00 (in Sweden), but by European Union standard EN 10025-2:2004 this steel is the grade S235JRG2 with material number 1.0038 [22]. Its magnetic properties expressed with $B = f(H)$ curve are given in Fig. 1.18 [177].

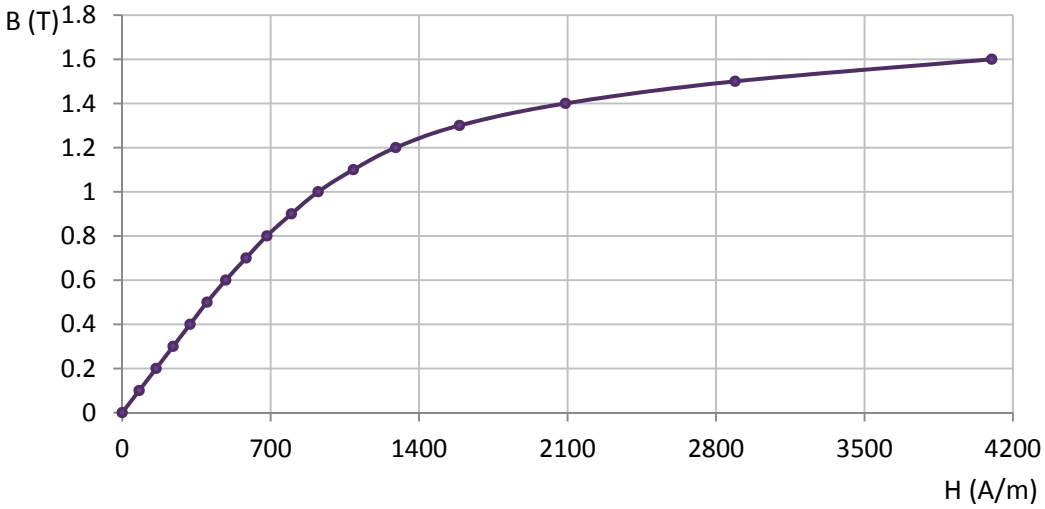

Fig. 1.18 $B = f(H)$ curve for steel Ст3 (grade S235JRG2, material # 1.0038)

These values are given as input data defining the MC yokes as steel in software *QuickField* [147].

1.3.3. Sealing screen

Usually the MCs are produced and used with a sealing screen. This screen can be made from different materials as provided by manufacturer, from those the most popular materials are made of carbon fibre, stainless steel or oxide ceramics. In this work the couplers with sealing screen made of stainless steel are researched.

Stainless steel is a steel class (Fig. 1.16) with at least 10.5 % of chromium and less than 1.2 % of carbon, and is subdivided (Fig. 1.19) according to European Union standard EN 10020:2000 “Definition and classification of grades of steel”.

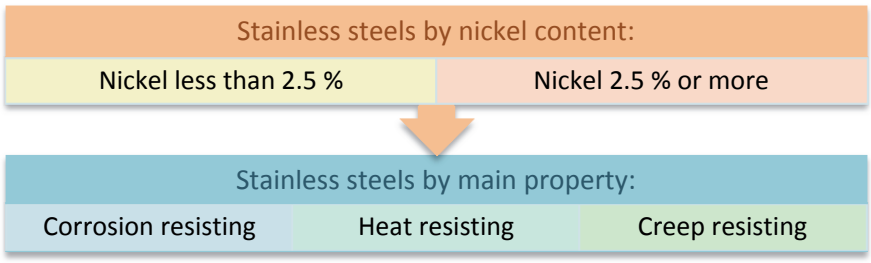

Fig. 1.19 Classification of stainless steel by standard EN 10020:2000

For stainless steels there are separated standards and as it follows from one of them [33], then the stainless steels are classified as given in Fig. 1.20.

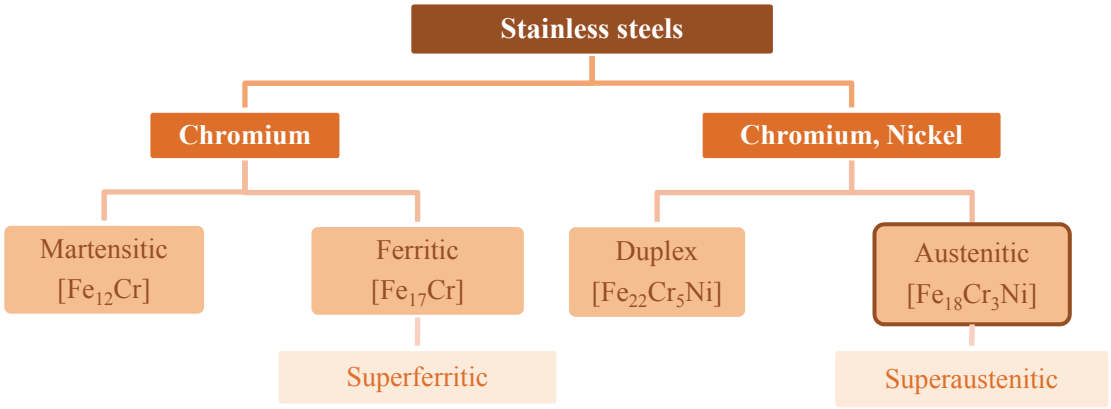

Fig. 1.20 Stainless steels classified by standard EN 10088-1:2012

Austenitic stainless steels may have a corrosion-resistance problem. *Intergranular corrosion* — corrosion type, when austenitic stainless steels are used in temperatures diapason 425–815 °C. At this temperature the carbon in the steel diffuses to the grain boundaries and thus precipitates the chromium carbide. This process leaves a lower chromium content adjacent to the grain boundaries. The grain boundaries become prone to preferential attack on subsequent exposure to a corrosive environment [9, 34].

Worldwide the two most popular austenitic stainless steels are the grades 1.4301 (or 304 according to AISI [2]) and 1.4401 (or 316), taking into account the commercial use [150]. The grade 1.4301 is also called the "18/8" steel for its composition: 18 % chromium and 8 % nickel. The grade 1.4401 is also called the "marine grade" thanks to its high corrosion resistance. The risk of intergranular corrosion can be reduced with adding titanium Ti, e.g. 1.4571 (or 316Ti).

In this research an austenitic stainless steel with grade 1.4401 (316) is used. This steel is corrosion resistant, but it has a specific production and that leads to expensive costs. Its magnetic properties are expressed with the relative permeability dependence from magnetic field strength: till 4 000 A/m the relative permeability of 1.4401 is $\mu_* = 1.003$, but till 16 000 A/m — $\mu_* = 1.004$ [33]. Even at higher magnetic field strength the relative permeability does not grow significantly, thus the relative permeability of austenitic stainless steel 1.4401 can be taken $\mu_* = 1.00$ for calculations and magnetic field modelling in this research.

1.4. CMC main characteristic

The previously given subchapters show that cylindrical magnetic couplers can be produced from a wide range of materials. And various materials have different magnetic properties. These properties influence the CMC mechanical torque. The values of mechanical torque depend on half coupling offset angle, when one of the half couplings is turned by an angle α relatively to other one. For such a turning Fig. 1.21 is given as an example, three CMCs with equal design are compared: axial length $l = 10$ mm, inner radius $R_1 = 10$ mm, outer radius $R_6 = 40$ mm, PM are made of NdFeB alloy, magnetic coverage coefficient $\beta = 0.9$, but with different pole pair numbers p (1, 4 and 8). As these curves may have unequal form it is more correct to compare the maximum value of coupler mechanical torque — maximum mechanical torque M_{max}.

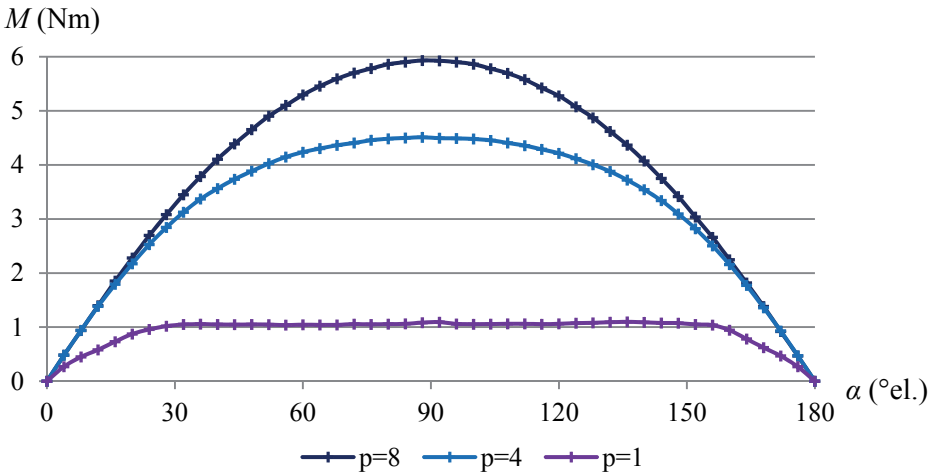

Fig. 1.21 Curves of CMC mechanical torque (PM made of NdFeB)

As it is considered that the main characteristic of cylindrical magnetic coupler is its maximum mechanical torque, the next aspect is the value of turning angle α at which the torque is maximum. In Fig. 1.21 the curves of mechanical torque are shown in electrical degrees, and the maximum value of torque is at $\alpha = 90$ °el. To obtain the curve in electrical degrees the CMC must be turned by angles in geometric degrees. In geometric degrees the torque dependence from turning angle varies for CMCs with different numbers of pole pairs (Fig. 1.22). In Fig. 1.22 the CMCs have PMs made of barium ferrite, but the influence of pole pair numbers remains the same for all types of permanent magnets. In this figure the values of mechanical torque M for CMCs with different numbers of pole pairs are scaled to show more obviously the regularity — at which turning angle α (in geometric degrees) the torque has its maximum value.

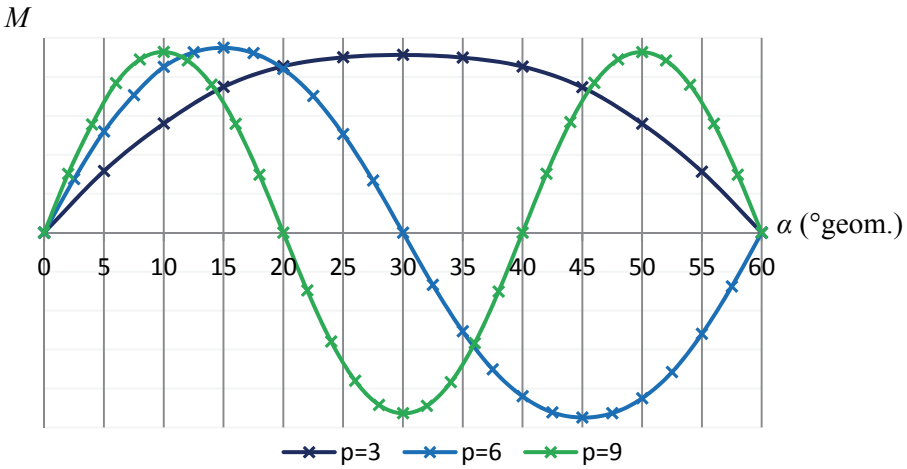

Fig. 1.22 Curves of CMC mechanical torque (PM made of Ba-ferrite)

The turning angle α at which the mechanical torque has it maximum value M_{max} for couplers with different pole pair numbers p can be calculated by (1.3).

$$\alpha = \frac{90°}{p}[°\text{geom}] \tag{1.3}$$

1.5. Conclusions

There are different types of magnetic couplers, but the cylindrical magnetic coupler (CMC) is researched in this work as the CMC is widely used in chemical industry, particularly in mixers, and the results of this research are already used in a company where the CMC mixers for laboratory equipment are manufactured (sent to and used in Germany).

The latest researches about CMC are overviewed, and they proved that in this work planned optimization has not been done and is necessary.

The main design and material parameters are chosen that influence the main coupler characteristic — mechanical torque.

A wide range of materials can be used in magnetic coupler manufacturing, but in this research the following materials are overviewed:

- for permanent magnets: barium ferrite, strontium ferrite, samarium cobalt alloy Sm_2Co_{17}, neodymium iron boron alloy;
- for sealing screen — austenitic stainless steel with grade 1.4401 ($\mu_* = 1.004$, but can be taken as air with $\mu_* = 1.000$);
- for coupler yokes — magnetically soft steel with grade S235JRG2 and material number 1.0038.

2. INFLUENCE OF DESIGN PARAMETERS ON MAXIMUM MECHANICAL TORQUE OF CMC

In the magnetic couplers the energy transfer between the inner and outer half couplings is ensured with the help of magnetic field. The nature of the magnetic field and its parameters prescribes the main coupler characteristic — mechanical torque. The magnetic field research methods will be described in this chapter.

In other words — the value of maximum mechanical torque M_{max} is influenced not only by the type of materials used in CMC, but also by the design parameters of the coupler. The latter influence will be overviewed in this chapter.

2.1. Active CMC

In the active CMC the permanent magnets are placed on both half couplings. In this work the CMC with equal number of PMs on both half couplings is researched.

2.1.1. Choice of influencing design parameters

The basic dimensions for a typical CMC in its cross section are given in Fig. 2.1. R_1 is the radius of the shaft on which the inner half coupling of CMC is placed/mounted, also called the *inner radius* of inner half coupling. R_2 is the inner half coupling radius not counting the height h_{PM} of permanent magnets, but R_3 is the inner half coupling radius counting the PM height, also called the *outer radius* of inner half coupling. R_4 is the outer half coupling radius counting the PM height h_{PM}, also called the *inner radius* of outer half coupling, but R_5 is the outer half coupling radius not counting the PM height. R_6 is the radius on which, e.g., the blades/paddles for CMC used in mixers are mounted, this radius is also called the *outer radius* of outer half coupling. The inner and outer half couplings are also characterized with their yoke height, accordingly h_{y1} and h_{y2}. Between the PMs on both half couplings there is the air gap δ in which the sealing screen is usually placed. R_δ is the radius by the middle of air gap, and at the surface made by this radius in axial length l the mechanical torque M is calculated. If the PMs have a rectangular form, then it is easier to place more magnets with smaller width b_{PM} than fewer, but wider magnets, because of the rounded surface.

The shaft (most often) is made from the same material as the yoke of CMC, thus also in this research the coupler model is reduced by the inner radius of inner half coupling (Fig. 2.2). So in the coupler base model one separate yoke (with its height h_y) is left — in the outer half coupling. The dimensions are correlated with each other with given relations (Fig. 2.3).

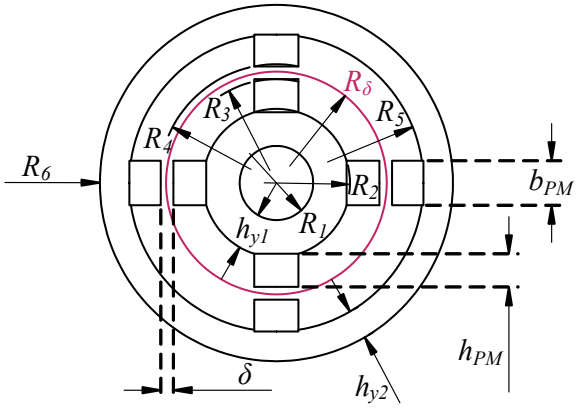

Fig. 2.1 Basic dimensions of CMC cross section

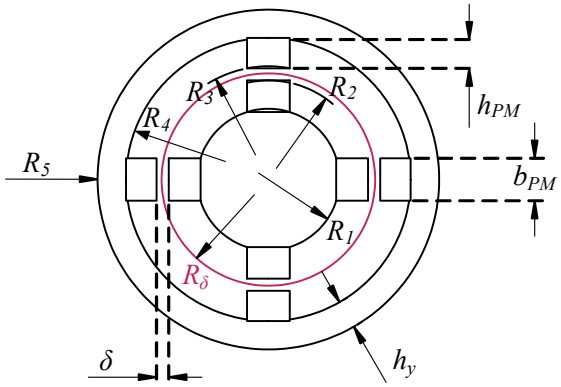

Fig. 2.2 CMC base model with dimensions in cross section

The most optimal PM form to be used in CMCs will be researched, and thus for practical reasons it has been chosen to use the magnetic coverage coefficient β ($\beta = \alpha_{PM}/\tau$, where α_{PM} is the angular width of PM in geometric degrees, but τ — pole pitch in geometric degrees) instead of PM width b_{PM}.

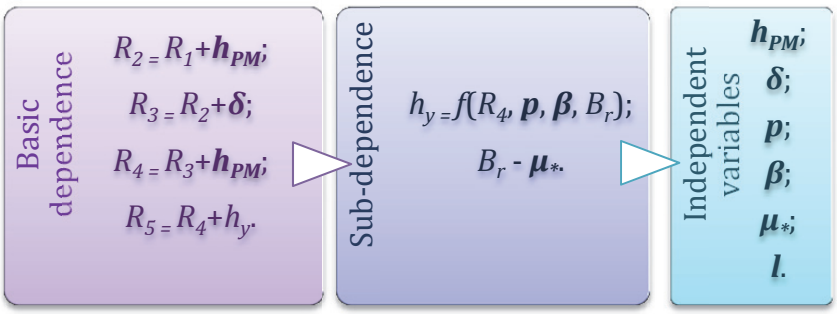

Fig. 2.3 Independent variables from basic dimensions

In the design optimization both — dependent and independent — variables are used. In the formula synthesis the dependent variables are: maximum mechanical torque M_{max}, maximum mechanical torque per volume M_{max}/V and the maximum values of magnetic flux densities $B_{max\ in}$ and $B_{max\ out}$. The following independent variables (design parameters) are

chosen: pole pair number p, magnetic coverage coefficient β, magnet height h_{PM}, air gap δ, relative permeability μ_* expressing the material that magnets are made of, and the coupler axial length l.

2.1.2. CMC mathematical model in QuickField software

The experiment plan consists of more than a thousand variations of chosen independent variables. It would not be practical to make every sample for all variations, so the use of special purpose computer simulation software is a very good solution.

To fulfil the analytic-type task — to research the influence of design parameters and PM material (permeability) on the nature of magnetic field (specifically, the magnetic saturation in steel), and on the coupler main characteristic (mechanical torque) — first of all it is necessary to research the CMC magnetic field.

The magnetic field research methods can be classified [166]:

- Analytical (where the magnetic field describing equations for simple or simplified models are used, the field linearity, etc., can be used);
- Numerical (based on the differential, integral, vector etc. equations, as *Maxwell equations*/equations of electromagnetic field);
- *Mathematical simulation* by terminology of the Latvian Academy of Sciences, but internationally more often known as the *mathematical modelling* (idealized and/or generalized object);
- *Physical simulation* by terminology of the Latvian Academy of Sciences, but internationally more often known as the *physical modelling* (the same models as real ones are used, but proportionally reduced);
- Experimental (a real object is used for which the magnetic field apportionment is researched; most reliable results).

Nowadays the numerical and mathematical modelling methods are the most popular for the magnetic field research [28, 75, 78, 166], because:

- An object with different form elements can be researched without principal changes;
- The nonlinear magnetization curves can be used without principal difficulties.

The simulation software for electromagnetic field modelling includes the numerical, mathematical modelling and other (e.g., for simulation iteration reduction) methods [138].

To model the magnetic field of CMC and calculate the necessary physical values many kinds of electromagnetic field simulation software can be used, such as *AMPERES* (three dimensional (3D)), *VSim* (3D), *OERSTED* (two dimensional (2D)), *ANSYS Maxwell*

(2D/3D), *QuickField* (2D), *MagNet* (2D/3D, as separate software and applied in *SolidWorks*), etc.

As the CMC has a symmetrical magnetic field in relation to the axial length, a simpler (two dimensional) electromagnetic field simulation software can be used. In this research the software *QuickField* (*QF*) [147] will be applied. This software is based on the finite element analysis. In the *QF* there are tools which can be used to protract the coupler model in cross section accordingly to the necessary design parameters and obtaining the geometry model, but it was chosen to use software *AutoCad* for the cross section drawings. In the *AutoCad* the drawings were saved as *.dxf* files, and these files were easily opened in *QF*. The process steps of working in *QF* are given in Fig. 2.4.

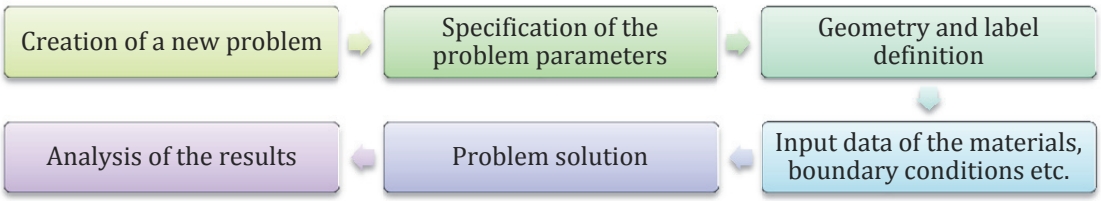

Fig. 2.4 Process steps in *QF*

At the new problem creation the problem type from given ones (Fig. 2.5) must be selected [147]. As the magnetic field is induced by permanent magnets in magnetic couplers, the PMs as the field source are magnetically static, and no other field sources are present, then the *Magnetostatics* is the most appropriate problem type, and it is selected for all CMC magnetic field modelling problems.

The model class must be chosen next. As the input is two dimensional, but real objects are three dimensional, then either the *plane-parallel* or the *axisymmetric* (axially symmetric) model class should be selected [147]. The cross section of CMC is equal at any length *l* point, thus the plane-parallel model class is selected for all further problems. And this length must also be input in the problem description dialog box. The units of length (microns, millimetres, centimetres, meters, kilometres, inches, feet or miles) can be chosen [147], the millimetres are chosen as the most suitable.

In the problem description dialog box the last two selections are the coordinate system and the precision. The precision is left by default the normal one. Between the Cartesian and polar coordinate systems the first one is chosen.

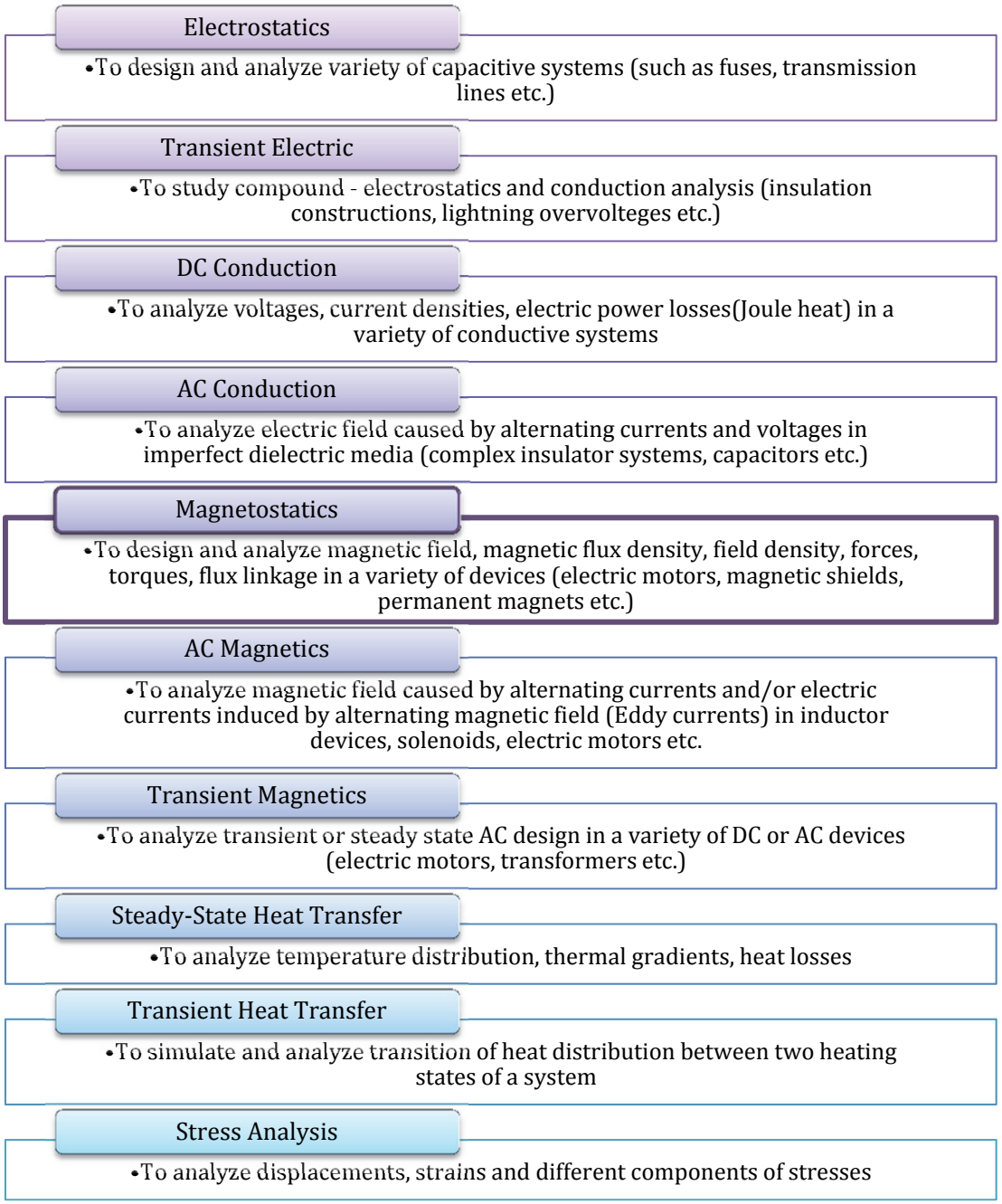

Fig. 2.5 Problem types in *QF*

After naming the problem file (with file extension .pbm) the same name is given to geometry file (.mod), data file (.dms) and result file (.res).

Next step is the creation of a model. As it is chosen to upload/import the previously prepared drawing files (.dxf), in this work the drawing tools for making the geometry model will not be overviewed. When the drawing file is imported and saved (automatically as the geometry model in geometry file .mod), the geometric objects (vertexes, edges and blocks) of the model can be defined and labelled. Then the boundary conditions must be defined, from which two are showed in Fig. 2.6. The Dirichlet condition is used at the circle made by outer

radius R_5 ($A_0 = 0$ Wb/m). Afterwards the mesh can be put on before the magnetic field calculation (/problem solution). A demonstrative example about CMC magnetic field calculation in *QF* is given in Appendix 5.

Dirichlet condition

- Specifies a known value of vector magnetic potential A_0;
- At the vertex or at the edge of the model;
- Can be defined as a function of coordinates ($x, y, z, r,$):

$$A_0 = a + bx + cy \text{ (planar problem)}$$

$$rA_0 = a + b \cdot zr + c \cdot \frac{r^2}{2} \text{ (axisymmetric problem)}$$

- a, b, c - constant parameters.

Neumann condition

- The tangent component of magnetic field intensity H_t is expressed with linear density of surface current σ:

$$H_t = \sigma \text{ (outward boundary)}$$

$$H_t^+ - H_t^- = \sigma \text{ (inner boundary)}$$

- "+" and "-"denotes quantities to the left and to the right side of the boundary.

Fig. 2.6 Boundary condition' types in *QF*

All the given information in this subchapter can be summarized as the methodology for physical parameters calculation of interest. The developed calculation methodology is given as an algorithm (Fig. 2.7).

This methodology is also used for permanent magnet synchronous motors to research their braking/cogging torques having different design parameters of interest [112, 114].

The developed calculation methodology allows to optimize the reactive cylindrical magnetic coupler only analyzing the results without a further necessity of synthesizing the formulas as it is in the active CMC case.

It is proposed to use rounded PMs instead of rectangular ones [110]. This transition — from rectangular form to rounded edges — is researched in this sub-chapter.

When the rectangular PMs are used, there are two additional radiuses, which must be considered, because of the PM embedding in the steel. These radiuses are also drawn (but are not numbered) in Fig. 2.8 and taken into account in calculations. In Fig. 2.8 the transition from rectangular PMs to rounded PMs is given.

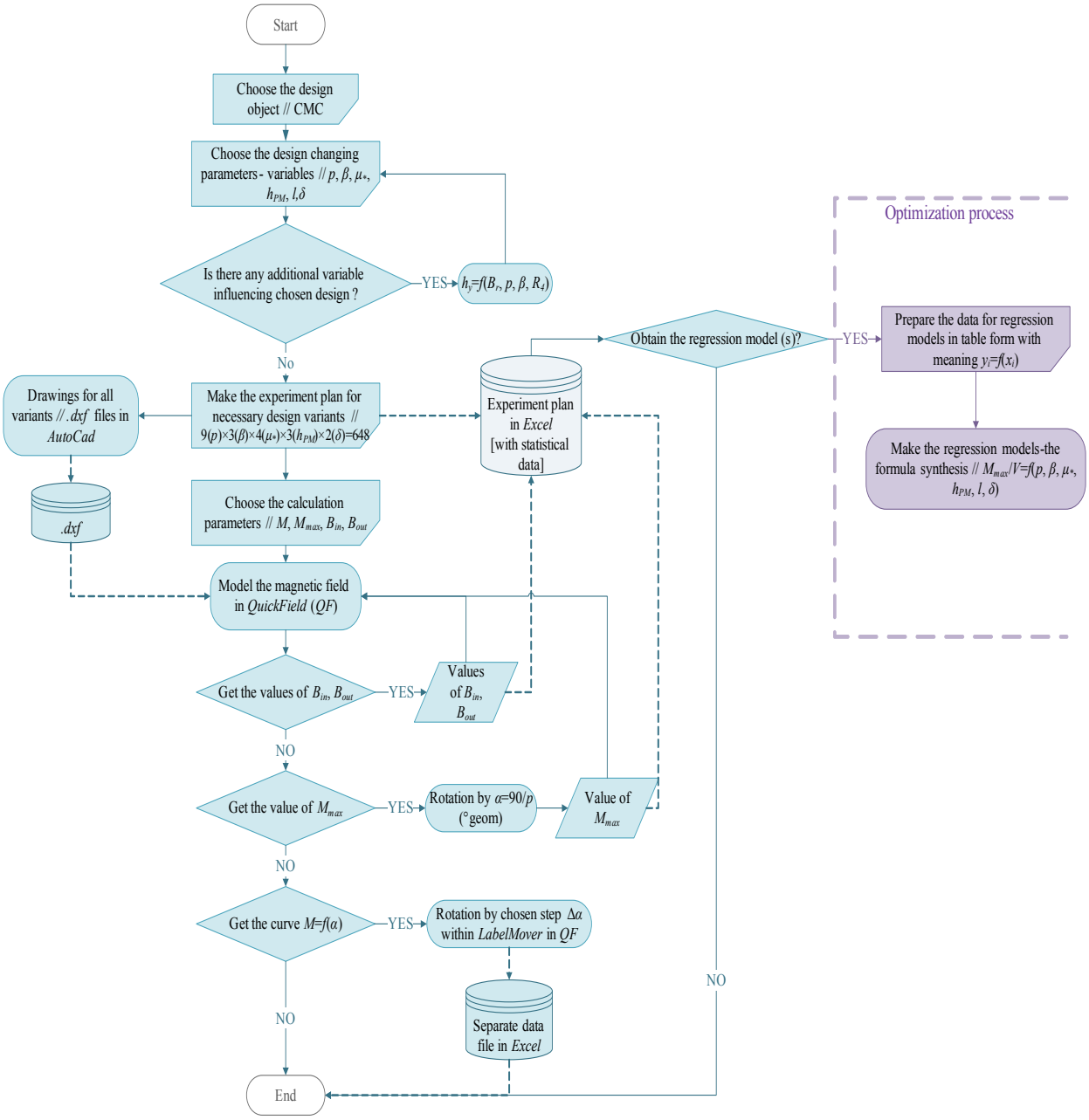

Fig. 2.7 Algorithm for the developed calculation methodology

2.1.3. Choice of PM shape

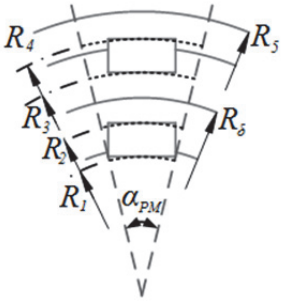

Fig. 2.8 Transition from rectangular to rounded PMs

Two-step transition is researched (Fig. 2.9). In the first step two of the edges are rounded, but the PMs angular width (corresponding length of the arc) is equal on both half couplings. In the second step the PMs on both half coupling are designed so that both — PM of inner half coupling and PM of outer half coupling — are equal by angle α_{PM}. And from here the magnetic coverage coefficient β can be used ($\beta = \alpha_{PM}/\tau$).

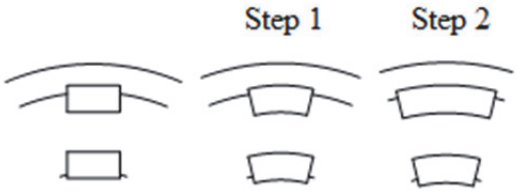

Fig. 2.9 Two-step transition of PM form

To research this transition a real CMC (produced in biotechnical centre for implementation in laboratory equipment BR-5 (Fig. 2.10)) is taken for the starting point. The inner half coupling 2 is fixed on the shaft 7 and thus is connected with the control block and motor 1, ensuring variable rotational velocity *n*. This half coupling is also supported to stainless steel tank 6 with Teflon axle box 5, ensuring the rotation. The outer half coupling 3 is placed in the cylindrical tank 6, and supported with Teflon axle box 5 to latter. This CMC has rectangular magnets 4 on both half couplings. On the outer part of outer half coupling the blades are embedded (not given in the figure).

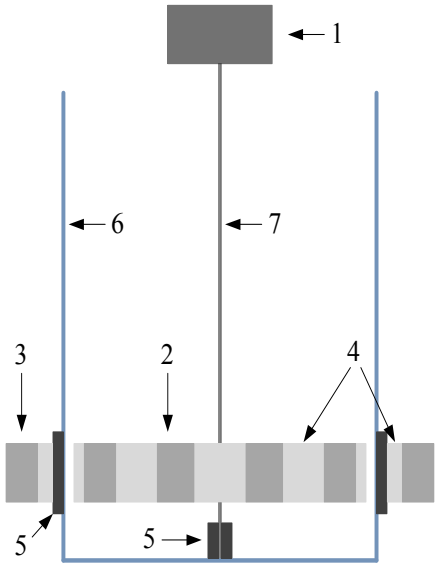

Fig. 2.10 Principal design of CMC as a part of mixer BR-5

This coupler has the following design parameters: axial length $l = 25.4$ mm (or 1 inch), pole pair number $p = 6$, magnet width $b_{PM} = 3.2$ mm (or 1/8″), $h_{PM} = 1.6$ mm (or

1/16″), radius R_1 = 6.6 mm, R_2 = 8.2 mm, air gap δ = 2.4 mm, R_3 = 10.6 mm, R_4 = 12.2 mm, R_5 = 13.5 mm, R_δ = 9.4 mm.

The maximum values of mechanical torque are compared for every transition step (table 2.1). It can be concluded that it is more useful to produce CMC with rounded permanent magnets than with rectangular ones, because the main characteristic — maximum mechanical torque M_{max} — grows for more than thirty per cent (>30 %).

Table 2.1

Comparison of CMCs with different form PMs

PM form	**Rectangular**	**Rounded**	
		Step 1	***Step 2***
Maximum mechanical torque M_{max} (Nm)	0.670	0.748	0.902
Growth (%)	–	**11.6**	**34.6**

2.1.4. Choice of boundary values for chosen design parameters

This research is made also with the intention of results' practical implementation in existing mixer (in CMC manufacturing at biotechnical centre). This is the basic reason for all chosen boundary values. These boundaries are necessary to later set the intervals of variables in which the optimization must be performed.

The radius R_1 is stated R_1 = 10 mm. From the practical implementation possibilities outcomes that the outer radius of inner half coupling can be R_2 = 14÷18 mm and the inner radius of outer half coupling can be R_3 = 16÷21 mm. This is taken into account in further boundary values' choice.

2.1.4.1. Pole pair number p

The smallest pole pair number with which the coupler could still work is p = 1 — CMC needs at least two magnets (or one pole pair) on both half couplings to operate as it is expected to.

The two real couplers with rectangular magnets are researched to choose which pole pair number should be taken as the largest for the CMC with rounded PMs [111].

The first coupler is named BR-5, but the second coupler — BR-30. The magnets' width was changed after chosen pole pair number so to fit as many magnets as possible on the surface made by R_1 (table 2.2). For these couplers the maximum mechanical torques were compared (Fig. 2.11, 2.12)

Table 2.2

BR-5 and BR-30 PM width b_{PM} corresponding to pole pair number p

	BR-5				BR-30			
	Original				Original			
p	6	5	4	3	7	6	5	4
***b_{PM}* (mm)**	3.2	4.1	5.2	6.6	6.3	7.6	9.2	11.1

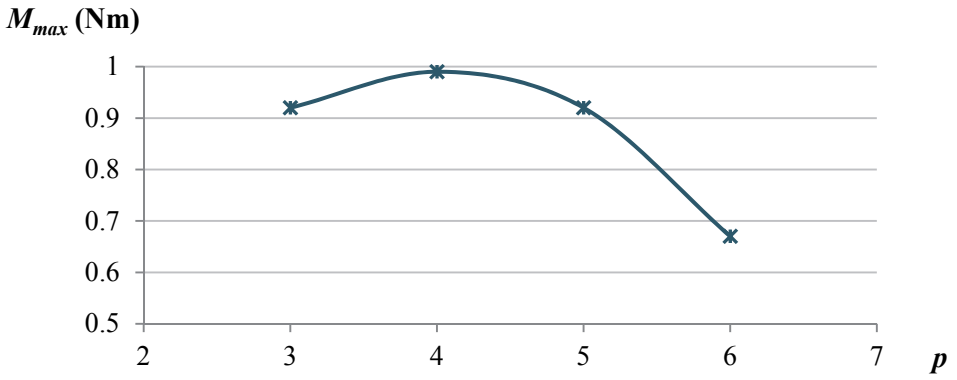

Fig. 2.11 Maximum mechanical torque from pole pair number for BR-5

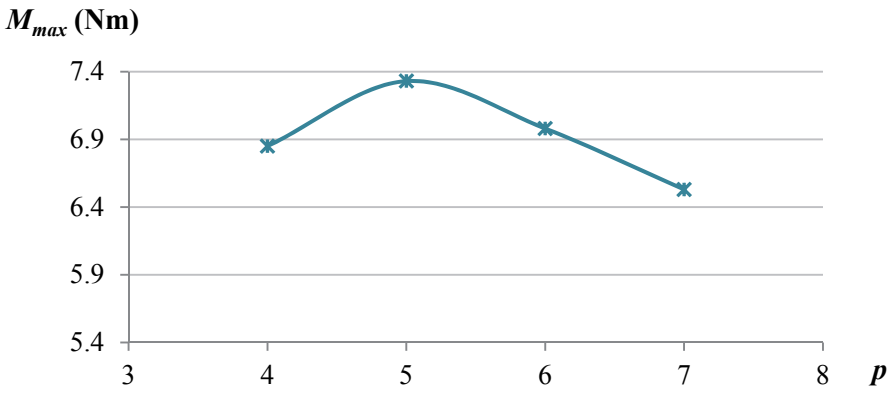

Fig. 2.12 Maximum mechanical torque from pole pair number for BR-30

These results show that the optimum could be around the pole pair number p = 5. The research of the coupler with rounded PMs must also be made for reliable choice. For this research two magnetic coverage coefficients β are also taken into account [109], to see if the optimal value of pole pair number p doesn't jump out the planned one. The sizes of coupler are taken as follows: $R_1 = 22$ mm, $h_{PM} = 4$ mm, $\delta = 2$ mm and $R_4 = 32$ mm, but $\beta = 0.7, 0.9$. The axial length $l = 25.4$ mm (= 1″). The pole pair number p is taken from one till ten, and the maximum mechanical torque is compared for these variants (Fig. 2.13).

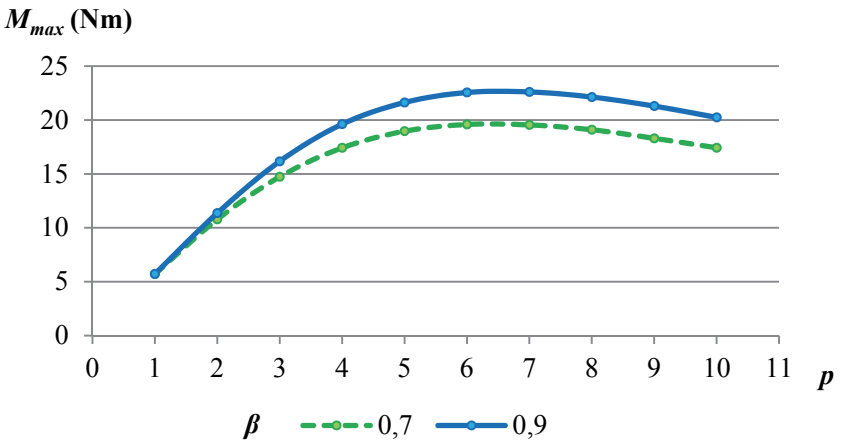

Fig. 2.13 Maximum mechanical torque for coupler with rounded PMs

As can be seen, the optimal value of maximum mechanical torque is at about pole pair number $p = 7$. Even at different magnetic coverage coefficients β the manner of the curve $M_{max} = f(p)$ remains the same.

Hence the maximum boundary value of pole pair number is taken $p = 9$. To sum up, in this research the interval of pole pair number is chosen $p = [1 \div 9]$.

2.1.4.2. Magnetic coverage coefficient β

For the choice of maximum boundary value of magnetic coverage coefficient β, the magnetic field calculations are made for three PM materials (Sr-ferrite, SmCo and NdFeB) and the following design variants: $p = 5$, $l = 10$ mm, $h_{PM} = 6$ mm, $\delta = 2$ mm and $\beta = 0.9 \div 0.97$ by a step $\Delta\beta = 0.01$. The maximum mechanical torque M_{max} (Fig. 2.14) and the maximum torque per unit volume M_{max}/V (Fig. 2.14) are compared for these variants.

The maximum torque M_{max} dependence from magnetic coverage coefficient β is almost linear and downward oriented at higher β value (in interval $0.9 \div 0.97$) in case of the PMs being made of simple ferrite as barium or strontium (fir. 2.14, a). In case of rare-earth PMs the opposite is true: the dependence has a wavy form and at higher β values the torque M_{max} can grow or drop-down (Fig. 2.14, b and c).

Then it is stated to take into account the manufacturing possibility — how easy it is to place two strong (rare-earth alloy) magnets vary close [25, 86] —, hence the maximum value of magnetic coverage coefficient is taken $\beta = 0.9$.

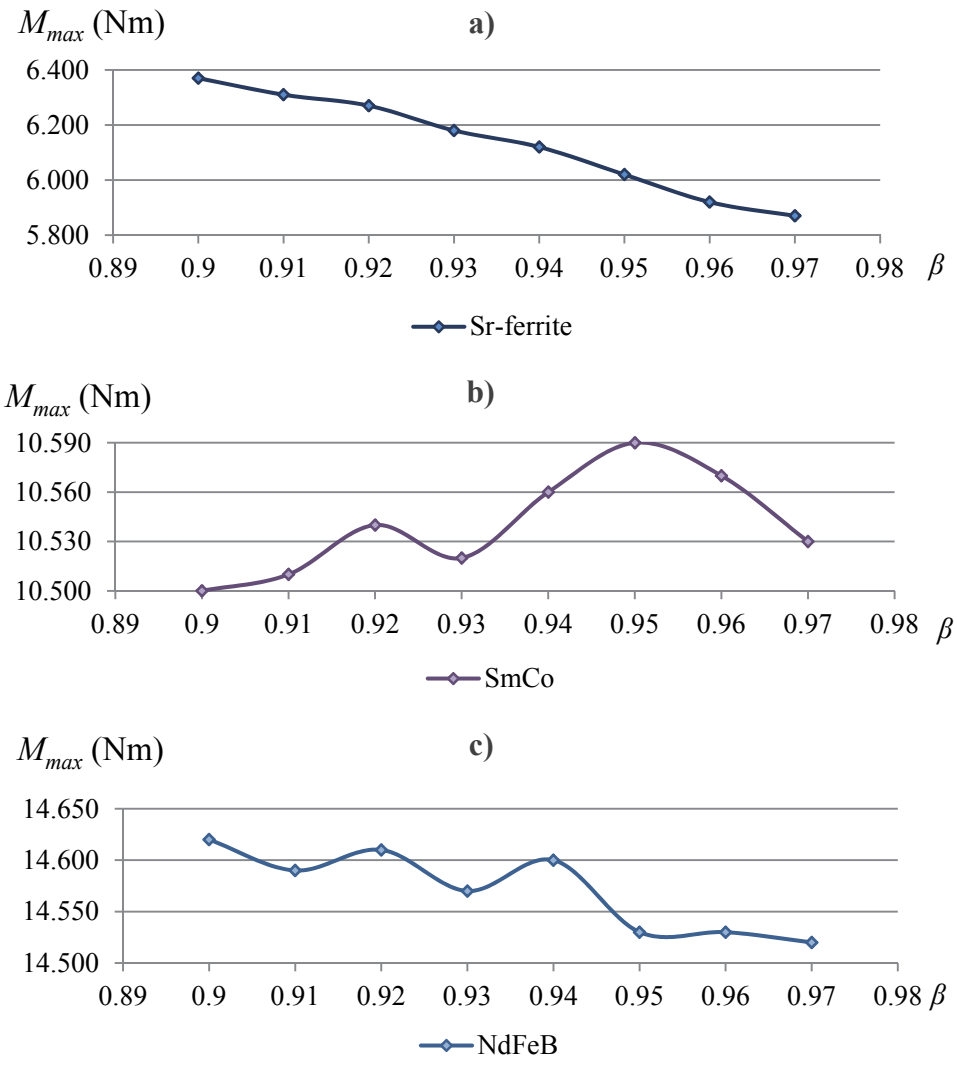

Fig. 2.13 M_{max} dependence from β for three PM materials:

a) — Sr-ferrite (strontium ferrite), **b)** — SmCo (samarium cobalt),
c) — NdFeB (nepdymium iron boron)

The minimal boundary value of magnetic coverage coefficient is not specifically researched because a similar situation exists in electrical machines — the smaller the magnetic field coverage on pole pitch is, the less effective the use of magnetic flux is [18, 33, 89, 101]. In electrical machines it is often suggested not to ensure the magnetic coverage less than 0.6 of pole pitch. The calculations (for case: $p = 1$, $l = 25.4$ mm, $R_1 = 22$ mm, $h_{PM} = 4$ mm, $\delta = 2$ mm, NdFeB magnets; Fig. 2.15) showed that the value of magnetic coverage coefficient β has a strong influence on the mechanical torque (when the pole pair number is 4 or less). The smaller the β, the more outstanding is the jump of torque. But at $\beta = 0.9$ the curve has a trapeze shape. This can be explained by the magnetic field property that it focuses at the corners — and when the magnets are very wide (just two magnets along the surface),

the main interaction (attraction and repulsion) forces are “wider” according to the turning angle α. This influence decreases at higher number of pole pairs (Fig. 2.16), when the torque M dependence from magnetic coverage coefficient β is the same according to its shape — all curves are parabolic. The value of maximum mechanical torque M_{max} is smaller at lower magnetic coefficient β.

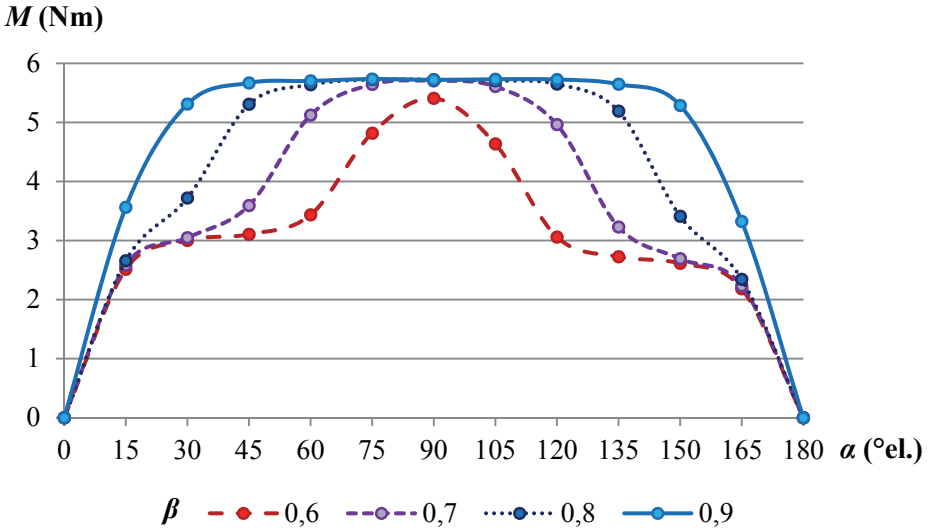

Fig. 2.15 The evolution of M by β (p = 1)

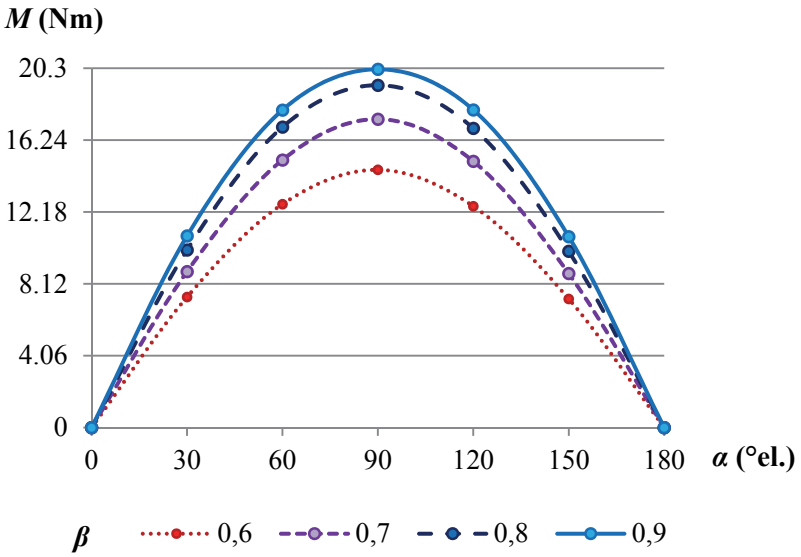

Fig. 2.16 The evolution of M by β (p = 10)

The author suggests taking the minimal boundary value of magnetic coverage coefficient β no less than 0.7 in active magnetic couplers, definitely in active cylindrical magnetic couplers.

Thus in this research for planned optimization the interval of magnetic coverage coefficient is chosen β = [0.7÷0.9].

2.1.4.3. PM height h_{PM}

The diapason of PM height is chosen accordingly to statement at the beginning of the subchapter *2.1.4.*, that radius R_2 should be 14 till 18 mm (and radius R_1 is constant — 10 mm). It is easy to check if the PM height h_{PM} conforms to this condition (table 2.3).

Table 2.3

PM height h_{PM} conformity to stated condition

h_{PM} (mm)	R_2 (mm)	$R_2 \geq 14$ AND $R_2 \leq 18$ (mm)
3	13	–
4	**14**	+
5	15	+
6	16	+
7	17	+
8	**18**	+
9	19	–

Hence the interval of PM height is $h_{PM} = [4 \div 8]$ mm.

2.1.4.4. Air gap δ

The sealing screen is produced no thinner than one millimetre [86]. The fixation elements (such as axle box) are also made about 0.5 mm thin, and an additional 0.5 mm width is counted. To sum up, the minimal value of the gap in the coupler between the inner and outer half couplings should be taken $\delta = 2$ mm. In calculations this gap is set as air gap.

To specify the maximum boundary value of air gap δ, similar conformity must be filled as it was given for PM height. The condition is as follows: the radius R_3 should be 16 till 21 mm. Another piece of common knowledge/condition is taken into account — the air gap should not be wider than the smallest value of PM height, i.e., $\delta \leq 4$ mm. This conformity is tested in table 2.4.

Table 2.4

Air gap δ conformity to stated condition

δ (mm)	R_2 (mm)	R_3 (mm)	$R_3 \geq 16$ AND $R_3 \leq 21$ (mm)
2	14	16	+
2	18	20	+
3	14	17	+
3	18	21	+
4	14	18	+
4	18	22	–

As in the case when the $h_{PM} = 8$ mm and $\delta = 4$ mm, the stated condition is not confirmed, then the value $\delta = 4$ mm is taken as inadequate for further research. Hence the interval of air gap is $\delta = [2 \div 3]$.

2.1.4.5. PM materials

Two types of material for permanent magnets are chosen: simple ferrite and rare-earth alloy. And for unbiased judgement two materials are taken for each type: barium ferrite ($BaFe_{12}O_{19}$), strontium ferrite ($SrFe_{12}O_{19}$), samarium cobalt alloy (Sm_2Co_{17}, grade 30H) and neodymium iron boron alloy (NdFeB, grade N38UH). The characteristics of these materials are given in table 2.5.

In the optimization algorithm a smooth interval for magnet materials cannot be used, because in such a situation, when an interval would be used $\mu_* = [1.061 \div 1.344]$, any value from it with a certain precision could be selected. Thus an optimum with a material that does not exist could be obtained. Hence, only given four materials are used with their fixed value of relative permeability μ_*, as given in the following table.

Table 2.5

Main characteristics for chosen PM materials

PM material	B_r **(T)**	H_c **(kA/m)**	BH_{max} **(kJ/m^3)**	μ_*	$t_{op\ max}$ **(°C)**
Sr-ferrite	0.38	225	27.9	**1.344**	200
Ba-ferrite	0.245	175	8.4	**1.114**	200
SmCo	1.1	800	220–240	**1.094**	350
NdFeB	1.2	900	280–300	**1.061**	180

These fixed values of residual induction B_r and coercive force H_c are used in magnetic field modelling and the necessary parameters' calculations.

2.1.4.6. Axial length l

The smallest unit for the CMC axial length is taken 10 mm (or 1 cm). And according to the manufacturing possibility (implementation in mixer) the length is taken no longer than 75 mm (or 7.5 cm). Hence the interval of axial length is $l = [10 \div 75]$ mm.

2.2. Reactive CMC

When a cylindrical magnetic coupler (CMC) has the permanent magnets only on one half coupling and the half coupling without PMs has the same toothed form as if the magnets were there, it is called the reactive CMC (Fig. 2.17). Such a design solution is necessary in

cases when the environment would be too aggressive to PMs: temperature too high, causing the magnets to noticeable lose their quality — repulsion and attraction forces-, or other influencing factors that could lead to magnet demagnetization, etc.

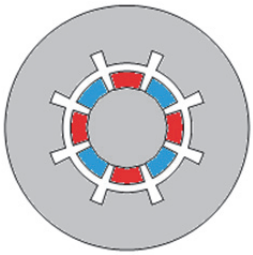

Fig. 2.17 Reactive CMC in cross section

The disadvantage of such design CMC is that it has much lower maximum mechanical torque than the active CMC with the same design parameters. As an example mechanical torque for active and reactive CMCs is given with identical design parameters ($p = 2$, $\beta = 0.6$, $l = 10$ mm, $R_1 = 10$ mm, $h_{PM} = 4$ mm, $\delta = 2$ mm, PMs are made of NdFeB alloy), except that reactive coupler instead of the magnets has the steel teeth with the same shape (as magnets for active coupler) on the outer half coupling (Fig. 2.18).

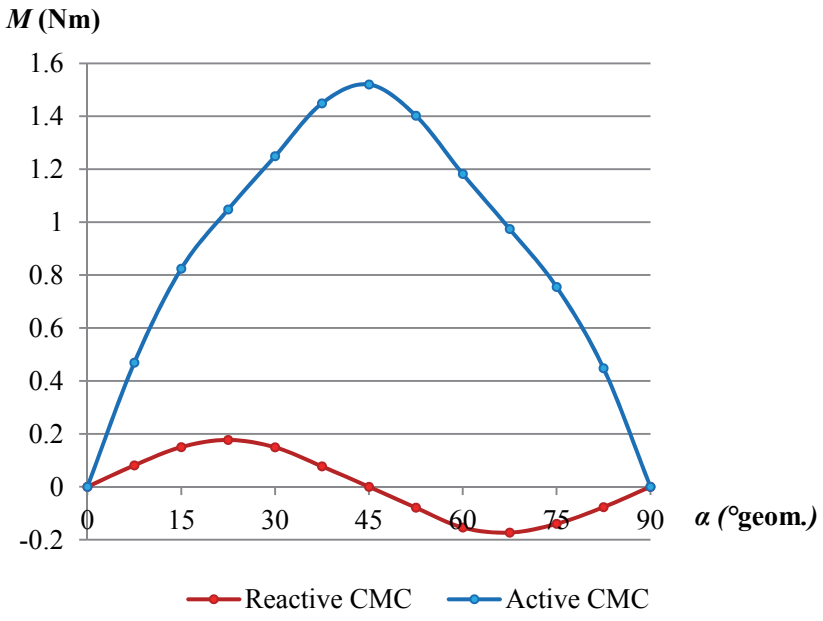

Fig. 2.18 Mechanical torque of active and reactive CMCs

As it has been mentioned, the active couplers have much higher value of maximum mechanical torque than the reactive ones with identical design parameters. This and other researched design variants showed that the reactive coupler has a pole pitch τ two times shorter compared to the active coupler, because the one half coupling is made of teeth-shaped steel. So there is no separate magnetic field source, and each steel tooth interacts with (/passes

through the field of) the north and following south direction magnets, while in active coupler at the same positions the PM tooth (with south or north direction) just has the higher or lower value of the torque in the same magnetic flux direction. However, the size of the pole pitch is not a disadvantage.

The main disadvantage, why the reactive couplers are used only in case of necessity to transfer the torque in aggressive environment, is the small value of its maximum mechanical torque, compared with the same design active CMC (Fig. 2.19). Hence a new design of reactive CMCs is proposed [133, 134] and researched [113].

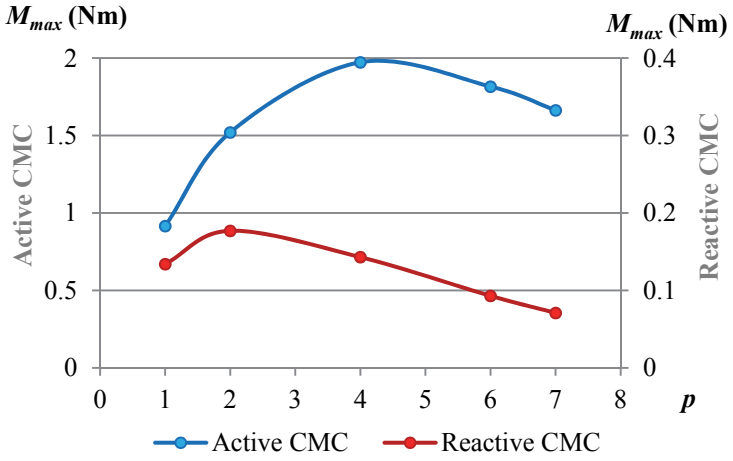

Fig. 2.19 Maximum mechanical torque M_{max} for active and reactive CMCs

The new design reactive CMC has also inner and outer half couplings as the standard reactive coupler (Fig. 2.20), and the permanent magnets 1 are placed only on one half coupling. The yoke 2, on which the PMs are mounted, is made of ferromagnetic material. In the new reactive coupler the second half coupling has sector-shaped poles 3 made of ferromagnetic material, which are separated from each other with nonmagnetic material air gap 4 and placed on a body 5, made of nonmagnetic and light material. Both half couplings are separated from each other with fixed sealing screen 6.

When the half coupling with PMs starts to rotate, the magnetic flux, induced by magnets, closes through conversely magnetized poles by steel teeth on the second half coupling. The maximum value of magnetic flux Φ_{max} in the air gap is in case when the angle θ between the magnets axis **m** and to **m** nearest ferromagnetic pole axis **p** is equal to $\theta = 45°$, calculated by (2.1) as the pole pair number is $p = 2$. The k in (2.1) is an unpaired integer: $k = 1, 3, ..., n$.

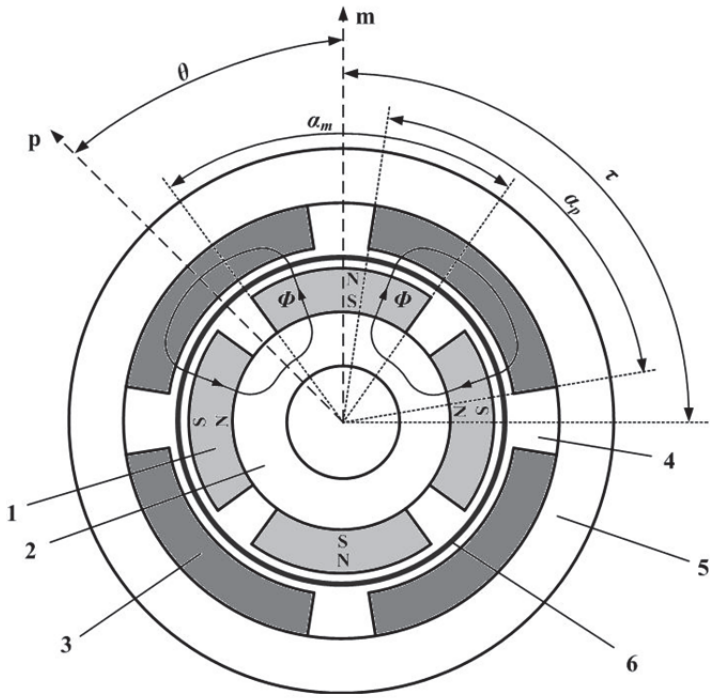

Fig. 2.20 New (patented) design reactive CMC

$$\theta = k\frac{90}{p}(^{\circ}\text{geom}). \tag{2.1}$$

If the angle between axes **p** and **m** comprises to the value from (2.1), the mutual placement of driving and driven half couplings conforms the idle or balance mode of the coupler, and the torque is equal to $M = 0$ Nm.

When the axes **p** and **m** match or the angle is θ = 0°, the magnetic flux in the air gap is minimal $\Phi = \Phi_{min}$ (Wb). The other angles, at which the magnetic flux is minimal, can be calculated by (2.1), but then the k is paired integer, $k = 2,4, ..., n$. In such a situation the mutual placement between the both half couplings has an unstable balance, but torque again is $M = 0$ Nm. The transition from the maximum to the minimal magnetic flux (also in the opposite direction) provides the torque between the driving and the driven half couplings. The maximum value of mechanical torque M_{max} is at angle θ according to (2.2).

$$\theta_{M\max} = k\frac{90}{2p}(^{\circ}\text{geom}), \tag{2.2}$$

where k — an integer, $k = 1, 2, ..., n$.

The value of M_{max} depends on magnetic coverage coefficient β and it is:

$$\beta = \frac{\alpha_p}{\tau} = \frac{\alpha_m}{\tau}(^{\circ}\text{geom}), \tag{2.3}$$

where α_p — the sector-shaped pole width (°geom),

α_m — the width of PM (°geom).

The three basic situations of reactive CMC magnetic field are given in Fig. 2.21

The new design reactive coupler (Fig. 2.22, a) is researched as well as the standard design reactive coupler with the same dimensions (Fig. 2.22, b).

For the comparison the characteristic M_{max}/V is chosen — maximum mechanical torque per volume — for objective results, because the new design coupler has a very light nonmagnetic yoke. The PMs are made of NdFeB alloy. Results are given for new (Fig. 2.23) and standard (Fig. 2.24) design reactive couplers.

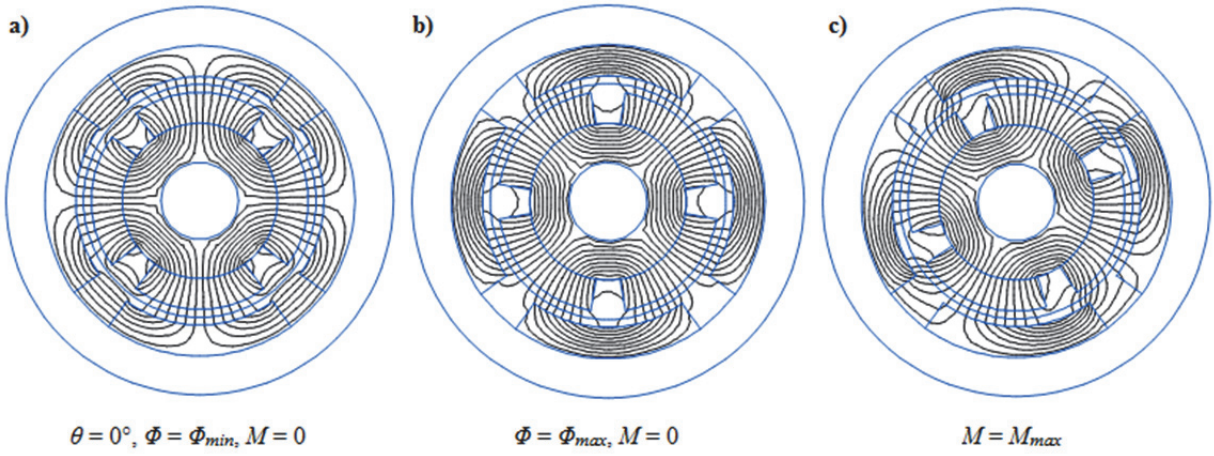

Fig. 2.21 Reactive CMC magnetic field

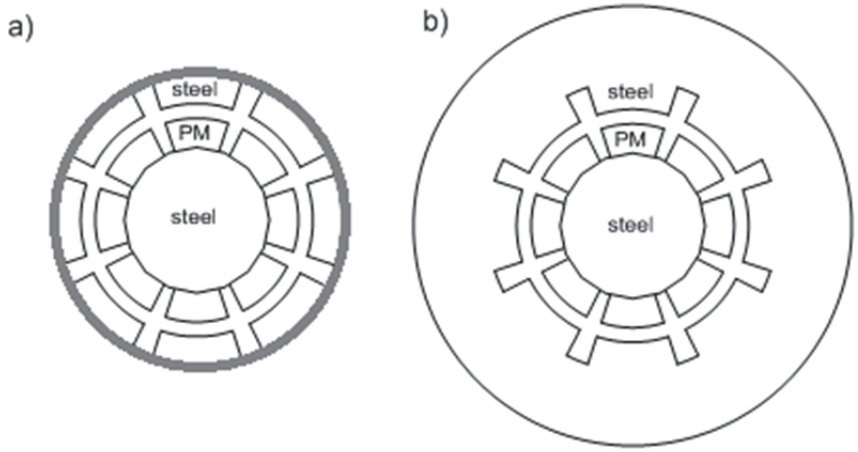

Fig. 2.22 New (a) and standard (b) design reactive CMCs in cross section

The highest values of M_{max}/V for standard design reactive coupler is at pole pair number $p = 4$ and with $\beta = 0.6$, but for the new reactive coupler design — at $p = 2$ with the values of magnetic coverage $\beta = 0.7 \div 0.8$. From these both graphs it can be seen that with standard design the reactive coupler has the values of M_{max}/V for about 9 times lower than with the new design.

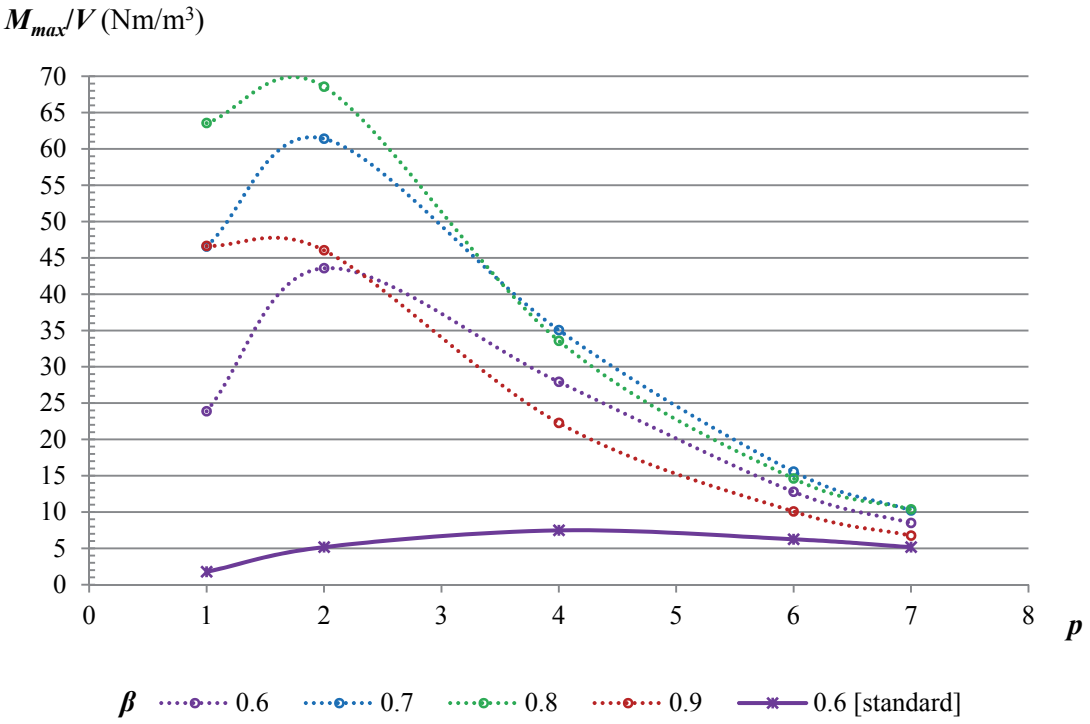

Fig. 2.23 $M_{max} = f(p, \beta)$ for new design reactive CMC

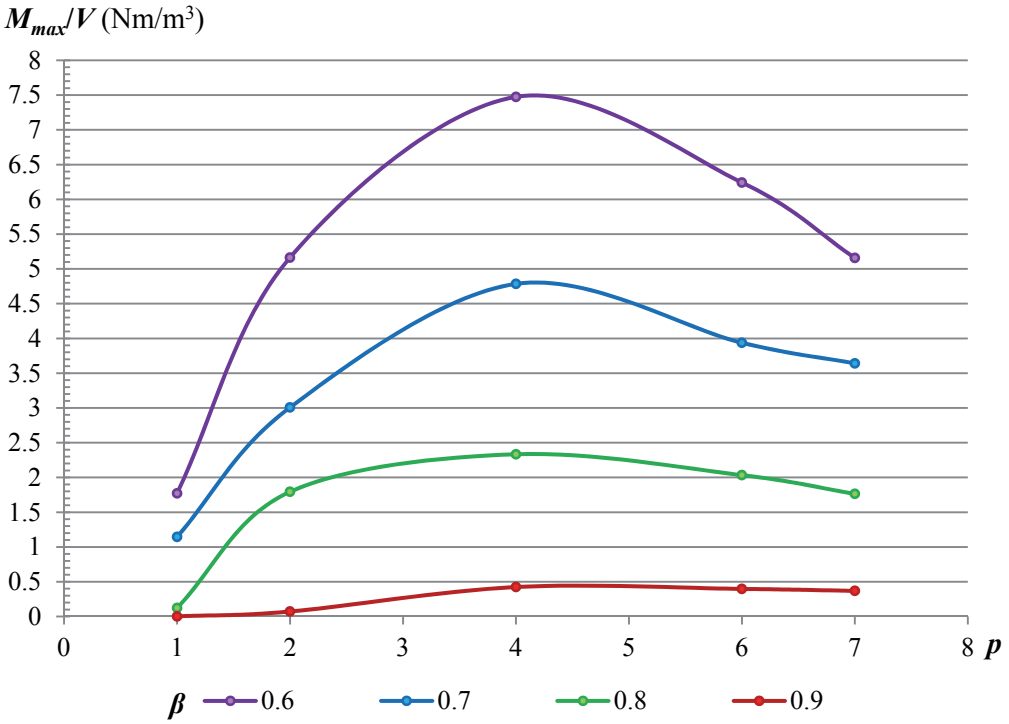

Fig. 2.24 $M_{max} = f(p, \beta)$ for standard design reactive CMC

The invention [133] provides:

1) The new sector-shaped ferromagnetic poles, which are separated from each other with sector-shaped air gap and placed on nonmagnetic, very light body;

2) The number of ferromagnetic poles is equal to the number of permanent magnets to ensure the operation of reactive coupler;
3) To increase the ratio M_{max}/V, the magnetic coverage coefficient of ferromagnetic poles and PMs must be increased to $\beta = 0.8$;
4) If the sector-shape poles are made of light polymer matrix composite containing magnetic filler (iron, ferrite) powder, the half couplings increase the weight-dimensions characteristics.

2.3. Comparison of active and reactive CMCs

As the standard design reactive couplers had a much smaller ratio M_{max}/V than the active ones, it was irrelevant to compare them. But the new design reactive couplers have better ratio M_{max}/V and it is important to know the effectiveness of them compared to the active coupler.

One example of each has been taken — active and new design reactive CMC — with identical dimensions: $R_1 = 10$ mm, $h_{PM} = 4$ mm, $p = 2$, $\beta = 0.6$, NdFeB magnets, $R_5 = 27$ mm (for active coupler), $l = 10$ mm. The magnetic fields in cross section for both of these couplers are given in Fig. 2.25.

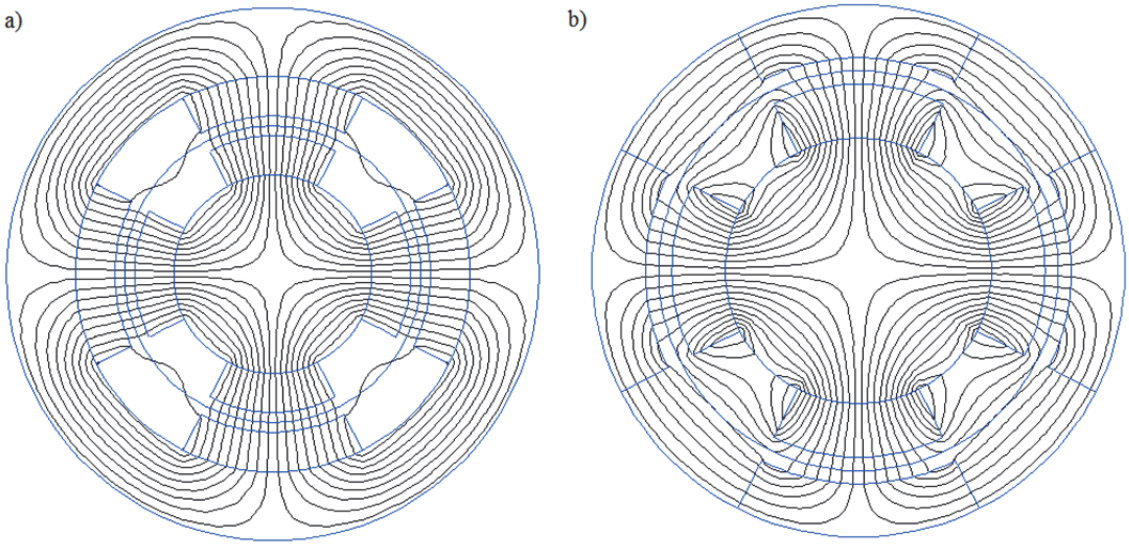

Fig. 2.25 Magnetic field in cross section for active (a) and new design reactive (b) CMCs

The value of maximum torque M_{max} for the new design reactive coupler still is smaller than for the active one (Fig. 2.26), but only 4.5 times smaller instead of about 8.6 times as it is in case of standard design reactive coupler. In percentage the comparison of M_{max} for reactive couplers to the active one is given in table 2.8.

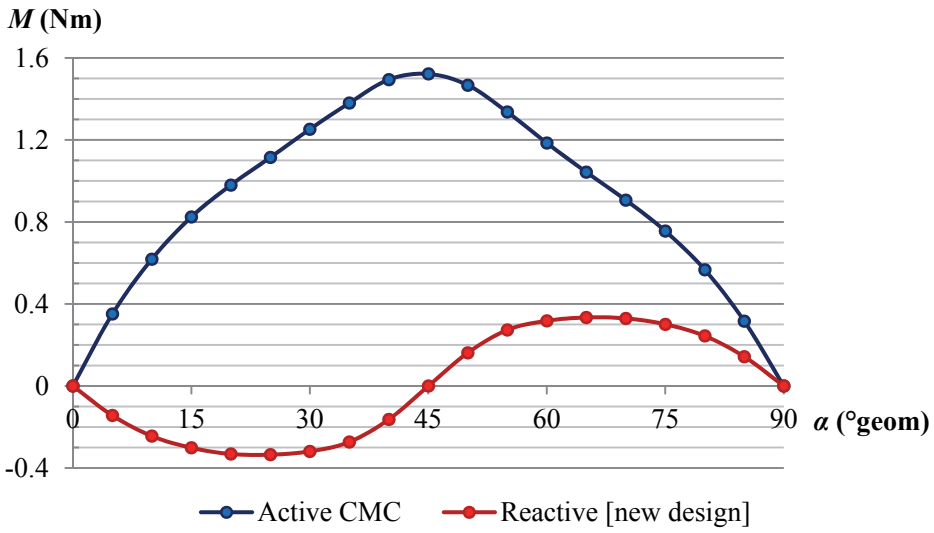

Fig. 2.26 Mechanical torque M of active and new design reactive CMCs

The ratio M_{max}/V is also compared for active and reactive CMC couplers (table 2.6). If only the torque is overviewed, then the new design reactive coupler has an improvement of about 2 times higher torque value than the standard design reactive coupler. But for the ratio M_{max}/V — about 9 times higher value.

Table 2.6

Main characteristics compared for active and reactive CMCs

Design	M_{max} **(Nm)**	M_{max}/V **(Nm/cm^3)**	M_{max} **(%)**	M_{max}/V **(%)**
Active CMC	1.523	79.54	–	–
Reactive CMC (new)	0.335	43.68	22.0	54.9
Reactive CMC (standard)	0.177	5.16	11.6	6.5

Important conclusion is that, while the maximum torque M_{max} of new design reactive CMC attains about 22 % of the active coupler maximum torque, the maximum torque per volume M_{max}/V is about 55 % from the value of active CMC M_{max}/V. Hence in very aggressive environments the new design reactive CMC is a very good alternative.

The developed calculation methodology allows obtaining the optimum of reactive CMC only analyzing the calculation results and without necessity of any further mathematical procedure. Thus further will be researched only the active CMC.

2.4. Conclusions

From the researched and overviewed materials in this chapter following conclusions can be made:

- The base model of active CMC for further research is chosen and the modification is defined.
- The influencing design parameters of coupler torque are researched and chosen, for which the boundary values are strictly grounded from scientific or practical reasons and these values are chosen to be used in further optimization.
- A methodology is developed to obtain the CMC characteristic and control parameters at different design parameters by magnetic field modelling, based on finite element method/analysis.
- The influence of permanent magnet shape on the coupler maximum mechanical torque M_{max} was researched. The transition from rectangular PMs to rounded PMs increases the M_{max} for about 35 %. The rounded PMs are used in further research and optimization of CMC.
- The reactive CMC was researched, and a new design reactive CMC was developed, which has improved M_{max} 2 times and M_{max}/V about 9 times. For the proposed new design reactive CMC the Latvian and European patents were obtained.
- The active and reactive CMCs are compared and it can be concluded that the new design reactive CMC is a very good alternative to active CMC if the environment where the coupler is placed is aggressive and thus the PMs would lose their good properties.
- The developed calculation methodology allows obtaining the optimum of reactive CMC without necessity of any further mathematical procedure.

3. SYNTHESIS OF MATHEMATICAL MODELS

In the magnetic couplers' designing the main task is to ensure the optimal distribution of the magnetic field in the elements which conduct the magnetic field. This distribution is directly related to the design parameters or sizes. Hence the main task transfers to one where the optimal combination of the design parameters must be chosen ensuring the best distribution of the magnetic field. With the best distribution of the magnetic field understand the magnetic field of the whole design system that either the field has no saturation (respectively, the design system is without extremely high values of the magnetic flux density) or no unnecessary magnetic field conducting elements are in the design (in some elements the magnetic flux density is not at all or is too small to be useful), so the raw materials are redundantly consumed.

It is chosen to use mathematical model of cylindrical magnetic coupler (CMC) for the planned optimization. Here and further with mathematical model the mathematical relation in equation forms for the relevant physical parameters depending on the design and other parameters is meant.

There are no such existing mathematical models for CMC that could be used in the optimization considering the chosen boundary values of the material and design parameters. Thus the subtask is to obtain such mathematical models (or formulas), including all the parameters of interest.

In any field of sciences every research is based on one of two aspects (to explore or to confirm) [145], from which all the research methods are divided in:

a) exploratory;
b) confirmatory.

The whole research process the author would divide as given in Fig. 3.1, and in this chapter the data analysis techniques are overviewed, from which one is chosen.

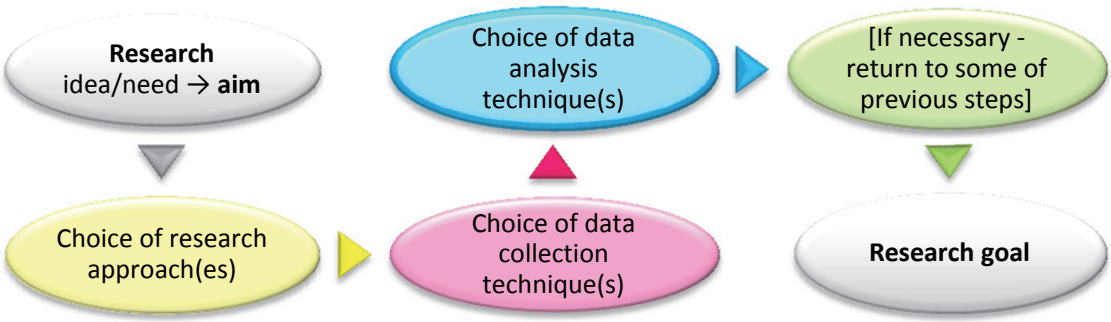

Fig. 3.1 Research process

There are a few general research approaches (in some literature also called methodologies) [19, 35, 52, 148, 158]:

- field study (in humanitarian and exact sciences);
- case study (more often in social sc.);
- laboratory experiment (in humanitarian and exact sc.);
- opinion research (more often in social sc.);
- experimental simulation (more often in biological and physical sc.)
- etc.

Any general research approach cannot be implemented without a data collection method/technique such as [4, 32, 119]:

- survey (more often in social sc.);
- individual interview (more often in social sc.);
- focus group(s) (more often in social sc.);
- observations – for objects or individuals (in humanitarian and exact sc.);
- experiment (in humanitarian and exact sc.);
- simulation (more often in exact sc.);
- etc.

After gathering the data, it must be analyzed (blue step in Fig. 3.1). Most often the data is a multivariate system and the two variables $y = f(x)$ is a simplified and derived case from multivariate data [39]. The *multivariate data analysis* (MDA) refers to all statistical techniques for analysis of multiple measurements of individuals and objects [44].

Variables can be quantitative (values are numerically measurable, e.g., voltage) and qualitative (descriptive meaning, e.g., hair colour). For both — quantitative and qualitative — variables can be used the MDA techniques/methods (Fig. 3.2, 3.3) [39, 44, 162].

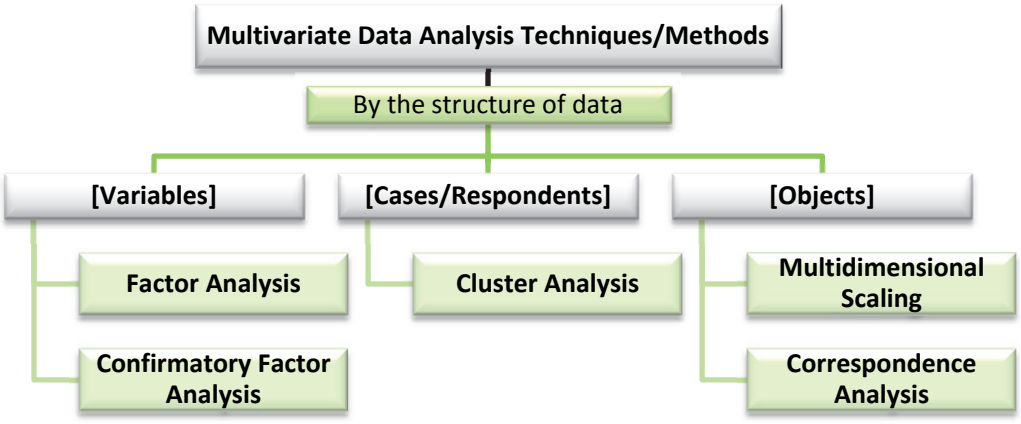

Fig. 3.2 Classification of multivariate data analysis' techniques by data structure

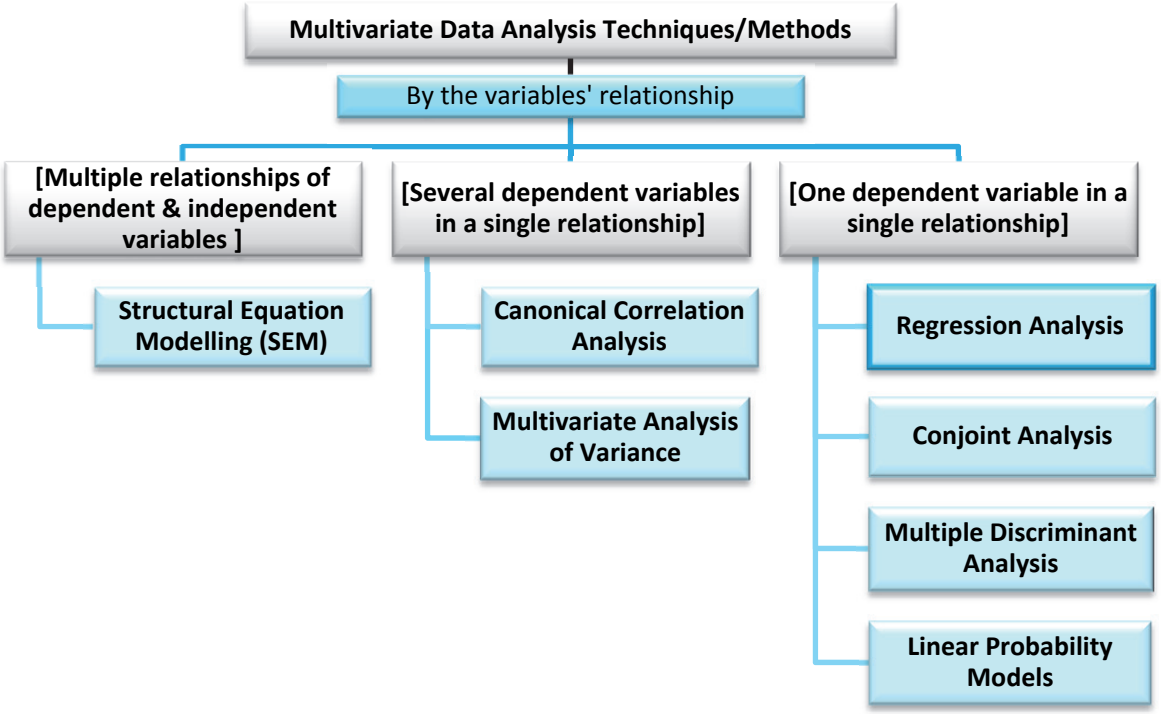

Fig. 3.3 Classification of multivariate data analysis' techniques by variables' relationship

Some more information about some of MDA methods will be given now [44].

In the *regression analysis* the dependent variable y_1 is quantitative but the independent variables x_1, ..., x_n can be both — quantitative and qualitative-, the relationship forms as follows:

$$y_1 = f(x_1, x_2, ..., x_n). \tag{3.1}$$

In the *conjoint analysis* the dependent variable y_1 may have either a quantitative or a qualitative value but the independent variables x_1, ..., x_n are only qualitative, in another way the relationship is the same as in (3.1).

The *multiple discriminant analysis* can be chosen if the dependent variable y_1 is qualitative, but the independent variables x_1, ..., x_n are quantitative, others as in (3.1).

The same relationship (3.1) is for *analysis of variance*. Just the dependent variable y_1 is quantitative, but the independent variables x_1, ..., x_n are only qualitative. In the *multivariate analysis of variance* the variables are the same — dependent variables y_1, ..., y_n are quantitative and independent variables x_1, ..., x_n are qualitative — but the relationship forms as in (3.2).

$$y_1, y_2, ..., y_n = f(x_1, x_2, ..., x_n) \tag{3.2}$$

The given relationship (3.2) remains valid for the *canonical correlation analysis* but the dependent (y_1, ..., y_n) and independent (x_1, ..., x_n) variables both may be mixed: quantitative and qualitative.

In the *structural equation modelling* (SEM) the dependent variables y_1, ..., y_n are only quantitative and the independent — mixed (quantitative and qualitative) —, but the relationship is:

$$\begin{aligned} y_1 &= f(x_{11}, x_{12}, ..., x_{1n}) \\ y_2 &= f(x_{21}, x_{22}, ..., x_{2n}) \\ &... \\ y_m &= f(x_{m1}, x_{m2}, ..., x_{mn}) \end{aligned}. \tag{3.3}$$

For easier comparison of these mentioned multivariate data analysis methods table 3.1 is given.

Table 3.1

Comparison of some MDA methods

MDA method	***Dependent variable(s)***	***Independent variables***	***Relationship type***
SEM	quantitative	quant.&qual.	$y_1 = f(x_{11}, x_{12}, ..., x_{1n})$ $y_2 = f(x_{21}, x_{22}, ..., x_{2n})$ ... $y_m = f(x_{m1}, x_{m2}, ..., x_{mn})$
Canonical correlation analysis	quant.&qual.	quant.&qual.	$y_1, y_2, ..., y_n = f(x_1, x_2, ..., x_n)$
Multivariate analysis of variance	quantitative	qualitative	
Regression analysis	quantitative	quant.&qual.	$y_1 = f(x_1, x_2, ..., x_n)$.
Analysis of variance	quantitative	qualitative	
Multiple discriminant analysis	qualitative	quantitative	
Conjoint analysis	quant.&qual.	qualitative	

The most suitable method is considered to be the *regression analysis* as the dependent variables are in a relation with independent variables from the same simulation/experiment set, and the chosen variables are quantitative. The regression analysis is used for the forecasting of the dependent variables as a response of the changes of independent variables [44].

In engineering sciences the regression analysis' models became popular only in the 60s–70s of last century. Earlier (and also nowadays) such models were used for social, philosophical and political issues to forecast how some human societies will act in a response to some changes or, e.g., in election forecasting [36, 38, 44, 156].

The regression analysis classification is given in Fig. 3.4. The regression models are also called the *metamodels* or *surrogate-models* [51, 78]. The difference between the linear and non-linear regression models is in the mathematical description: the non-linear regression models are expressed with a multiplication of independent variable(s) or factor(s) and the coefficient(s) as in *gravity model* [83, 115], the linear models are classically expressed as follows [38, 44, 156]:

$$y_i = \alpha_i + \beta_i(x_m) + \varepsilon_i, \tag{3.4}$$

where y_i — dependent variable for i-th combination of elementary functions;

α_i — i-th coefficient;

β_i — i-th coefficient for elementary functions of independent variables x_m;

m — number of independent variables;

ε_i — i-th error (with mean equal to zero).

The (3.4) is a simplified expression for one dependent variable in a multivariate regression model, also for one level in a multilevel regression model. For a multilevel regression model as an example the two-level regression model is given (3.5). In such a situation the first level is the dependent variable y_i, but the second level is configured by the coefficients $\alpha_{j[i]}$ and $\beta_{j[i]}$, which also are in a relation with independent variables x_m forming the elementary functions u_j and having the errors η_j [38]. The multilevel regression models are much more complicated than the multivariate ones because of their mathematical structure. Another common regression model is Bayesian [44, 105], but the multivariate regression model will be used in the formula synthesis.

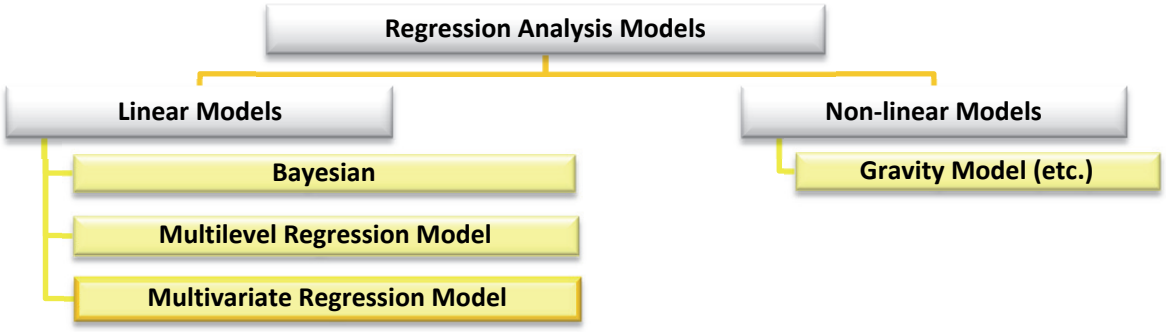

Fig. 3.4 Classification of regression analysis' models

$$\begin{aligned} y_i &= \alpha_{j[i]} + \beta_{j[i]}(x_m) + \varepsilon_i \\ \alpha_j &= a_0 + b_0 u_j + \eta_{j1} \\ \beta_j &= a_1 + b_1 u_j + \eta_{j2} \end{aligned} \tag{3.5}$$

3.1. Definition of objective function and control parameters

In the optimization the obtained models or synthesized formulas of objective function and the control parameters will be used. The objective function should include the main physical characteristic and some design or economical parameter for an unbiased judgement as in all optimization problems. Thus the maximum mechanical torque M_{max} is the physical characteristic. The optimization will be made by design parameters and magnets' material indirectly indicating the economical aspect — the less material is used and the smaller are the design parameters, the cheaper the coupler can be made with the characteristic of interest.

The maximum mechanical torque M_{max} can be the same for more CMCs with a different design parameters' combination, thus the maximum mechanical torque per volume unit M_{max}/V is chosen as a reliable characteristic.

The objective function is the function of maximum mechanical torque per volume unit M_{max}/V depending on PM material (expressed with its relative permeability μ_*), coupler axial length l, PM height h_{PM}, PM width per pole pitch (expressed with magnetic coverage coefficient β), coupler air gap δ and the number of PMs (expressed with pole pair number p) as given in (3.6).

$$M_{\max}/V = f(\mu_*; l; h_{PM}; \beta; \delta; p) \tag{3.6}$$

There are two types of control parameters taken into account: practical — outer half coupling yoke height h_y, the thinnest possible in manufacturing process — and the theoretical — maximum value of magnetic flux density B_{max} in the yokes that should not be exceeded to ensure optimal distribution of magnetic field.

The control parameter yoke height h_y of outer half coupling is taken already into account making the drawings for creation of mathematical models in software *QF*, i.e. a $h_y \geq 5$ mm. Thus it is also indirectly included in the formation of the value of maximum mechanical torque per volume M_{max}/V.

For the control parameters maximum values of magnetic flux density in yokes — $B_{in\,max}$ and $B_{out\,max}$ — the dependence of pole pair number p, PM height h_{PM}, coefficient of magnetic coverage β and the width of air gap δ is relevant, because the axial length l doesn't influence the saturation of magnetic field in the direction of cross section, and the values of flux density are in a wide range for simple ferrite and rare-earth alloy magnets, thus the formulas as function (3.7) are synthesized for every magnet material type — simple ferrite and rare-earth alloy — separately.

$$B_{\max} = f(h_{PM}; \beta; \delta; p) \tag{3.7}$$

These formulas will be used to forecast the values of maximum magnetic flux density in the yokes for the calculated optimal combination of design parameters. The optimal combination will be dismissed if the value of maximum flux density exceeds the 1.8 T, i.e., should be that $B_{max} \leq 1.8$ T.

3.2. Short description of program for formula synthesis

It is important to mention the Latvian scientist V. Eglājs who had worked on the development of multivariate regression models in 1970s and 80s and also introduced a rational system of experiment planning in such cases [170, 171, 190]. Thanks to his research another Latvian scientist O. Onževs later developed a programs-complex based on multivariate regression models described in detail in his dissertation [107]. This tool is used in the further formula synthesis, and the algorithm of formula synthesis is given in the block diagram (Fig. 3.5).

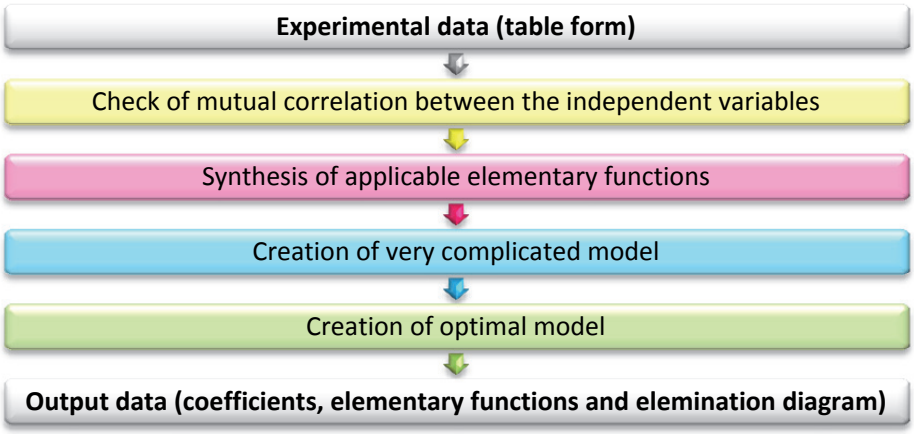

Fig. 3.5 Algorithm of formula synthesis

3.3. Choice of synthesized formulas

The formulas are synthesized for the objective function (M_{max}/V) and the control parameters ($B_{in\ max}$ and $B_{out\ max}$).

The first trials of formula synthesis [110] showed that the wide range of pole pair number p (from 1 till 9) used in one formula gives enough high relative error and thus analyzing all the calculated variants the pole pair numbers p are arranged in groups for both objective function and control parameters.

The choice is based on the elimination diagrams (appendix 6), given with the results of synthesized elementary functions in O. Onževs' program.

The measurement unite of M_{max}/V calculated by formula is the Newton meters per cube meter (Nm/m^3), but the PM height h_{PM} and air gap δ must be input in millimetres (mm), the pole pair number p and magnetic coverage coefficient β are non dimensional. The same is with the calculation of maximum magnetic flux density B_{max} in the yokes, just the flux density is in Tesla (T).

3.3.1. Objective function

As in the calculation of coupler volume V the axial length l is included and in the calculation of M_{max} the length l correlates directly, in result the axial length l is not taken in the formula synthesis for M_{max}/V, because it is already taken into account in M_{max} and V in a direct relation with them ($M_{max}(l)/V(l) \rightarrow M_{max}/V \neq f(l)$).

For the permanent magnets made of rare-earth alloys — NdFeB with $\mu_* = 1.061$ and SmCo with $\mu_* = 1.094$ — the according formulas are (3.8)–(3.10) and (3.11)–(3.13). For the rare-earth alloy magnets the pole pair number p is ranked in the following groups: p = 1–4, p = 5–6, p = 7–9. For the simple ferrite magnets — Ba-ferrite with $\mu_* = 1.114$ and Sr-ferrite with $\mu_* = 1.344$ — the according formulas are (3.14)–(3.16) and (3.17)–(3.19). For CMC with Ba-ferrite magnets the pole pairs are ranked as — p = 1–2, p = 3–5, p = 6–9 —, but with Sr-ferrite magnets — p = 1–2, p = 3–6, p = 7–9.

The formulas are chosen as follows: first, attention is paid to the breaking point, then, even if the breaking point is small and the first one in the elimination diagram, attention is paid to the value of correlation: about 95 % or 90 %.

For the CMC with $\mu_* = \mathbf{1.061}$ (PMs made of NdFeB) and pole pair $\boldsymbol{p = 1–4}$ the formula with correlation ρ = 95.28 % is:

$$\begin{aligned} M_{\max}/V = {} & -19.43 + +27.26p + 20.04\frac{p \cdot h_{PM}}{\delta} - 8.758\frac{\beta \cdot h_{PM}}{\delta} - 1.932\frac{p \cdot h_{PM}^2}{\delta^2} - \\ & - 0.067p^3 \cdot h_{PM} + 2.872p^2 \cdot \beta^2 - 2.958p \cdot h_{PM} \cdot \beta^2 + 0.338h_{PM}^2 \cdot \beta^2 - \\ & - 0.177p^4, \end{aligned} \tag{3.8}$$

if $\boldsymbol{p = 5–6}$, then (with ρ = 94.30 %):

$$\begin{aligned} M_{\max}/V = {} & -352.5 + 124.5\frac{h_{PM}}{\delta} + 27.7h_{PM} + 770.0\beta - 16.38\frac{h_{PM}^2}{\delta^2} - 16.07h_{PM} \cdot \beta - 408.6\beta^2 - \\ & - 3.17h_{PM}^2 - 6.44\frac{p \cdot h_{PM}}{\delta} + 14.04\frac{p \cdot h_{PM} \cdot \beta^2}{\delta} - 0.052p^3 \cdot h_{PM} + \\ & + 0.191\frac{h_{PM}^4}{\delta^4} - 59.32\frac{h_{PM} \cdot \beta^3}{\delta} + 0.036p \cdot h_{PM}^3, \end{aligned} \tag{3.9}$$

and for ***p* = 7–9** with ρ = 95.51 % the formula is:

$$M_{\max}/V = -61.52 + 125.6\frac{h_{PM}}{\delta} - 12.76p - 24.69h_{PM} + 439.9\beta - 24.66\frac{h_{PM}^2}{\delta^2} + \\ + 1.076h_{PM}^2 - 255.9\beta^2 + 2.067\frac{h_{PM}^3}{\delta^3}. \tag{3.10}$$

For the CMC with $\mu_* =$ **1.094** (SmCo magnets) the formulas are as follows:

- ***p* = 1–4**, ρ = 94.08 %

$$M_{\max}/V = -13.47 + 31.76p + 14.28\frac{p \cdot h_{PM}}{\delta} - 30.18\beta^2 - 1.519\frac{p \cdot h_{PM}^2}{\delta^2} - 2.207p \cdot h_{PM} \cdot \beta + \\ + 1.827h_{PM} \cdot \beta^2 - 1.442p^3 + 3.949\beta \cdot p^2, \tag{3.11}$$

- ***p* = 5–6**, ρ = 90.21 %

$$M_{\max}/V = -118.4 + 62.42\frac{h_{PM}}{\delta} - 37.55p + 642.7\beta - 5.987\frac{h_{PM}^2}{\delta^2} + \\ + 33.5\beta \cdot p - 9.26h_{PM} \cdot \beta - 459.0\beta^2, \tag{3.12}$$

- ***p* = 7–9**, ρ = 95.37 %

$$M_{\max}/V = -50.0 + 102.2\frac{h_{PM}}{\delta} - 10.46p - 20.17h_{PM} + 362.3\beta - 19.93\frac{h_{PM}^2}{\delta^2} + \\ + 0.880h_{PM}^2 - 212.1\beta^2 + 1.66\frac{h_{PM}^3}{\delta^3}. \tag{3.13}$$

For the coupler with $\mu_* =$ **1.114** (Ba-ferrite magnets) the formulas are:

- ***p* = 1–2**, ρ = 95.56 %

$$M_{\max}/V = -1.07 + 0.9172h_{PM} + 0.5577\frac{p \cdot h_{PM}}{\delta} + 0.9608p \cdot \beta - 0.035h_{PM}^2 - \\ - 0.482h_{PM} \cdot \beta - 0.052\frac{p \cdot h_{PM}^2}{\delta^2} + 0.06p \cdot h_{PM} \cdot \beta, \tag{3.14}$$

- ***p* = 3–5**, ρ = 93.59 %

$$M_{\max}/V = -14.53 + 3.0\frac{h_{PM}}{\delta} + 1.98p + 25.93\beta + 0.682h_{PM} - 0.795\frac{h_{PM}^2}{\delta^2} - \\ - 0.153h_{PM} \cdot p + 0.232\frac{p \cdot h_{PM}}{\delta} - 0.22p^2 - 0.29\beta \cdot h_{PM} - \\ - 14.51\beta^2 + 0.067\frac{h_{PM}^3}{\delta^3}, \tag{3.15}$$

- ***p* = 6–9**, ρ = 90.20 %

$$M_{\max}/V = -10.86 + 4.09\frac{h_{PM}}{\delta} - 0.646h_{PM} + 32.51\beta - 0.561\frac{h_{PM}^2}{\delta^2} + 0.0352h_{PM}^2 - \\ - 0.265\beta \cdot h_{PM} - 0.628p \cdot \beta - 15.38\beta^2 + 0.006\frac{h_{PM}^4}{\delta^4}. \quad (3.16)$$

For $\mu_* = 1.344$ (Sr-ferrite magnets) the formulas are chosen as follows:

- ***p* = 1–2**, ρ = 95.35 %

$$M_{\max}/V = 4.573 - 2.683p - 0.1962h_{PM} + 1.510\frac{p \cdot h_{PM}}{\delta} + 4.077p \cdot \beta - 5.671\beta^2 + \\ + 0.298h_{PM} \cdot p - 0.167\frac{p \cdot h_{PM}^2}{\delta^2}, \quad (3.17)$$

- ***p* = 3–6**, ρ = 90.05 %

$$M_{\max}/V = -26.78 + 5.102\frac{h_{PM}}{\delta} + 2.575p + 56.87\beta + 0.7385h_{PM} - 0.548\frac{h_{PM}^2}{\delta^2} - \\ - 0.254h_{PM} \cdot p + 0.351\frac{p \cdot h_{PM}}{\delta} - 0.349p^2 - 1.402\frac{\beta \cdot h_{PM}}{\delta} - \\ - 35.15\beta^2 + 0.995p \cdot \beta, \quad (3.18)$$

- ***p* = 7–9**, ρ = 95.93 %

$$M_{\max}/V = -7.193 + 10.15\frac{h_{PM}}{\delta} - 1.02p - 1.60h_{PM} + 39.53\beta - 1.972\frac{h_{PM}^2}{\delta^2} + \\ + 0.0833h_{PM}^2 - 0.439\beta \cdot h_{PM} - 22.52\beta^2 + 0.165\frac{h_{PM}^3}{\delta^3}. \quad (3.19)$$

This is a more complicated system — use of sub-distribution for function M_{max}/V —, but, as mentioned before, the merging of pole pair numbers p and magnets' relative permeability μ_* in one formula give the correlation for just about ρ = 45 %. When the magnets material was separated in rare-earth alloys and simple ferrites and all numbers of pole pairs were included in one formula, the correlation was about ρ = 60 %. To achieve better results (correlation ρ≥90 %) and in analyzing the obtained magnetic field calculations data the above given sub-distribution is chosen, on which the author insists instead of one formula $M_{max}/V = f(\mu_*, l, h_{PM}, \beta, \delta, p)$!

3.3.2. Control parameters

There are three control parameters, but, as the outer half coupling yoke height h_y is already taken into account in making of the drawings, the formulas are synthesized just for

two parameters: maximum magnetic flux density in inner and outer half couplings ($B_{max\ in}$, $B_{max\ out}$).

The analysis of all obtained data showed that for the CMC with the magnets made of simple ferrite the maximum flux densities in both half couplings do not exceed the value of one Tesla ($B_{max} \leq 1.3$ T). Here it can be concluded that in case of such CMC the saturation in steel doesn't have to be controlled/ monitored, so the formulas are not synthesized for couplers with simple ferrite PMs.

For the CMC with rare-earth PMs the curves are very different for $B_{max} = f(p)$. As the highest values of $B_{max\ in}$, $B_{max\ out}$ are at design parameters $h_{PM} = 8$ mm and $\delta = 2$ mm, then at these parameters (and with NdFeB magnets) as the example the flux density in outer half coupling $B_{max\ out} = f(\beta, p)$ is given (Fig. 3.6).

As can be seen in Fig. 3.6 the curve of maximum magnetic flux density in outer half coupling $B_{max\ out} = f(\beta, p)$ can be very different: almost linear ($p = 1$–3) and parabolic-style oriented upwards ($p = 4,6,8$) or downwards ($p = 5,7,9$). This sub-distribution is also used in formula synthesis.

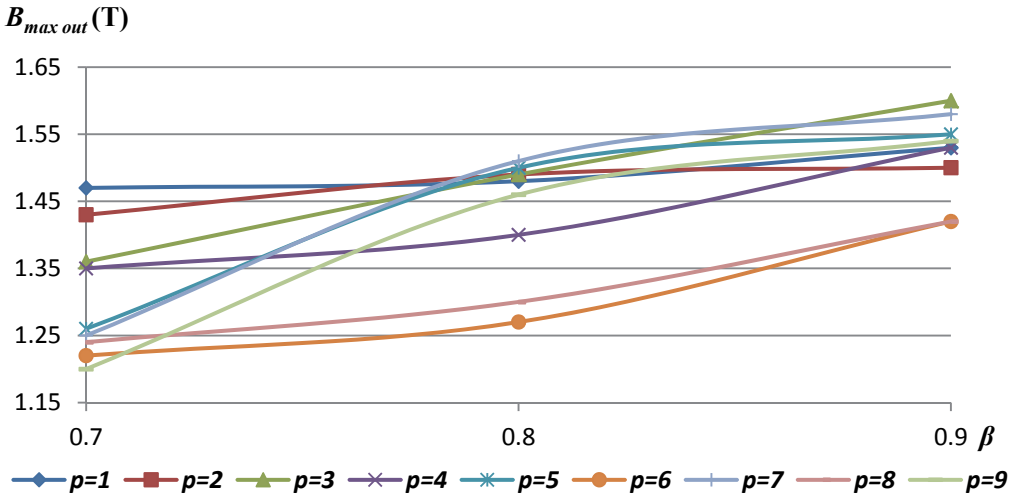

Fig. 3.6 Maximum magnetic flux density in outer half coupling $B_{max\ out} = f(\beta, p)$

The formulas are synthesized only for pole pair numbers $p = 1$–3, because for $p = 4$–9 the values of maximum magnetic flux density are as follows: $B_{max\ in} \leq 1.7$ T, $B_{max\ out} \leq 1.6$ T. The formulas are real for CMC with PMs made of NdFeB or SmCo. The formulas are chosen from the elimination diagrams (appendix 7) and the correlation of maximum flux density in inner half coupling ρ_{Bin} and in outer half coupling ρ_{Bout} is taken into account, and the formulas are:

- $\boldsymbol{p = 1}$, $\rho_{Bin} = 98.73$ % and $\rho_{Bout} = 99.96$ %

$$B_{\max in} = 2.881 - 3.182\beta + 0.0851 h_{PM} + 0.0326 \frac{h_{PM}^2}{\delta^2} + 3.116\beta^4 - 0.0002 \frac{h_{PM}^5}{\delta^5}, \quad (3.20)$$

$$B_{\max out} = 1.712 - 0.436\beta^2 - 0.1363 h_{PM} + 0.1736 \frac{h_{PM}}{\delta} + 0.01 h_{PM}^2 - 0.0068 \frac{h_{PM}^3}{\delta^3} + \\ + 0.4723\beta^5 + 0.0001 \frac{h_{PM}^5}{\delta^5}, \quad (3.21)$$

- ***p* = 2–3**, ρ_{Bin} = 80.40 % and ρ_{Bout} = 89.91 %

$$B_{\max in} = 2.532 + 0.0913 p - 5.11\beta + 0.125 h_{PM} - 0.033 h_{PM} \cdot p + 0.036 \frac{h_{PM}}{\delta} + 4.121\beta^2, \quad (3.22)$$

$$B_{\max out} = 1.387 + 1.12\beta - 0.70 p + 0.8495 p \cdot \beta + 0.0056 p \cdot h_{PM} + 0.0086 \frac{h_{PM}^2}{\delta^2} + \\ + 0.0005 h_{PM}^2 - 1.543\beta^2 + 0.0447 \frac{p \cdot h_{PM}}{\delta} - 0.0061 \frac{h_{PM}^2 \cdot p}{\delta}. \quad (3.23)$$

3.3.3. Formula testing

The chosen regression models/synthesized formulas are tested with some variants of variables (table 3.2). All four PM materials (μ_* = 1.061, 1.094, 1.114, 1.344) are chosen, just one value of air gap (δ = 2.4 mm) as the range is δ = 2–3 mm, two middle values (accordingly to the base values used in formula synthesis) for PM height (h_{PM} = 5, 7 mm) and magnetic coverage coefficient (β = 0.75, 0.83). To prove the previously given information about axial length *l* (that it is not in the formula, but anyway taken into account), its values are chosen randomly for each testing variant. For these variants the regression models are compared with data obtained in magnetic field modelling (table 3.3).

Table 3.2

Tested variants

No.	μ_*	h_{PM} **(mm)**	δ **(mm)**	***p***	β	***l*** **(mm)**
1.	1.061	5	2.4	3	0.75	20
2.	1.094	5	2.4	3	0.83	22
3.	1.114	5	2.4	7	0.75	25
4.	1.344	5	2.4	7	0.83	28
5.	1.061	7	2.4	3	0.75	24
6.	1.094	7	2.4	3	0.83	26
7.	1.114	7	2.4	7	0.75	30
8.	1.344	7	2.4	7	0.83	32
9.	1.061	5	2.4	3	0.75	13
10.	1.094	5	2.4	3	0.83	15
11.	1.114	5	2.4	7	0.75	18

12.	1.344	5	2.4	7	0.83	21
13.	1.061	7	2.4	3	0.75	45
14.	1.094	7	2.4	3	0.83	47
15.	1.114	7	2.4	7	0.75	47
16.	1.344	7	2.4	7	0.83	49

Table 3.3

Comparison of regression models with data from magnetic field modelling

No.	*Data (magn. field model.)*			*Regression models*			*Relative error (%)*		
	M_{max}/V (Nm/m^3)	$B_{max\ in}$ (T)	$B_{max\ out}$ (T)	M_{max}/V (Nm/m^3)	$B_{max\ in}$ (T)	$B_{max\ out}$ (T)	M_{max}/V	$B_{max\ in}$	$B_{max\ out}$
1.	123.28	1.6	1.43	119.71	1.496	1.393	2.90	6.47	2.59
2.	101.89	1.6	1.40	99.87	1.609	1.491	1.98	0.53	6.53
3.	4.449	0.37	0.31	4.430	–	–	0.43	–	–
4.	9.325	0.66	0.56	9.302	–	–	0.24	–	–
5.	131.46	1.56	1.38	131.15	1.578	1.403	0.24	1.18	1.68
6.	108.17	1.68	1.47	108.11	1.691	1.502	0.05	0.63	2.15
7.	4.992	0.38	0.31	4.977	–	–	0.31	–	–
8.	10.367	0.67	0.60	10.216	–	–	1.45	–	–
9.	123.28	1.59	1.43	119.71	1.496	1.393	2.89	5.88	2.59
10.	101.89	1.59	1.41	99.87	1.609	1.491	1.99	1.17	5.78
11.	4.448	0.37	0.31	4.430	–	–	0.43	–	–
12.	9.325	0.68	0.56	9.302	–	–	0.24	–	–
13.	131.46	1.58	1.44	131.15	1.578	1.403	0.24	0.10	2.55
14.	108.17	1.66	1.48	108.11	1.691	1.502	0.05	1.84	1.46
15.	4.992	0.38	0.31	4.977	–	–	0.31	–	–
16.	10.366	0.68	0.62	10.216	–	–	1.45	–	–

The CMC design in cross section is different for variants from 1 till 8, and then in the same order these variants are repeated. That has been intentionally done to prove that even not including the axial length l in the synthesised formulas it is taken into account — for longer l the torque M_{max} is higher, but also the volume V increases, thus the ratio M_{max}/V stays identical, and the values of M_{max}/V by formulas is calculated correctly.

The testing results show that the use of regression models gives high precision — not more than 5 % — for the model of M_{max}/V. For control parameters the precision is lower, but also acceptable: less than 10 %.

3.4. Conclusions

Analyzing the available multivariate data analysis techniques or methods the regression method/analysis models is considered to be the most suitable for the obtained data from the magnetic field modelling to acquire the mathematical model (in a formula form) for the cylindrical magnetic couplers (CMCs).

A ready programs-complex is used (developed by *Dr. sc. eng.* O. Onževs) for the formula synthesis and the program is based on multivariate regression model, chosen from the many regression analysis models and this choice is grounded in his dissertation.

For the optimization problem the objective function is defined

The analysis of results obtained from CMC magnetic field modelling showed that the formulas of control parameters as maximum magnetic flux density B_{max} must be synthesized only for the case, when PMs are made of rare-earth alloys as NdFeB and SmCo, because for couplers with simple ferrite PMs the values of B_{max} do not exceed 1.3 T and $B_{max} \leq 1.8$ T.

Even for couplers with rare-earth alloy PMs the formulas of B_{max} are not synthesized for all pole pair numbers p because by such dependence the nature of the magnetic flux density is not uniform and a synthesized formula gave small correlation. The next step was the grouping of pole pair number p, excluding the $p = 4–9$, because also in such cases the value of maximum flux density does not have to be controlled — not exceeding the 1.7 T. Thus te formulas are synthesized for maximum magnetic flux density in inner half coupling $B_{max\ in}$ and in outer half coupling $B_{max\ out}$ in range $p = 1–3$.

Similar situation was with the main characteristic M_{max}/V. Combining all PM materials and pole pair number gave a critically small correlation ρ (with the data obtained in magnetic field modelling) — $\rho < 40$ %, thus the formulas were synthesized for every material and from analysis groups of pole pair numbers chosen separately, increasing the correlation $\rho > 90$ %.

The synthesized formulas were tested, and the results showed that the separation of PM materials and pole pair numbers have been appropriate and the relative errors for the main characteristic M_{max}/V is $\varepsilon_{M/V} < 5$ % and for the control parameters B_{max} is $\varepsilon_B < 10$ %, acquiring valid mathematical (in formula form) models.

4. OPTIMIZATION OF CMC

By the *mathematical optimization* usually is understood [146]:

a) the formulation and

b) the solution of a constrained optimization problem described in general mathematical form (4.1).

$$\min_{\text{w.r.t.x}} f(\text{x}), \text{with constraints} \begin{cases} g_j(\text{x}) \le 0, \;\; j = 1,2,...,m \\ h_j(\text{x}) = 0, \;\; j = 1,2,...,r, \end{cases} \tag{4.1}$$

where min — minimize;

w.r.t. — with respect to;

$f(\text{x})$, $g_j(\text{x})$, $h_j(\text{x})$ — scalar functions of column vector $\text{x} = [x_1, x_2, ..., x_n]^T \in \text{R}^n$;

x_i — (design/independent) variables;

$f(\text{x})$ — objective function (dependent variable);

$g_j(\text{x})$ — inequality constraint functions;

$h_j(\text{x})$ — equality constraint functions.

The formulation a) would be: the optimum vector x denoted by x^* with corresponding optimum function value $f(\text{x}^*)$ solves problem (4.1). In case of no specified constraints the problem is called *unconstrained minimization* [30, 101, 116, 146, 161, 164]. In CMC optimization there are two constraints (inequality functions) — $B_{max\ in} \le 1.8$ and $B_{max\ out} \le 1.8$ —, and the problem is a constrained optimization.

In (4.1) the problem is defined as minimization task, but for CMC the aim is to obtain such combination of the variables where the value of M_{max}/V is the highest. The maximization task in standard form is:

$$\min_{\text{x}} F(\text{x}), \tag{4.2}$$

where $F(\text{x}) = -f(\text{x})$ mathematically is (4.3).

$$\max_{\text{x}} f(\text{x}) = -\min_{\text{x}} [-f(\text{x})] \tag{4.3}$$

So the optimum x^* in minimization problem gives the optimum of original maximization problem by $-\text{F}(\text{x}^*)$.

The *mathematical optimization* is also called *nonlinear programming*, *mathematical programming* or *numerical optimization* [30, 101, 116, 146, 161, 164]. Sometimes the term *mathematical optimization* is used for describing the science of determining the best solutions of mathematically defined problems (as models of physical reality or manufacturing processes or systems).

At the beginning of 1940s the *optimization* was called a *mathematical programming*. The term *programming* was defined with the connotation — intended meaning: the problem formulation and the algorithm design and analysis [101]. Afterwards the word programming became linked with computer software.

Though people of all times have tried to optimize everything they can, the optimization as a science section was developed just somewhat more than 70 years [101].

The classification of optimization problems is given in Fig. 4.1 [30, 101, 116, 146, 161, 164, 169].

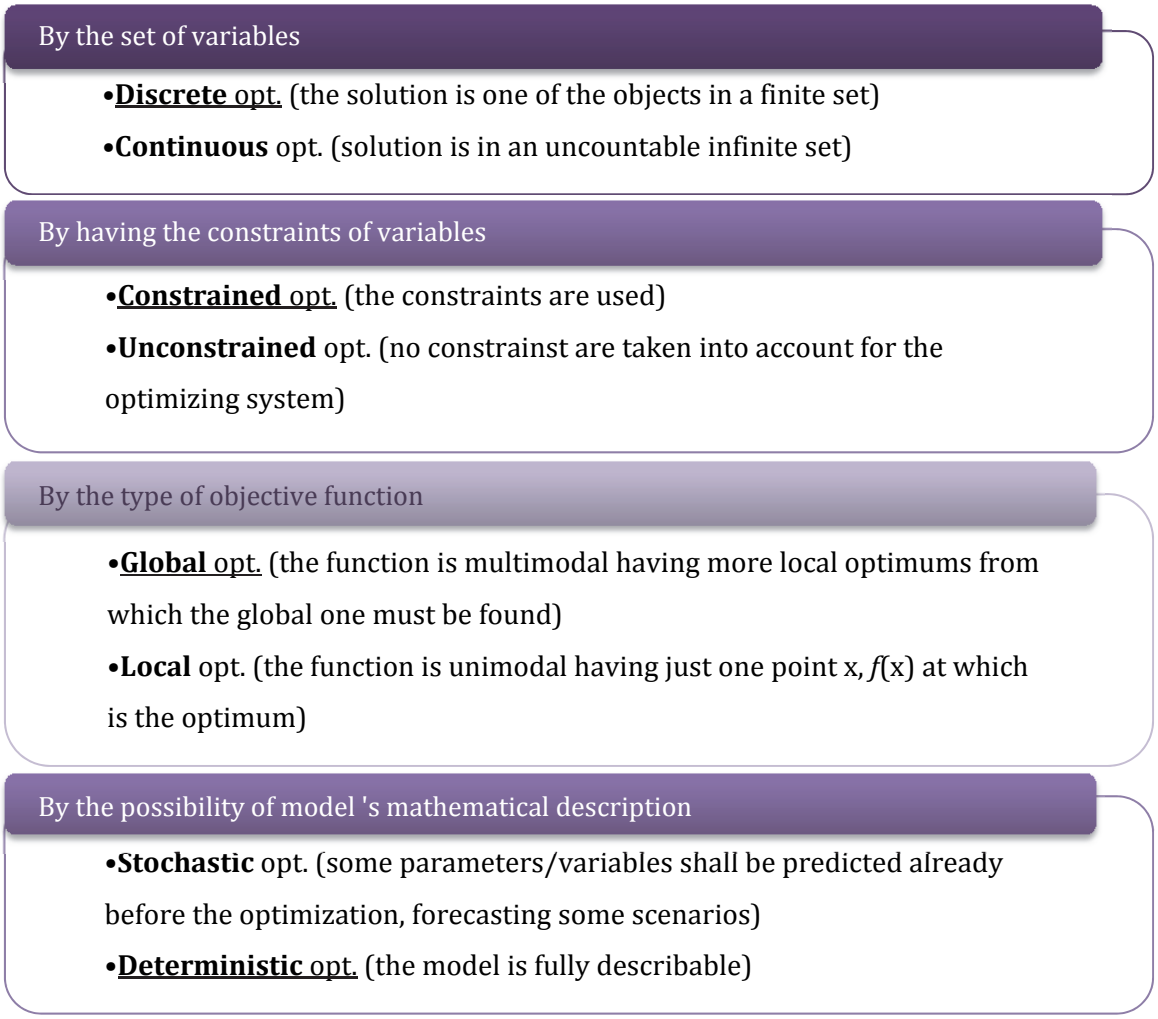

Fig. 4.1 Classification of optimization problems

According to the classification (Fig. 4.1) the stated CMC optimization is deterministic, discrete and constrained.

At the choosing of most suitable optimization method such parameters (which often conflict) are considered [101, 146]:

1) robustness — the method should perform well enough in a wide range of variables in the chosen model class;
2) efficiency — should perform in reasonably short period of time or with small computer storage;
3) accuracy — the solution should be identified with chosen precision, without being overly sensitive to the data errors or to the arithmetic rounding errors that occur in the algorithm implementation on a computer.

Further the most often in electrical engineering used optimization methods are given and afterwards the information of the newest optimization methods is given.

4.1. Most commonly used optimization methods in electrical engineering

As the CMC is a subtype of electrical machines the optimization methods used in electrical engineering shall be used. Before the choosing of optimization method some of them must be analyzed, thus in the subchapters the most often used (and for more than one dimension/variable) are given [101, 169]. For one-dimensional optimization tasks such methods as *function parabolic approximation*, *golden section method*, *Powell's quadratic interpolation* etc. can be used [146, 169].

4.1.1. Gradient method

The gradient method is one of the *iteration methods* using *derivatives*. The name of the method comes from the basic principle: the optimum is found at the point were the *gradient vector* $g(x)$ is close to zero or to the desired precision ε, because the vector shows the way were the function has the most rapid changes (the growth or reduction), and when there are no changes, the optimum is found [164, 170]. The gradient vector is the vector of function $f(x)$ first order derivatives (partial derivatives) at the point x [164]:

$$g(\mathrm{x}) = \nabla f(\mathrm{x}) = \begin{bmatrix} \frac{\partial f}{\partial x_1}(\mathrm{x}) \\ \frac{\partial f}{\partial x_2}(\mathrm{x}) \\ \vdots \\ \frac{\partial f}{\partial x_n}(\mathrm{x}) \end{bmatrix}. \tag{4.4}$$

The optimization algorithm for the gradient method is given in Fig. 4.2 [146, 169],

where i — the number of iteration;

s_0 — first value of the step s (!for every variable of x);

s — a constant step value at every i-th iteration (for every variable of x);

ε — chosen precision;

x_{min}, x_{max} — the minimal and the maximum values or boundary values of each variable from x;

x_{opt} — the vertor x (of variables x_1, x_2, ..., x_n) at the optimum point.

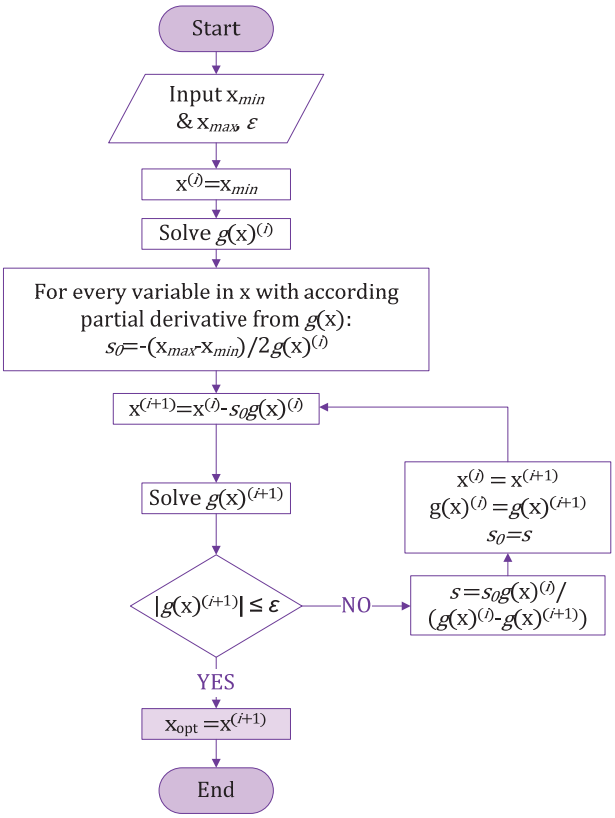

Fig. 4.2 Algorithm of gradient method

The calculation of the first step s_0 is started from the middle point of the given interval for each variable from x to ensure the reliability: when the step s is taken too small, the optimum point is reached very slowly, when too big — there is a high risk of exceeding the optimal value of $f(x)$, even jumping out of the search interval [168, 169].

With a choice of appropriate step s the gradient method is considered to be a good method reviewing the convergence of iterations, which is important in iteration methods. This method is popular because ensuring the quick convergence the optimum can be found in comparing small number of iterations.

This method is applicable if the optimizing system is given as a function, otherwise the first order derivatives cannot be obtained and thus the method cannot be applied.

Another disadvantage is that the solution may be just the local optimum instead of a global one. To avoid this situation it is necessary to know or to predict enough of a small region (minimal and maximum values of variable) were the global optimum point should be.

4.1.2. Interval exclusion method

To use the interval exclusion method the boundaries (of variables in which the optimization is planned) must be set and the optimizing system must be known in equation(s) form. The principle is based on the size of variable interval length L that is compared with the chosen precision ε and, when the precision is not satisfied, in every next iteration i the interval length L is reduced excluding the rest of the interval (therefore the name). When every next interval length L is reduced by a half the *interval exclusion method* is called *bisection method* (bisects the interval) [101, 169].

The optimization (minimization) algorithm of *bisection method* is given in Fig. 4.3.

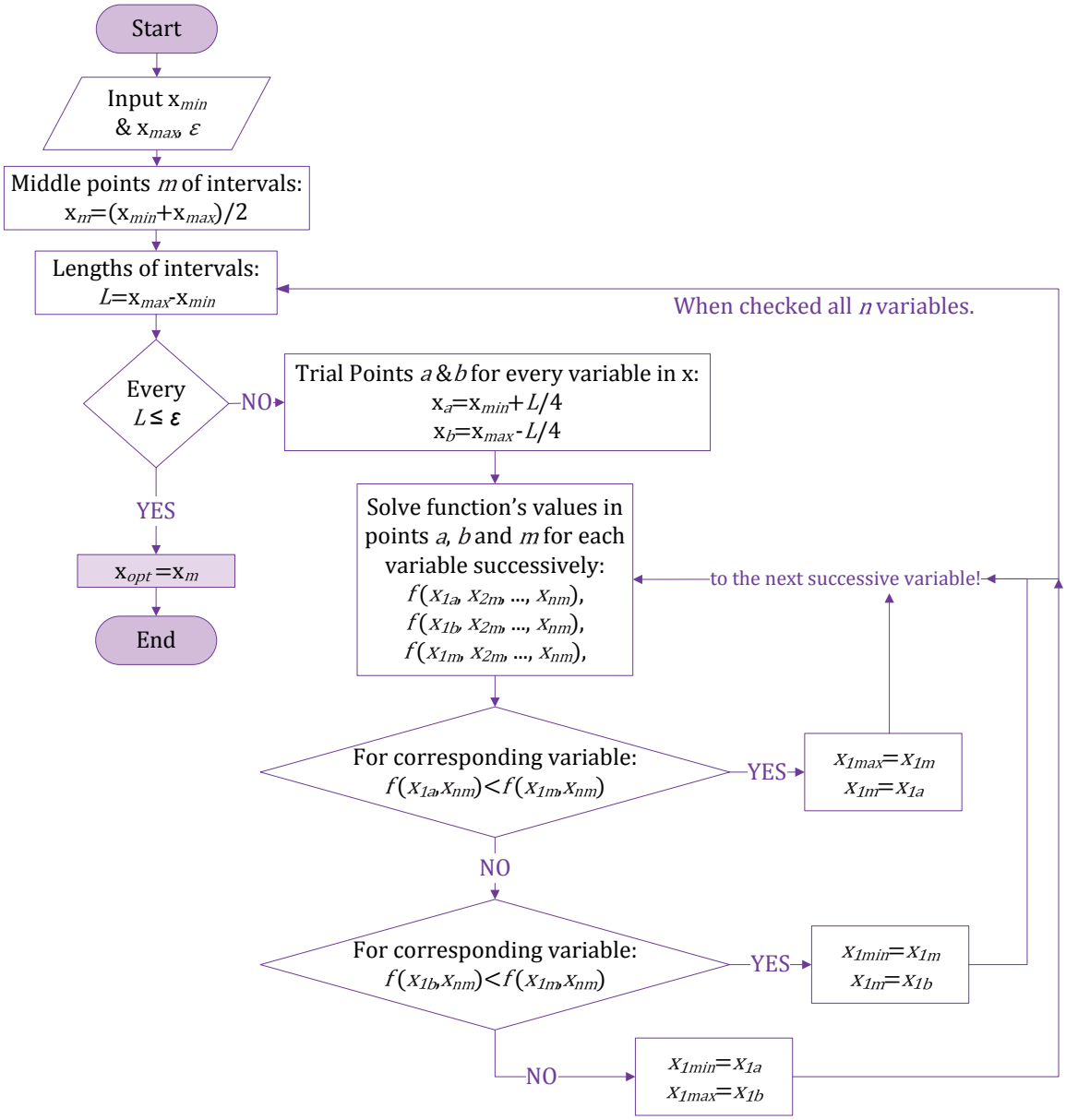

Fig. 4.3 Algorithm of bisection method

This method can be used when the dependent and independent variables are given as functions instead of table form. The method is quick if the number of independent variables is less than five ($n \leq 4$).

An advantage also is no necessity to use the derivatives. The method will also be fast when setting high precisions/tolerances ε [146, 169].

4.1.3. Newton's method

The *Newton's method* (sometimes also called *Newton-Raphson method*) is used in unconstrained minimization problems and these necessary and sufficient conditions must be complied:

1) First order condition — functions partial derivatives ∇f at the optimum point x_{opt}

$$\nabla f\left(\mathrm{x}_{opt}\right)=\begin{bmatrix}\frac{\partial f}{\partial x_1}\left(\mathrm{x}_{opt}\right)\\ \frac{\partial f}{\partial x_2}\left(\mathrm{x}_{opt}\right)\\ \vdots\\ \frac{\partial f}{\partial x_n}\left(\mathrm{x}_{opt}\right)\end{bmatrix}=0, \tag{4.5}$$

2) Second order condition or Hessian matrix at the optimum point $H(\mathrm{x}_{opt})$

$$H\left(\mathrm{x}_{opt}\right)=\begin{bmatrix}\frac{\partial^2 f}{\partial x_1^2}\left(\mathrm{x}_{opt}\right) & \frac{\partial^2 f}{\partial x_1 \partial x_2}\left(\mathrm{x}_{opt}\right) & \cdots & \frac{\partial^2 f}{\partial x_1 \partial x_n}\left(\mathrm{x}_{opt}\right)\\ \frac{\partial^2 f}{\partial x_2 \partial x_1}\left(\mathrm{x}_{opt}\right) & \frac{\partial^2 f}{\partial x_2^2}\left(\mathrm{x}_{opt}\right) & \cdots & \frac{\partial^2 f}{\partial x_2 \partial x_n}\left(\mathrm{x}_{opt}\right)\\ \vdots & \vdots & \ddots & \vdots\\ \frac{\partial^2 f}{\partial x_n \partial x_1}\left(\mathrm{x}_{opt}\right) & \frac{\partial^2 f}{\partial x_n \partial x_2}\left(\mathrm{x}_{opt}\right) & \cdots & \frac{\partial^2 f}{\partial x_n^2}\left(\mathrm{x}_{opt}\right)\end{bmatrix}>0. \tag{4.6}$$

The algorithm for classical *Newton's method* is given in Fig. 4.4.

The advantage of this method is the quadratic convergence near the solution. At the same time the method applied in one-dimensional optimization task may not be convergent at all and in multi-dimensional optimization task the situation with convergence is even more complicated [146].

The necessity to calculate the Hessian matrices in each iteration is also considered as a disadvantage because the computation of the Hessian matrix represents the major task in the optimization program. Therefore the classical Newton's method is not recommended in practice [146].

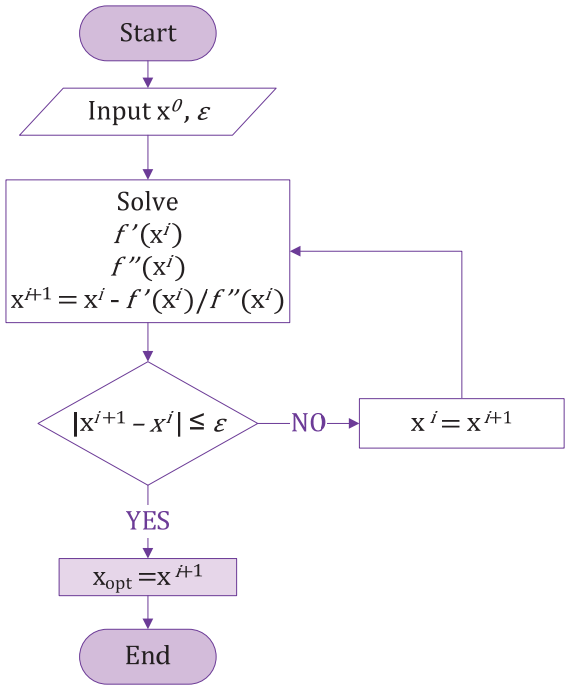

Fig. 4.4 Principal algorithm of Newton's method

4.1.4. Lagrangian method

Used in equality constrained minimization problems! The method is named after its introducer — Lagrange — in 1760 transforming the classical optimization task (4.1) into the *Lagrangian function* (4.7) using the, so-called, *Lagrangian multipliers* λ_j ($j = 1, 2, ..., r$ and $r<n$) and such that the necessary conditions (4.8) are ensured [101, 146].

$$L(\mathrm{x},\lambda) = f(\mathrm{x}) + \sum_{j=1}^{r} \lambda_j h_j(\mathrm{x}) \text{ or } L(\mathrm{x},\lambda) = f(\mathrm{x}) + \lambda^T \mathrm{h}(\mathrm{x}), \tag{4.7}$$

where $L(\mathrm{x}, \lambda)$ — Lagrangian function;

$f(\mathrm{x})$ — objective function;

x — column vector of variables: $\mathrm{x} = [x_1, x_2, ..., x_n]^T$;

λ_j — j-th Lagrangian multiplier in column vector λ^T;

$h_j(\mathrm{x})$ — j-th equality constraint function in vector of equality constraint functions $\mathrm{h}(\mathrm{x})$.

$$\begin{aligned} &\frac{\partial L}{\partial x_i}\left(\mathrm{x}_{opt}, \lambda_{opt}\right) = 0 \qquad i = 1,2,...,n \\ &\frac{\partial L}{\partial \lambda_j}\left(\mathrm{x}_{opt}, \lambda_{opt}\right) = 0 \qquad j = 1,2,...,r \end{aligned}, \tag{4.8}$$

where x_{opt} — candidate point for optimal values x_i;

λ_{opt} — stationary point with values λ_j accordingly to candidate point.

The principal algorithm for *Lagrangian method* is given in Fig. 4.5.

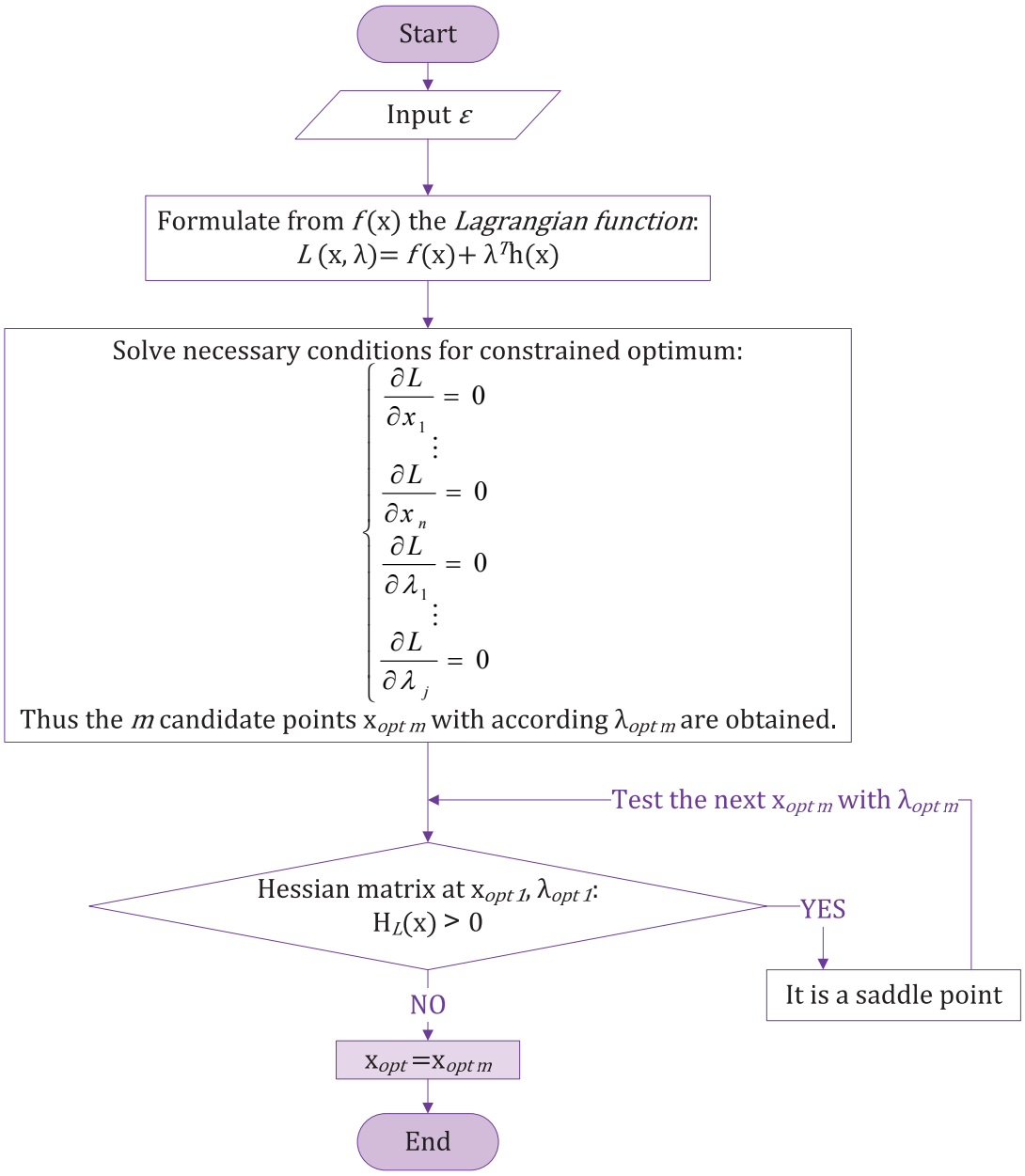

Fig. 4.5 Principal algorithm of Lagrangian method

The *Lagrangian method* for simple optimization tasks can give the result in the very first step(s), also, the candidate points of optimum in more complex optimization tasks can be quickly found, but it is important to note that before any tests of convergence the candidate points must be tested, because often they are so called *saddle points* [101, 146]. In a constrained minimization task the *Hessian matrix of the Lagrangian functions* is positive definite at the saddle point, i.e. $H_L(x) > 0$ [146].

Another disadvantage of the Lagrangian method is the necessity to calculate the $n + r$ equations, slowing the computational speed, as well as appropriate method of such equation solving must be chosen.

4.2. Other popular optimization methods

Since the 1980s the so called *multiplier methods* became more popular, were the classical Lagrangian method is combined with others. The first were the *zero order* methods, which used the functions directly with any order derivatives, though it is simpler for students to understand these methods in program environment, they are much slower and computationally much more expensive [146].

The latest and popular methods are as follows: the combined Lagrangian method with some other one and the modified Newton's methods such as the DFP method.

For the author less known methods are given in the subchapters.

4.2.1. Powell's quadratic interpolation

This method is an *interpolation method*, which successively fits the quadratic interpolation curves to function data with a sequent approximation to the minimum point x_{opt}. The *Powell's method* is a conjugate-gradient method that does not require derivatives [26, 121–123, 146].

Usually applied for one-dimensional optimization tasks with given i data points, from which one initial point x_0 is taken, though in the algorithm with it two more points are substituted using defined step h [118, 121, 146].

The quadratic polynomial with its coefficients a_i is as follows:

$$\begin{gathered} p_2(x) = a_0 + a_1(x - x_0) + a_2(x - x_0)(x - x_1) \\ a_0 = f(x_0), \qquad a_1 = f[x_0, x_1], \qquad a_2 = f[x_0, x_1, x_2], \end{gathered} \tag{4.9}$$

where $p_2(x)$ — quadratic polynomial;

a_i — polynomial coefficients (i = 0, 1, 2);

x — one-dimensional parameter/variable;

x_i — known values/points;

$f[x_0, ..., x_i]$ — first (i = 1) and second (i = 2) order divided differences (4.10).

$$\begin{aligned} f[x_0] &= f(x_0) \\ f[x_0, x_1] &= \frac{f(x_1) - f(x_0)}{x_1 - x_0} \\ f[x_1, x_2] &= \frac{f(x_2) - f(x_1)}{x_2 - x_1} \\ f[x_0, x_1, x_2] &= \frac{f[x_1, x_2] - f[x_0, x_1]}{x_2 - x_0}, \end{aligned} \tag{4.10}$$

where $f(x_i)$ — the function value at x_i point.

In the optimization process so called *turning point* x_m is used, and it occurs when slope is zero (4.11).

$$\frac{\partial p_2(x)}{\partial x} = 0$$
$$a_1 + 2a_2 x - a_2 x_1 - a_2 x_0 = 0 \tag{4.11}$$
$$x_m = x = \frac{a_2(x_0 + x_1) - a_1}{2a_2}$$

All mentioned parameters are used and must be calculated in the necessary steps in the algorithm of *Powell's* method (Fig. 4.6).

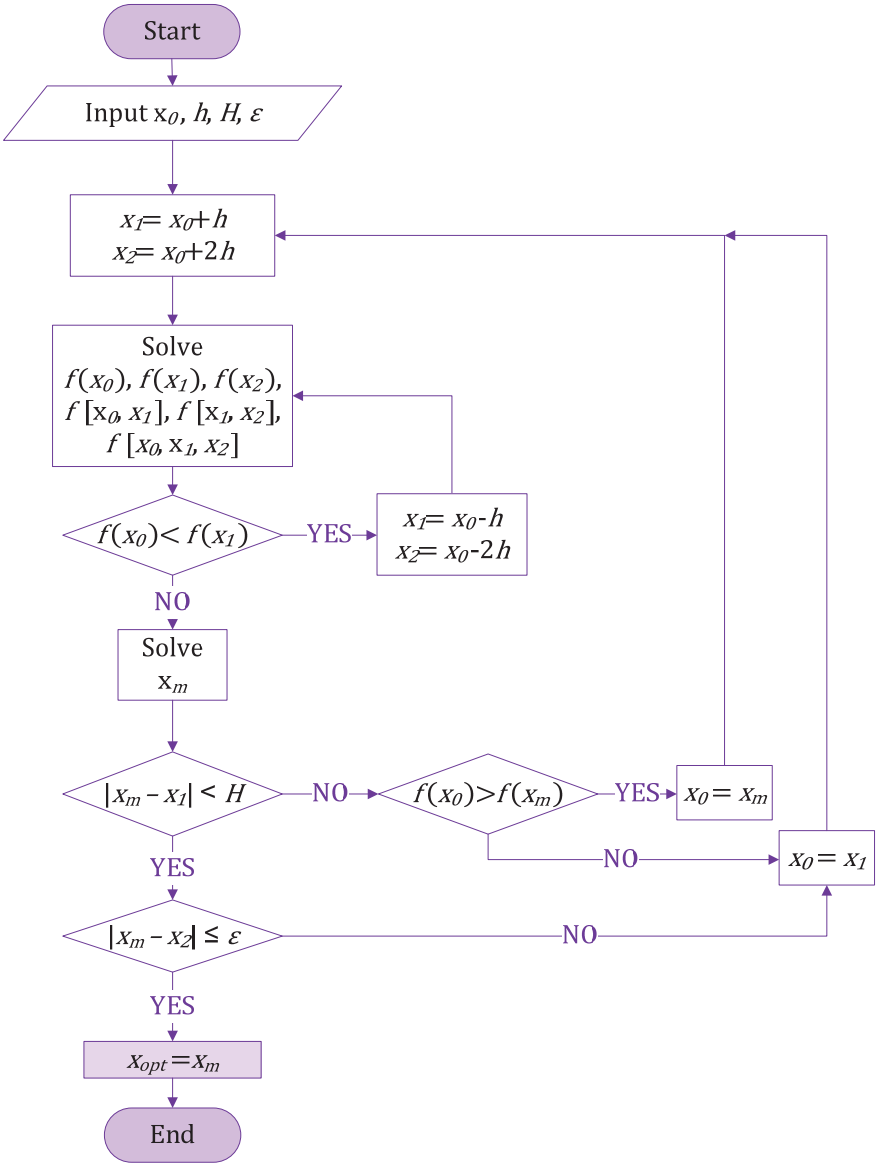

Fig. 4.6 Algorithm of Powell's quadratic interpolation method

The *Powell's quadratic interpolation* method and the *Davidon cubic interpolation* method are considered to be the most efficient and accurate methods for one-dimensional (one

variable) functions [101, 118, 146]. For multi-dimensional optimization tasks, the modified quadratic interpolation methods can be used [26, 43, 101, 118, 142].

4.2.2. Davidon-Fletcher-Powell (DFP) method

This is a *Newton's modified* method belonging to *iteration methods* that use *derivatives*. It is named after its authors — Davidon, Fletcher and Powell —, though often is used its abbreviation DFP [146].

Usually the *search direction* or the *normalized steepest descent direction* u was equal to *Newton step* Δ, i.e., $\mathrm{u}^i = \Delta$ (4.12) [169, 173, 174].

$$\mathrm{u}^i = \Delta = -\mathrm{H}^{-1}\left(\mathrm{x}^{i-1}\right)\nabla f\left(\mathrm{x}^{i-1}\right), \tag{4.12}$$

where for the *i*-th direction u^i is taken the values of x in (*i*-1)-th iteration;

H — the Hessian matrix at x^{i-1};

$\nabla f(\mathrm{x}^{i-1})$ - gradient vector at x^{i-1}.

The Hessian matrix H must be calculated at each *i*-th iteration, but in this DFP method the use of approximation G_0 to H^{-1} for the first iteration ($i = 1$) is introduced, and the approximation G is updated after calculation of each search direction (4.13) [146]. There are also used an (auxiliary) substitution variable λ, and coefficients A_i (4.14) and B_i (4.15) calculated through auxiliary parameters v^i (4.16) and y^i (4.17).

$$\mathrm{u}^i = -\mathrm{G}_{i\text{-}1}\nabla f\left(\mathrm{x}^{i-1}\right), \tag{4.13}$$

$$\mathrm{A}_i = \frac{\mathrm{v}^i\mathrm{v}^{iT}}{\mathrm{v}^{iT}\mathrm{y}^i} \tag{4.14}$$

$$\mathrm{B}_i = \frac{-\mathrm{G}_{i-1}\mathrm{y}^i\left(\mathrm{G}_{i\text{-}1}\mathrm{y}^i\right)^T}{\mathrm{y}^{iT}\mathrm{G}_{i\text{-}1}\mathrm{y}^i} \tag{4.15}$$

$$\mathrm{v}^i = \lambda_i\mathrm{u}^i \tag{4.16}$$

$$\mathrm{y}^i = \nabla f\left(\mathrm{x}^i\right) - \nabla f\left(\mathrm{x}^{i-1}\right) \tag{4.17}$$

The algorithm of this method is given in Fig. 4.7.

The *DFP method* does not require the evolution of Hessian matrix H or the explicit solution of a system, thus is succeed the quickness of this method [101, 146].

Mathematically important is that the G_i would be positive-definite, and with a theorem (given and proved in [146]): if G_{i-1} is positive-definite and the G_i is obtained from G_{i-1} then also G_i is positive-definite.

The *DFP method* is considered to be a computationally quick and simple method with a good convergence to the set precision ε.

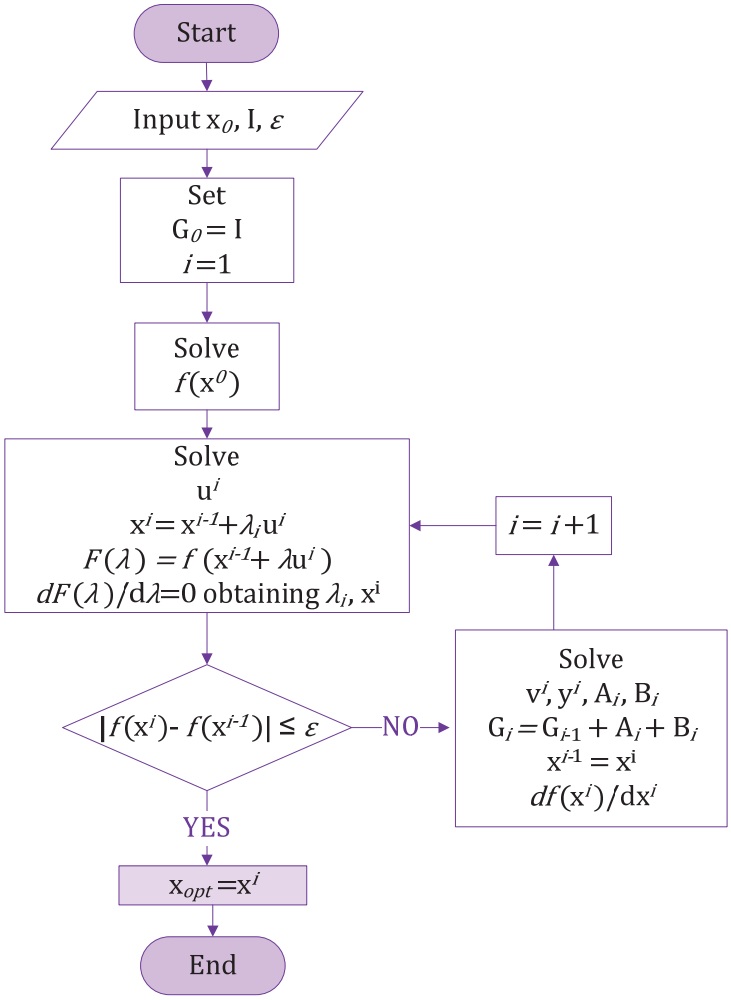

Fig. 4.7 Algorithm of Powell's quadratic interpolation method

4.2.3. Fletcher-Reeves directions

Usually for quadratic functions, but used also for other function types. It is an *iteration method* using derivatives. Here the so called *directions* $u_i (i = 1,2, ..., n)$ are used. For the initial point x_0 the directions is $u^1 = -\nabla f(x^0)$, but for i-th iteration till $i = n - 1$:

$$u^{i+1} = -\nabla f(x^i) + \beta_i u^i, \tag{4.18}$$

where x^i is calculated by (4.19) and the *optimal descent step* β_i by (4.20) with corresponding i-th substitution variable λ_i, and when $\lambda_i \ge 0$ line search is ensured.

$$x^i = x^{i-1} + \lambda_i u^i \tag{4.19}$$

$$\beta_i = \frac{\left\|\nabla f\left(\mathrm{x}^i\right)\right\|^2}{\left\|\nabla f\left(\mathrm{x}^{i-1}\right)\right\|^2} \tag{4.20}$$

So in general the algorithm is as given in Fig. 4.8:

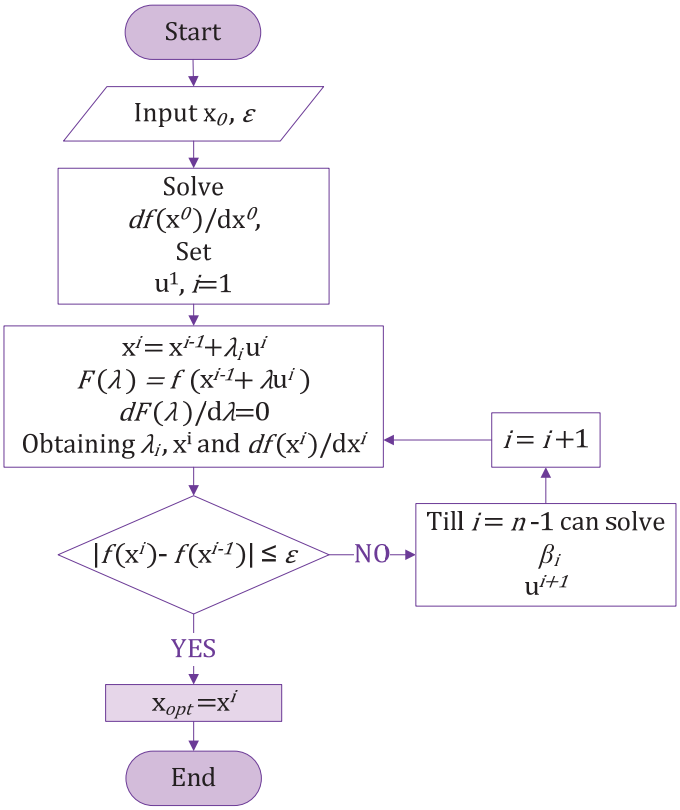

Fig. 4.8 Algorithm of Fletcher-Reeves directions

4.2.4. Multiplier method for inequality constraints

This is a *multiplier method*, so are called the methods there the *Lagrangian method* is combined with the use of *penalty function*, thus the disadvantage of Lagrangian method for its difficult determination analytically is avoided.

The *augmented Lagrangian function* L is introduced and defined as in (4.21).

$$L\left(\mathrm{x},\lambda,\rho\right) = f(\mathrm{x}) + \rho \sum_{j=1}^{m} \left\langle \frac{\lambda_j}{2\rho} + g_j(\mathrm{x}) \right\rangle^2, \tag{4.21}$$

where $f(\mathrm{x})$ — optimization (minimization) function;

$g_j(\mathrm{x})$ — inequality constraints ($g_j(\mathrm{x}) \le 0, j = 1, 2, ..., m$);

λ_j — j-th Lagrangian multiplier;

ρ_j — j-th penalty parameter.

In the optimization process the stationary point x^* is found in each i-th iteration ($i = 1, 2, ..., n$):

$$\frac{\partial L}{\partial x_i} = \frac{\partial f}{\partial x_i} + 2\rho \sum_{j=1}^{m} \left\langle \frac{\lambda_j}{2\rho} + g_j \right\rangle \frac{\partial g_j}{\partial x_i} = 0. \tag{4.22}$$

The Lagrangian multiplier λ_j^* in stationary point x^* is found in subcalculation obtaining penalty parameter ρ and then:

$$\lambda_j^* \cong \lambda_j^{k+1} = \left\langle \lambda_j^k + 2\rho_k g_j\left(\mathrm{x}^{*k}\right) \right\rangle. \tag{4.22}$$

The algorithm of minimization of augmented Lagrangian function is very similar to the algorithm of Lagrangian method (Fig. 4.5) and is not given separately.

This method is considered as quick and precise, and it could be used in CMC optimization as there are the objective function and the inequality constraints.

4.2.5. Sequential quadratic programming (SQP)

The *SQP method* is based on the *Newton's method*, and is applied for optimization problems with equality $h_j(\mathrm{x}) = 0 (j = 1, 2, ..., r)$ and inequality $g_j(\mathrm{x}) \le 0$ $(j = 1, 2, ..., m)$ constraints [101, 142, 146, 168].

The solution of quadratic programming (QP) problem is equal to determination of the *Newton step* Δ, but further named as "s", for x_{opt}, λ_{opt}. The *k*-th (x^k, λ^k, μ^k) QP problem is to minimize (4.23) such that (4.24) and (4.25) [146].

$$F(\mathrm{s}) = f\left(\mathrm{x}^k\right) + \nabla^T f\left(\mathrm{x}^k\right)\mathrm{s} + \frac{1}{2}\mathrm{s}^T \mathrm{H}_L\left(\mathrm{x}^k\right)\mathrm{s} \tag{4.23}$$

$$g\left(\mathrm{x}^k\right) + \left[\frac{\partial g\left(\mathrm{x}^k\right)}{\partial \mathrm{x}}\right]^T \mathrm{s} \le 0 \tag{4.24}$$

$$h\left(\mathrm{x}^k\right) + \left[\frac{\partial h\left(\mathrm{x}^k\right)}{\partial \mathrm{x}}\right]^T \mathrm{s} = 0 \tag{4.25}$$

The hessian matrix H is for the classical Lagrangian function *L* with respect to x:

$$\mathrm{H}_L\left(\mathrm{x}^k\right) = \nabla^2 f\left(\mathrm{x}^k\right) + \sum_{j=1}^{m} \lambda_j^k \nabla^2 g_j\left(\mathrm{x}^k\right) + \sum_{j=1}^{r} \mu_j^k \nabla^2 h_j\left(\mathrm{x}^k\right). \tag{4.26}$$

The algorithm is not given, because in general the principle of algorithm for the *SQP method* is the same as for *Newton method* (can see Fig. 4.4), only the *quadratic programming* methods must be applied in the solving of subsystems [26, 144].

There are some more methods which are used to solve global constrained and unconstrained problems, as *feasible descent cone (FDC) method*, the *leap-frog (LF) method*, and *modified bouncing ball (MBB) trajectory method* etc., which are not closer overviewed, because at the beginning the author planned to make an optimization program by himself and

so the optimization methods were overviewed, but later the author decided to use an existing optimization tool.

4.3. Choice of optimization tool

There are much optimization software as an existing optimization tool to solve the desired problem and the most suitable – taking into account the optimization method it is based on and the type of the necessary optimization problem (OP) – can be freely chosen. Most of them are for charge, so the comparison for some of these software is made showing also the period of the trial version if offered (table 4.1). These data are last time checked in January 2015. Used abbreviations: "API" — application programming interface, "NLP" — nonlinear programming, "MDA" — multivariate data analysis, "ANOVA" — analysis of variance.

Table 4.1

Comparison of some optimization software

No.	*Title of product*	*Type of OP*	*Method(s) based on*	*Some facts*	*Trial version (weeks)*
1	Xtreme [108]	Global opt.; From data sheets	Advanced genetic algorithms (including Pareto-front genetic algorithm) coupled with artificial neural networks	• Graphical user interface; • Microsoft Excel Add-In; • Available API for Python, C, C++.	2
2	WORHP [132]	For large scale sparse nonlinear opt.	Use the sequential quadratic programming (SQP), for the subproblems — the interior point methods	• Written in hybrid of Fortran and C; • Can be used in C/C++ and Fortran; • Available as API for MATLAB; • Free of charge for academic use.	–
3	VisSim [130]	For different dynamic systems	–	• Instead of writing and solving equation systems the visual block diagram language — dynamical systems and model based design — is used; • Usually used for optimization of dynamic flow systems, electronics' circuits etc. though the electric motor simulation library is for AC induction,	–

				brushless DC, and stepper motors; • For academic use a 35 % discount (starting with 5 seats), for more information must contact directly.	
No.	***Title of product***	***Type of OP***	***Method(s) based on***	***Some facts***	***Trial version (weeks)***
4	SmartDO [128]	Multidisciplinary design opt.	Gradient-based direct global search methods and finite element analysis (FEA), computer-aided design (CAD), computational fluid dynamics (CFD) etc.	Used, e.g., for turbine rotor structural optimization.	–
5	PottersWheel [126]	MDA tool with optimization possibilities; For any ordinary differential equation based model	Multi-experiment fitting; Regression models, Bayesian networks, Boolean models, and stochastic models	• A MATLAB® toolbox, based on C files and FORTRAN integrators; • For experimental measurements from biochemical, engineering or other dynamical system; • Allows ordinary differential equation (ODE) based modelling; • Can discriminate competing hypothesis; • Graphical user interface; • Data can be imported from .xls and .txt files; • API is available; • Free for academic use	–
6	solidThinking Evolve [129]	Design opt. tool	High-quality photorealistic rendering	• New design forms can easily be implemented in the base model of initial drawing; • Generates renderings in real time; • Turns the initial pencil drawings into the real 3D objects; • Provides parametric control; • Trial version by request	–
7	OptiStruct [125]	Linear and non-linear opt.	Structural opt., FEA, and multi-body dynamics methods; multilevel substructuring Eigen solver	• E.g., for the weight reduce of aircraft engine; • Allows users to combine topology, topography, size and shape opt. methods; • Trial version by request	–
8	NMath	Linear, quadratic and non-linear	Matrix and vector classes, Fast Fourier	• A no numbered discount is applied for students;	4

	[124]	opt.	transforms (FFT), linear programming, linear regression, curve and surface fitting, cluster analysis, ANOVA etc.	• Provides libraries to be used on Microsoft .NET platform; • Has API for NVIDIA GPU's	
No.	***Title of product***	***Type of OP***	***Method(s) based on***	***Some facts***	***Trial version (weeks)***
9	What's*Best* [131]	Linear, non-liner (convex and non-convex/ global), quadratic (constrained or not), second order cone, stochastic and integer opt.	Not specified but according to the type of OP	• An add-in to Excel; • Provides the trial versions with limits of variables and problem dimensions, the period of trial version is not given	–
10	*SIMCA* [127]	MDA tool with optimization possibilities	Equations of derivatives, Savitzky-Golay, different filters, group observation, Regression models, class modelling, cluster analysis, discriminant analysis etc.	• .xlsx, .txt etc. can be imported; • Imports qualitative variables as they are given; • Supports multiple datasets; • The spectra plots, fast statistics, cross-correlation, values of minimum & maximum and mean etc. are available; • Operates with first, second and third order derivatives.	4

From the overviewed optimization tools the SIMCA is chosen to be used for CMC optimization. The SIMCA trial version with number of release 13.0.3 (32-bit) is downloaded and installed.

4.4. CMC optimization

A data table with independent and dependent variables is prepared for input to SIMCA. The data table is designed taking into account the boundary values and some middle values of independent variables, and the objective function and the control parameters are designed with respective synthesized formulas.

After multivariate data analysis and optimization (appendix 8), the following optimization results are obtained:

- For rare-earth alloys with M_{max}/V = 172.27 (Nm/m^3) and M_{max} = 36.97 (Nm):
  - Relative permeability μ_* = 1.061;
  - Axial length l = 75 mm;

- Pole pair number $p = 5$;
- Magnetic coverage coefficient $\beta = 0.80$;
- PM height $h_{PM} = 8$ mm;
- Air gap $\delta = 2$ mm;

- For simple ferrites with $M_{max}/V = 14.64$ (Nm/m^3) and $M_{max} = 3.09$ (Nm):
  - Relative permeability $\mu_* = 1.344$;
  - Axial length $l = 75$ mm;
  - Pole pair number $p = 4$;
  - Magnetic coverage coefficient $\beta = 0.8$;
  - PM height $h_{PM} = 8$ mm;
  - Air gap $\delta = 2$ mm.

If the two material types that PMs are made of are put together, the optimum will be in case of CMC with rare-earth magnets, of course.

The simple ferrite magnets are used to provide the potential alternative to decide to use either much expensive magnets with more higher characteristic M_{max}/V or much cheaper simple ferrites thus having smaller characteristic M_{max}/V of the coupler.

4.5. Optimization methodology

The made optimization process of active CMC allows developing the new optimization methodology (Fig. 4.9) for obtaining the optimum of desired parameters of CMCs within the chosen boundary values and according to necessary control parameters.

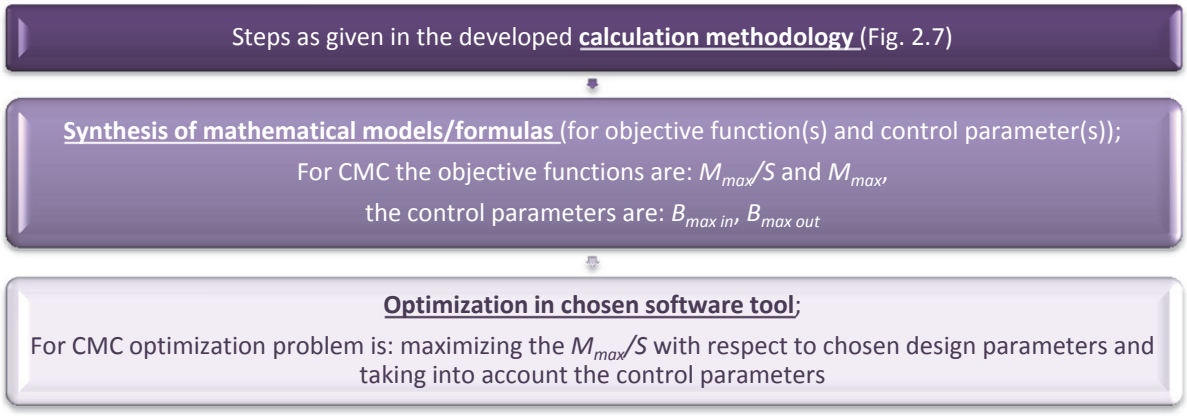

Fig. 4.9 Main steps of developed optimization methodology

4.6. Conclusions

From the overviewed and analyzed methods the combined Lagrangian methods and the modified Newton's methods are considered by the author to be the most suitable for the

CMC optimization; however the author has decided to use an optimization tool developed by professionals.

Some of many optimization tools are overviewed, from which the SIMCA is chosen as the most suitable.

The optimum of CMC design is found maximizing its main characteristic M_{max}/V and applying SIMCA. The optimum for whole researched system, of course, is for CMC where PMs are made of rare-earth alloy. The optimum point with $\boldsymbol{M_{max}/V = 172.27}$ (Nm/m^3) and $\boldsymbol{M_{max} = 36.97}$ (Nm) is following: $\mu_* = \mathbf{1.061}$, $\boldsymbol{p = 5}$, $\beta = \mathbf{0.8}$, $\boldsymbol{l = 75}$ mm, $\boldsymbol{h_{PM} = 8}$ mm, and $\delta = \mathbf{2}$ mm. When the coupler optimization system is reduced to the following — coupler with magnets made of simple ferrites-, the optimum point with $\boldsymbol{M_{max}/V = 14.67}$ (Nm/m^3) and $\boldsymbol{M_{max} = 3.09}$ (Nm) is following: $\mu_* = \mathbf{1.344}$, $\boldsymbol{p = 4}$, $\beta = \mathbf{0.8}$, $\boldsymbol{l = 75}$ mm, $\boldsymbol{h_{PM} = 8}$ mm, and $\delta = \mathbf{2}$ mm.

The optimum cannot be solved only by one characteristic M_{max}/V, because the analysis shows that in the designed optimization system three optimum points appear at once, thus the second characteristic must be taken. The formulas of maximum mechanical torque M_{max} were synthesized in parallel with the ones of M_{max}/V. The sub problem of optimization was set for the obtained results — maximize the M_{max} with the respect to axial length l (only l, because the rest of independent variables were according equal).

The situation that occurred in the optimization was noticed already in the synthesis of formulas and in the formulas' testing, though the effect of it highlighted only in the optimization steps. Now it is clear that, though to take the M_{max}/V seems to be physically rational step, for cylindrical magnetic coupler optimization the formulas should be synthesized for M_{max}/S, where S is the area of its cross section, instead of M_{max}/V.

The made optimization process of active CMC allows developing the new optimization methodology for obtaining the optimum of desired parameters of CMCs within the chosen boundary values and according to necessary control parameters.

5. EXPERIMENTS AND FURTHER RESEARCH POSSIBILITIES

In this chapter the experiments and the further research possibilities for CMC design optimization are given. The experiments for the comparison of obtained curves of mechanical torque are given, then the experiments for comparison of prediction of the maximum mechanical torque are given, and finally the author's opinion is given how the design of CMC could and should be optimized in future.

5.1. The first set of experiments

5.1.1. Objective, assignments and methods

Place — Institute of Physical Energetics.

Date — May 2014.

The objective of the experiment — to obtain the mechanical torque curve of CMC and compare it with the one calculated in *QuickField* (*QF*).

Object of the experiment — cylindrical magnetic coupler (CMC) with rectangular PMs.

Subject of the experiment — values of mechanical torque *M*.

Assignments of the experiments' set:

1. Prepare the object and the stand of the experiment;
2. Obtain the curve of mechanical torque in experimental way;
3. Obtain the curve of mechanical torque by simulation in *QF*;
4. Compare the results — both curves of mechanical torque.

Method of traditional experiment — the work principle of Dynamometer, by knowing the radius and added weight (or force), the torque can be calculated.

Method of simulation — for the simulation of CMC rotation the software QF is used and it is based on magnetic field modelling by the finite element analysis (FEA). The rotation can be made by desired angle and the program outputs the corresponding values of mechanical torque.

5.1.2. Steps of the experiments

Step 1

For the experiment a specifically designed object with implemented CMC was made to obtain the curve of mechanical torque (Fig. 5.1, 5.2). The whole object is made on the foot

stand 1, thus it is portable and can be fixed at any stand. The CMC 3 has inner and outer half couplings with rectangular permanent magnets. The inner half coupling is turned by an angle by the rotation axis 2.

The CMC has NdFeB magnets with pole pair number $p = 6$. Other design parameters are given in previous description about the coupler BR-5 (see chapter *2.1.3*.).

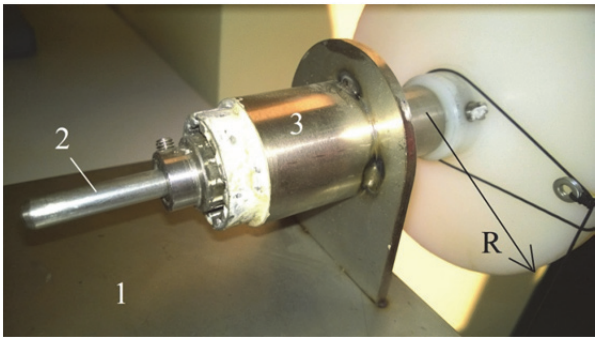

Fig. 5.1 The prepared object for the experiment (back side)

Fig. 5.2 The prepared object for the experiment (front side)

Step 2

The weights with summarized mass m_i are added at certain turning angle α_i (Fig. 5.3).

Fig. 5.3 The adding of weights at certain turning angles

For chosen angles α_i the mass m_i is known, which has to be added to balance out the torque in the air gap between the half couplings, and the radius R is known (R = 56 mm). The torque's value M_i is calculated by (5.1.) at the certain turning angle α_i. (table 5.1).

$$M_i = R \cdot F_i = 0.056 \cdot gm_i \,(\mathrm{Nm}) \tag{5.1}$$

Table 5.1

Mechanical torque M obtained experimentally

i	α_i ***(°el.)***	M_i **(Nm)**	***i***	α_i ***(°el.)***	M_i **(Nm)**
1	0	0	7	81	0.6
2	30	0.25	8	87	0.61
3	39	0.35	9	87	0.615
4	52.5	0.45	10	90	0.62
5	60	0.5	11	90	0.623
6	67.5	0.55			

Step 3

For this coupler a drawing was prepared and its magnetic field was modelled in *QF*. From the modelled magnetic field (Fig. 5.4), the mechanical torque M was calculated at different turning angles α (table 5.2).

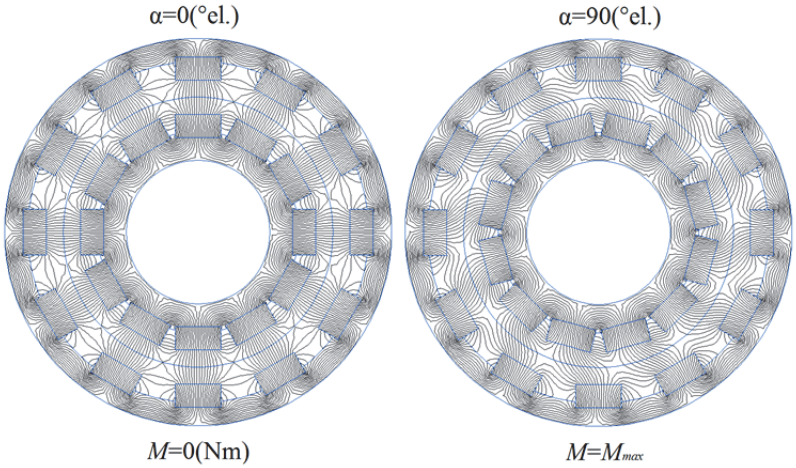

Fig. 5.4 Magnetic field of CMC BR-5 modelled in *QF*

Table 5.2

Mechanical torque *M* obtained in *QF*

i	α_i ***(°el.)***	M_i **(Nm)**	***i***	α_i ***(°el.)***	M_i **(Nm)**
1	0	0	8	105	0.57474
2	15	0.14345	9	120	0.50911
3	30	0.28770	10	135	0.42195
4	45	0.40497	11	150	0.30092
5	60	0.50346	12	165	0.15391
6	75	0.56623	13	180	0
7	90	0.59147			

Step 4

These results — obtaining the mechanical torque curves in experimental way and by magnetic field simulation — are compared and given in Fig. 5.5.

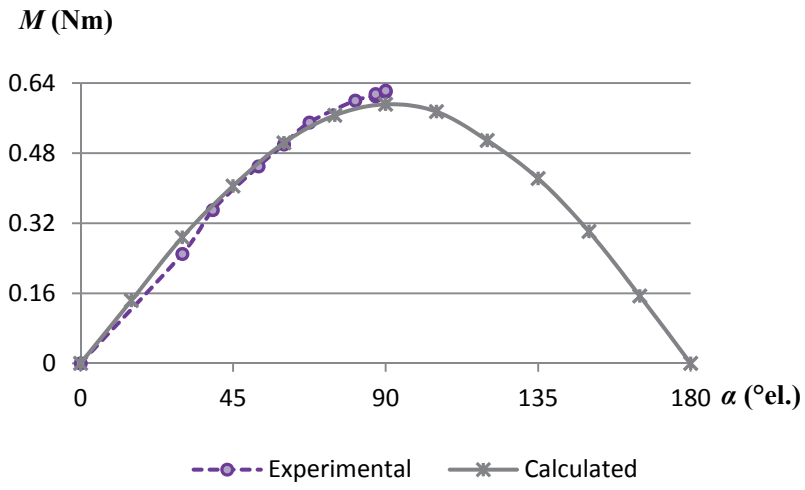

Fig. 5.5 Mechanical torque of CMC BR-5

5.1.3. Conclusions of the experiments

An experiment for CMC was made to obtain its mechanical torque M. The experimental torque was compared with the calculated one using the developed methodology. The difference of the calculated torque from the experimentally taken was not higher than 5 %, hence the developed methodology for torque and other parameter calculation is approved to be used in formula synthesis and coupler optimization.

Conclusions:

- The weights-adding principle is not a very precise method, thus the experimental curve is grooved;
- The experimental curve almost overlaps the curve obtained in simulation of magnetic field;
- As in the optimization the maximum value of mechanical torque is used, these values are separately compared: $M_{max\ exp}$ = 0.623 Nm and $M_{max\ QF}$ = 0.591 Nm. The difference is ΔM_{max} = 0.032 Nm or 5.4 % (according to M_{max} = 0.591 Nm);
- From the good overlapping of experimental torque curve on the curve's part that is obtained in magnetic field simulation software *QF*, and the small difference between the main (maximum) torque values (about 5 %) it may be concluded that the software *QuickField* is permissible for obtaining the mechanical torque maximum values to be used further in CMC design optimization.

5.2. The second set of experiments

5.2.1. Objective, assignments and methods

Place — Laboratory of BTC [86].

Date — January 2015.

The objective of the experiment — to obtain the mechanical torque curve of CMC and compare its maximum value with the one calculated by synthesized formula.

Object of the experiment — cylindrical magnetic coupler (CMC) with rounded PMs.

Subject of the experiment — values of mechanical torque M.

Assignments of the experiments' set:

1. Prepare the object and the stand of the experiment;
2. Obtain the maximum value of mechanical torque in experimental way;

3. Obtain the maximum value of mechanical torque by forecasting (using synthesized formula);
4. Compare the results — maximum values of mechanical torque.

Method of traditional experiment — the torque values are obtained at certain angles similar to work principle of Dynamometer, by knowing the radius and added force, the torque is calculated by oscilloscope (see the description of stand in "Step 1").

Method of forecasting — for the necessary boundary conditions (different from overviewed and from those that are taken for the base of formula synthesis, given in "Step 3") a new formula is synthesized in program made by O. Onževs (see chapter 3.1 and 3.2), which is based on the multivariate regression analysis.

5.2.2. Steps of the experiments

Step 1

A specifically designed object with implemented CMC is made to obtain the curve of mechanical torque in the experimental way (Fig. 5.6). The whole object is made on the foot stand 1; it is portable and can be fixed at any stand. The CMC 2 has inner and outer half couplings with rounded permanent magnets. To hold the coupler inner half coupling in one position an added weight 3 is needed.

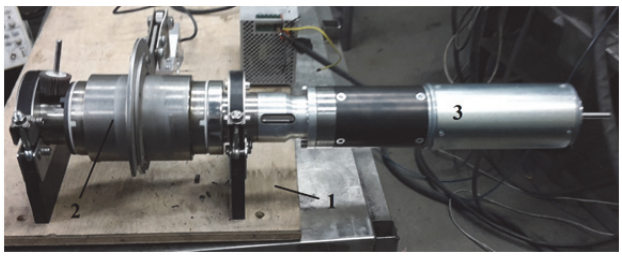

Fig. 5.6 The prepared object for the experiment

The CMC has rounded (or sector form) NdFeB magnets with pole pair number $p = 5$, height $h_{PM} = 9.5$ mm and magnetic coverage coefficient $\beta = 0.95$. The axial length is $l = 76.2$ mm and air gap is $\delta = 4.3$ mm. The radiuses are: $R_1 = 17.75$ mm and $R_5 = 50.85$ mm (Fig. 2.2).

The inner half coupling is turned by an angle measured with voltage sensor that is placed on the inner half coupling (Fig. 5.7) and connected with oscilloscope.

After fixing the turning angle the interaction forces between the PMs on both half couplings try to turn the outer half coupling on which the support system 1 is mounted (Fig. 5.8).

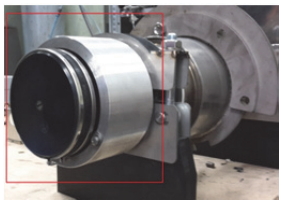

Fig. 5.7 The voltage sensor placed on the shaft of inner half coupling

When the outer half coupling tries to rotate (red arrow), the pressure force F is made by the arm of force l' = 200 mm and measured by the sensor 2 (Fig. 5.8).

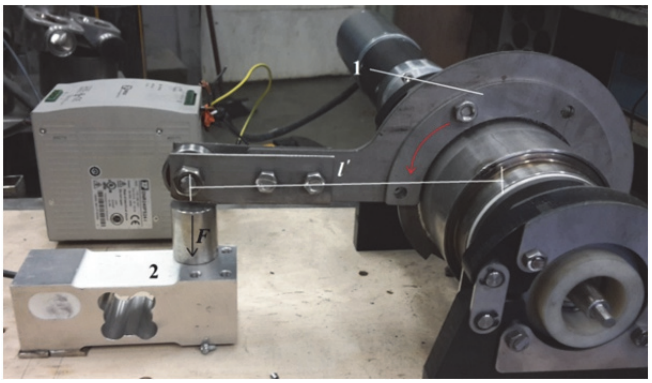

Fig. 5.8 The support system and sensor of pressure force

Step 2

The curve of mechanical torque is obtained in the oscilloscope, where the certain values of the turning angle α_i given by voltage sensor and the force F_i are used to calculate the torque value M_i (5.2). The stand for obtaining the mechanical torque in the experiment way is given in Fig. 5.9. Only the maximum value of mechanical torque M_{max} is taken and it is M_{max} = 76.13 Nm.

$$M_i = l' \cdot F_i \ (\text{Nm}) \tag{5.2}$$

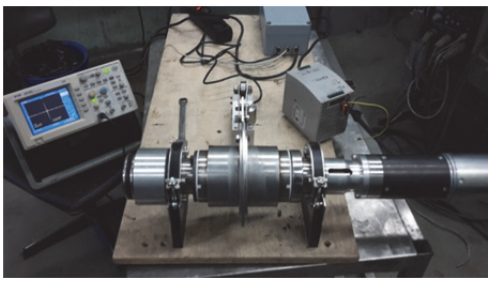

Fig. 5.9 The whole stand of experiment

Step 3

For this case to get to know the optimal design of coupler a separated formula was synthesized (5.3). The modelled design of CMC is simpler because the magnets' material is NdFeB (μ_* — const), magnetic coverage coefficient is β = 0.95 (also constant) and the air gap as well is known (δ = 4.3 mm).

The formula is true for models with following variable ranges: $l = 70–80$ mm, $h_{PM} = 8–10$ mm and $p = 4–6$. The ranges are small, but the result calculated with formula should be precise.

$$M_{\max} = l \cdot \left(0.3 + 0.09 h_{PM} - 0.007 h_{PM} \cdot p + 0.0023 h_{PM}^2\right) \tag{5.3}$$

From the results calculated with this formula one model is chosen, and it is the one after which the CMC is made described in "Step 1".

Inserting the variables $p = 5$, $h_{PM} = 9.5$ (mm) and $l = 76.2$ (mm) the value of maximum mechanical torque is $M_{max} = 78.492$ Nm.

Step 4

These results — obtained values of maximum mechanical torque in the experimental way and by synthesized model (formula) — are compared and given in table 5.3.

Table 5.3

Maximum mechanical torque M_{max}

	M_{max} (Nm)	ΔM_{max} (Nm)	ΔM_{max} (%)
Experimental	76.13	–	–
Modelled	78.49	2.36	3.10

5.2.3. Conclusions of the experiments

An experiment for CMC was made to obtain its maximum mechanical torque M_{max}. The experimental torque was compared with the modelled one using the synthesized formula (/model).

Conclusions:

- The pressure force F measuring system is more precise than the weights-adding principle;
- From modelled variants of CMC design one is chosen and its prototype model is made. The case with $h_{PM} = 10$ mm, of course, gives higher value of M_{max}, but the control parameter $B_{max\ out}$ exceeds the 1.8T limit, thus the variant with $h_{PM} = 9.5$ mm is chosen for prototype.
- The comparison of values of M_{max} shows that the error is less than 5 % ($\Delta M_{max} = 3.1$ %), hence can be concluded that the developed formula(/model) based on the multivariate regression analysis is a very useful tool in the forecasting of M_{max} values, and the author suggests to synthesize some more formulas/models for wider range of variable, according to axial length and outer radius of outer half coupling.

5.3. Potential improvements of CMC in future

In the author's opinion the further potential improvements of CMC design that should be researched are following:

a) The shape of inner and outer half coupling yokes could be made *teeth-rounded*, reducing the used raw materials and increasing the main characteristic M_{max}/V;
b) The CMC models should be expanded including one more independent variable — inner radius of inner half coupling, and for that model the formulas should be synthesized;
c) The author insists that the new formula synthesis should be made for following subgroups: for PMs made of rare-earth alloys and simple ferrites separately, for pole pair numbers p in groups that are respective to obtained results;
d) The influence of different numbers of permanent magnets on inner (N_{in}) and outer (N_{out}) half couplings on the coupler maximum mechanical torque M_{max};
e) The difference of maximum value of the magnetic coverage coefficient β for rare-earth magnets and for simple ferrite magnets.

5.4. Conclusions

The first set of experiments is the acquisition of the CMC (with rectangular PMs) torque. First experiment is made by method based on Dynamometer working principle, and the torque of the same coupler is obtained applying the *QuickField* software. The results are compared and outline that the software can be used for the torque (and other necessary parameters) curve acquisition, having the error for less than 6 per cent.

The second set of experiments is the acquisition of maximum value of CMC (with rounded PMs) torque. The torque maximum value from the first experiment way is compared with the value obtained calculating by the synthesized model/formula. The results outline that the use of synthesize models can be a very useful way in the forecasting of M_{max}, having the error for less than 5 per cent.

In the author's opinion further researches of CMC design optimization can be made in the previously given directions (chapter 5.3).

MAIN CONCLUSIONS

The analysis of latest researches about the cylindrical magnetic coupler (CMC) prove that the research of influencing design parameters and the optimization of CMC design based on magnetic field calculations made in this work was not done yet.

As the main characteristic of CMC the maximum mechanical torque M_{max} is chosen because the curves of mechanical torque M for different couplers may vary by amplitude and period. To avoid the mistakes that appear in an inappropriate comparison, one characterizing value (M_{max}) from the whole torque curve is taken. The CMC has many design parameters, but only 5 (pole pair number p, magnetic coverage coefficient β, PM height h_{PM}, air gap δ and axial length l) are chosen to be optimized. The 6th parameter is relative permeability μ_* characterizing the material from which the permanent magnets (PMs) are made of, this parameter also indirectly influences the CMC design and its main characteristic M_{max}. For these parameters the boundary values are researched and consequently chosen.

The base design is the CMC with rectangular PMs. The offered transition from rectangular PMs to rounded (or sector form) ones gives the improvement of M_{max} for more than 30 %. The optimization is made for the CMC with rounded PMs. As the values of M_{max} can be equal or very similar to couplers with very different design parameters, the characteristic as maximum torque per volume M_{max}/V is taken.

The calculation methodology is developed to obtain the desired parameters: main characteristic M_{max} and the control parameters — maximum values of magnetic flux density in inner and outer half coupling yokes — $B_{max\ in}$ and $B_{max\ out}$. The developed methodology includes the application of drawing software *AutoCad* and magnetic field modelling software *QuicField* (*QF*).

The reactive CMC is also researched and a new patented design is developed having improved M_{max} 2 times and M_{max}/V about 9 times when compared with the analogue (/standard design reactive CMC with yoke of outer half coupling) reactive CMC.

The optimum of reactive CMC can be found only by developed calculation methodology without any further mathematical procedures.

For the set boundaries and defined objective function, completely new CMC design models/formulas are synthesized, from which are chosen the most appropriate ones. The testing of these models proves that the precision is high: less than 5 % for M_{max}/V and less than 10 % for B_{max}.

The optimization algorithms are analyzed and the optimization tool *SIMCA* is chosen. The optimization process proves that the M_{max}/S (maximum mechanical torque per area) will be more correct to use in the optimization instead of M_{max}/V. The first step in the optimization problem is the maximization of M_{max}/V with the respect to chosen variables (design parameters), and, as more than one optimum is found, the sub-problem is the maximizing of M_{max} with respect to the one left variable — axial length. The optimum is found and it (with $\boldsymbol{M_{max}/V = 172.27}$ Nm/m^3 and $\boldsymbol{M_{max} = 36.97}$ Nm) is following: $\mu_* = \mathbf{1.061}$, $\boldsymbol{p = 5}$, $\beta = \mathbf{0.8}$, $\boldsymbol{l = 75}$ mm, $\boldsymbol{h_{PM} = 8}$ mm, and $\delta = \mathbf{2}$ mm.

When the coupler optimization system is reduced to the following — coupler with magnets made of simple ferrites-, the optimum point with $\boldsymbol{M_{max}/V = 14.67}$ (Nm/m^3) and $\boldsymbol{M_{max} = 3.09}$ (Nm) is following: $\mu_* = \mathbf{1.344}$, $\boldsymbol{p = 4}$, $\beta = \mathbf{0.8}$, $\boldsymbol{l = 75}$ mm, $\boldsymbol{h_{PM} = 8}$ mm, and $\delta = \mathbf{2}$ mm.

The made researches and optimization of active CMC allow developing a new optimization methodology.

The first set of experiments is the acquisition of the CMC (with rectangular PMs) torque. First experiment is made by method based on Dynamometer working principle, and the torque of the same coupler is obtained applying the software *QF*. The results are compared and mark out that the software can be used for the torque (and other necessary parameters) curve acquisition, having the error for less than 6 per cent. Thus the developed methodology of M_{max} and B_{max} acquisition is correct.

The second set of experiments is the acquisition of maximum value of CMC (with rounded PMs) torque. The torque maximum value from the first experiment way is compared with the value obtained calculating by the synthesized model/formula. The results mark out that the use of synthesized models can be a very useful way in the forecasting of M_{max}, having the error for less than 5 %.

A new optimization methodology is offered for obtaining the optimal combination of CMC design parameters, and it is following: start with obtaining the necessary physical parameters depending on chosen design parameters by the magnetic field calculations; next step is the synthesis of mathematical models/formulas (based on results from calculations of magnetic field) which allow the forecasting of the chosen characteristics such as M_{max} and M_{max}/S; the last step includes the choice of optimization tool and the coupler optimization.

APPENDICES

Appendix 1

Magnetic coupler application examples

In Fig. A.1 a device with MC that is used as a mixer or agitator is given. This particular sample is used in chemical, pharmaceutics and food processing industry. The PMs are made of samarium-cobalt (SmCo) alloy. The admissible working temperature is 150 °C. The seal is made of stainless steel (1.4571) and covered with silicon carbide for smooth sliding. The device can be used for solid substance grain mixing/agitation for grains with maximum hardness 700 HV and with maximum diameter 0.1 mm. Device is intended for operating speed $n = 400\ \text{min}^{-1}$.

Fig. A.1 Mixer/agitator with magnetic coupler

In Fig. A.2 a device with MC that is used as a centrifugal/gear pump, fan or blower is given. This device can be used in refining technology and in such industries as chemical, gas and oil, pharmaceutics and food processing. The PMs are made of SmCo or neodymium-iron-boron (NdFeB) alloy. The admissible working temperature for the respective alloy magnet is 250 °C and 120 °C. The seal can be made of either the stainless steel (1.4571) and covered with silicon carbide for smooth sliding, or ceramic or carbon fibre. The pump admissible operating pressure is 25 bars. It can be used for solid substance grains with maximum hardness 700 HV and with maximum diameter 0.1 mm. Device is intended for operating speed $n = 3600\ \text{min}^{-1}$ and maximum torque till 462 Nm.

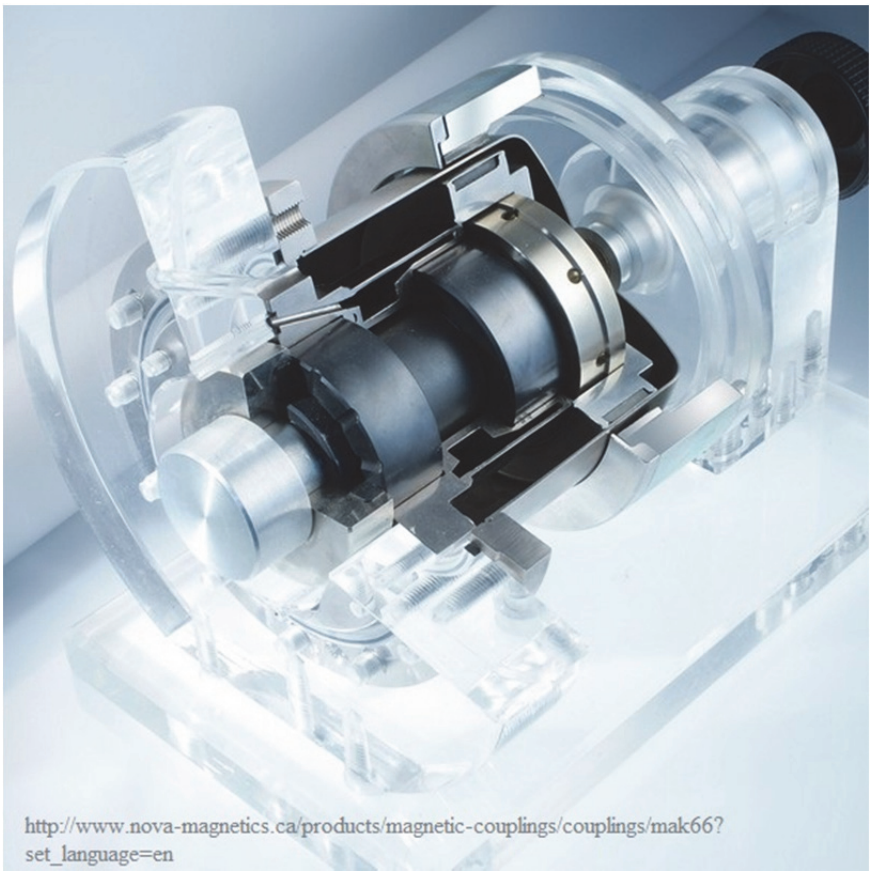

Fig. A.2 Pump with magnetic coupler

It is given (Fig. A.3) a device with MC that is used in extreme conditions: operating pressure is 45 bars and operating temperature is more than 100 °C. The device is used as a centrifugal/gear pump, fan, and blower or as a part of autoclave. These devices are used in chemical, oil and gas, pharmaceutics and food processing industry and in refining technology. The PMs are made of SmCo or NdFeB alloy. The admissible operating temperature for the respective alloy magnet is 250 °C and 120 °C.

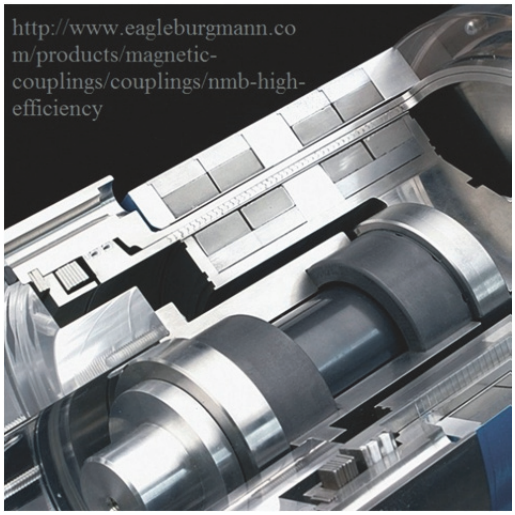

Fig. A.3 Pump with magnetic coupler

The seal is made of stainless steel (1.4401/1.4436) and covered with PTFE (polytetrafluorethylen). One metal lay of the sealing can is slotted to reduce the Eddy currents to a minimum (approximately 2 % of motor power). Device is intended for operating speed $n = 3000\ \text{min}^{-1}$. It can be applied for large torques (from 18 till 1879 Nm), high speed and pressure.

In Fig. A.4 a centrifugal pump (a) and an MC (b) used in it are given. The MC is used in compressors, vacuum pumps and agitators. This device is used in chemical, oil and gas, pharmaceutics industries and in refining technology. The PMs are made of SmCo or NdFeB alloy. The admissible operating temperature for the respective alloy magnet is 300 °C and 150 °C [16].

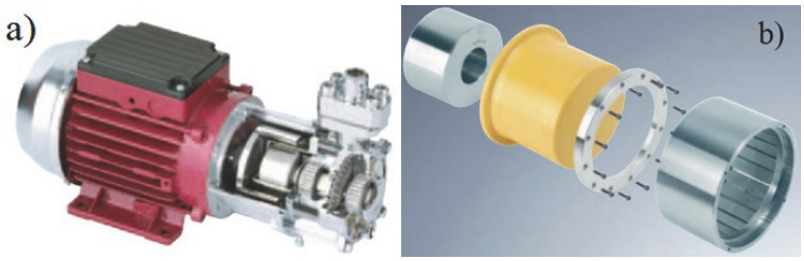

Fig. A.4 Centrifugal pump (a) and magnetic coupler used in it (b)

The seal is made of oxide ceramics or stainless steel. The available torque range is from 25 till 550 Nm (at operating temperature 20 °C) [16].

Appendix 2

Examples of reactive, Eddy current and hysteresis MCs

An active magnetic coupler has permanent magnets placed on both half couplings so that each magnet interacts with other half coupling magnets. The PMs on both half couplings are inducing the magnetic field conducted through the air gap and in parts made of steel.

A reactive MC (Fig. A.5) has permanent magnets mounted only on one half coupling. The other half coupling has similar design (according to PM form) and it is made only of steel (more info in chapter 2.2.).

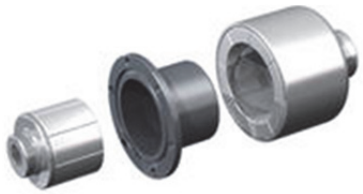

Fig. A.5 Reactive cylindrical magnetic coupler

A hysteresis MC (Fig. A.6) also has PMs only on one half coupling, but the second half coupling is made of easily magnetizable/demagnetizable material. The north-south PMs magnetize and demagnetize the material. This magnetization-demagnetization cycle results in synchronously coupled magnetic circuit. The magnetic energy is utilized to magnetize and demagnetize the easily magnetizable material, but this loss is much less than in Eddy current couplers.

http://www.dextermag.com/products/magnetic-assemblies/magnetic-couplings

Fig. A.6 Hysteresis linear magnetic coupler

An Eddy current coupler (Fig. A.7) is made as follows: on one half coupling sequent north-south PMs are placed, but the other half coupling is made of electrically conductive material (most often aluminium or copper). The coupler is asynchronous. When the magnets rotate, the alternating magnetic field occurs in the second half coupling inducing an electrical

current in the conductive material. These currents make opposite magnetic fields to the permanent magnets, so the half couplings are joined. The utilized energy from the magnetic field is converted into flowing electrical currents (thus converted also in heat).

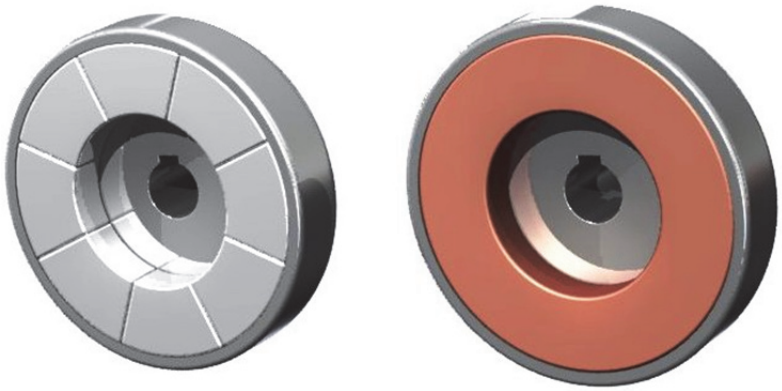

Fig. A.7 Eddy current disc form magnetic coupler

Appendix 3

Most commonly used magnetic units and their ratio

Magnetic property	Units	Ratio (between the SI and English units)
Induction *B*	Tesla (T) or millitesla (mT)	T (or Wb/m^2) = G/ 10 000
	Gauss (G) or kilogauss (kG)	mT = G/ 10
		T = kG/ 10
		kG = 10 T
Field strength *H*	Amperes per meter (A/m) or kiloamperes per meter (kA/m)	kA/m = 0.079577472 Oe kA/m = 79.577472 kOe
	Oersteds (Oe) or kilooersteds (kOe)	Oe = 12.5663706 kA/m
Maximum energy product BH_{max}	Kilojoules per cubic meter (kJ/m^3)	kJ/m^3 = 7.9577 MGOe
	Megagauss Oersteds (MGOe)	MGOe = 0.12566445

Appendix 4

Experiment "Demagnetization curve"

Equipment: Hystograph (Fig. A.8) with its software MAG-Expert;

Fig. A.8 Hystograph

Object: two (2) samples of permanent magnets (PM) made of NdFeB (Fig. A.9), nickel coated (produced by *K&J Magnetics* [117]);

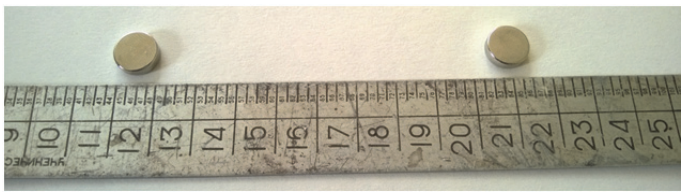

Fig. A.9 NdFeB permanent magnet samples

Subject: demagnetization curve of permanent magnet.

Date: 24.10.2011.

Place: Institute of Physical Energetics (Fizikālās enerģētikas institūts, FEI), Laboratory of Electrophysical Process Modelling.

Experiment steps:

The hystograph is an analog/digital measuring equipment for obtaining the hysteresis loop of PM [91].

1. Turn on the hystograph and run the MAG-Expert, after which a dialog window occurs;
2. Define the sample in "Sample Data" subwindow. Four material types are offered: "Alnico", "Ferrite", "SmCo/NdFeB" and "Ni-ref. material". Mark the "SmCo/NdFeB"

material type. For every material type there are automatically set the ranges for the magnetic field strength (H_{min}, H_{max}) and the polarisation (J_{min}, J_{max}). There are two fluxmeters to measure the values of polarization J and flux density B [91].

3. Give the diameter (11.11 mm or 7/16 in [117]) and height (3.18 mm or 1/8 in) of the sample and the sample shape (disk), from which the sample area (cm^2) is calculated.
4. Give the sample weight (2.54 g), from which the sample density is calculated.
5. Give the temperature of the sample (23 °C), which is the temperature of room where the samples are kept.
6. Give the sample name ("Sample 1", "Sample 2") and if necessary the specific sample number.
7. Give the person name that makes the test ("Ose").
8. Choose the coil ("J26_COMP", Fig. A.10) in "Winding system" subwindow, between two coils: "J26_COMP" and "J10_COMP". The difference is in the diameters: accordingly 26 mm and 10 mm. In turn the diameter of coil is chosen from sample diameter.

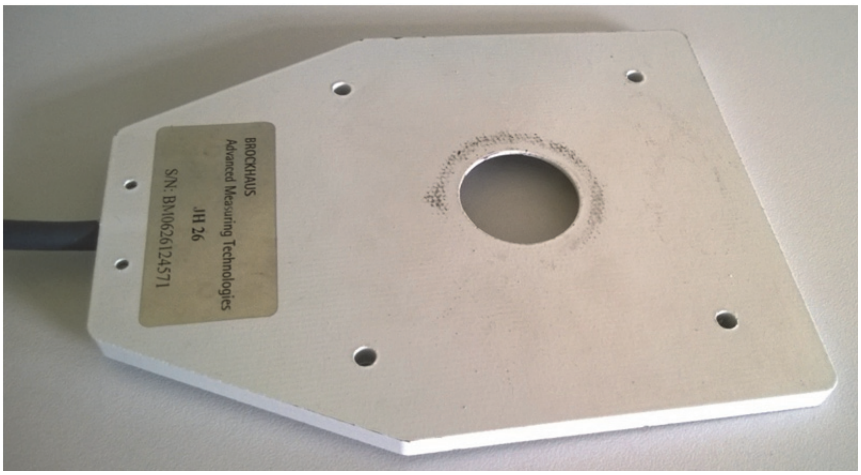

Fig. A.10 Coil "J26_COMP"

9. In the main MAG-Expert window push the button "Start", after which the zero point is set. The PM is not yet placed in the coil. Then the notification that the zero point is set appears.
10. Insert the magnet. And press the button "OK", after which the measuring of hysteresis loop is started.
11. As in the interests there is the part of demagnetization curve (to know the values of residual induction, coercive force and maximum product energy), so it is chosen to show the report in the second quadrant, instead of showing whole hysteresis loop.

Results:

The results from MAG-Expert are in a view of report (Fig. A.11, A.12) and summarized in table A.1.

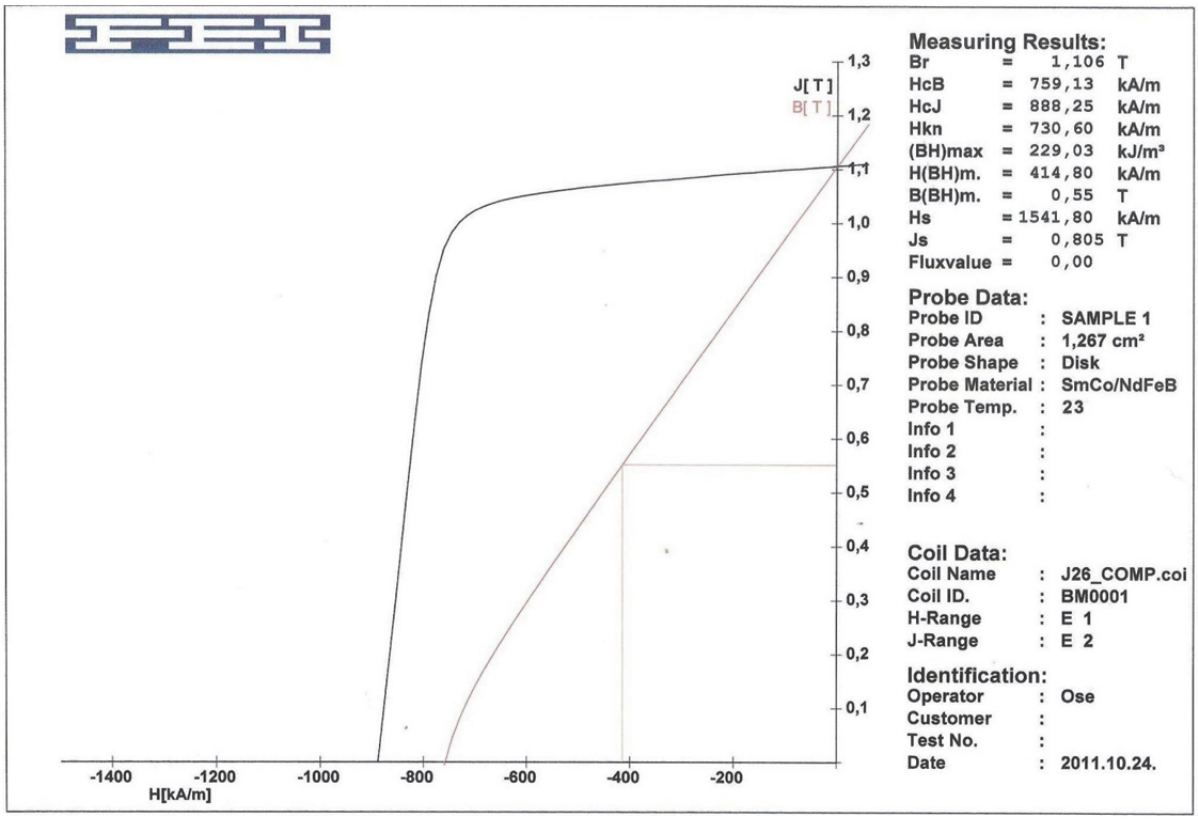

Fig. A.11 Test report for the first sample

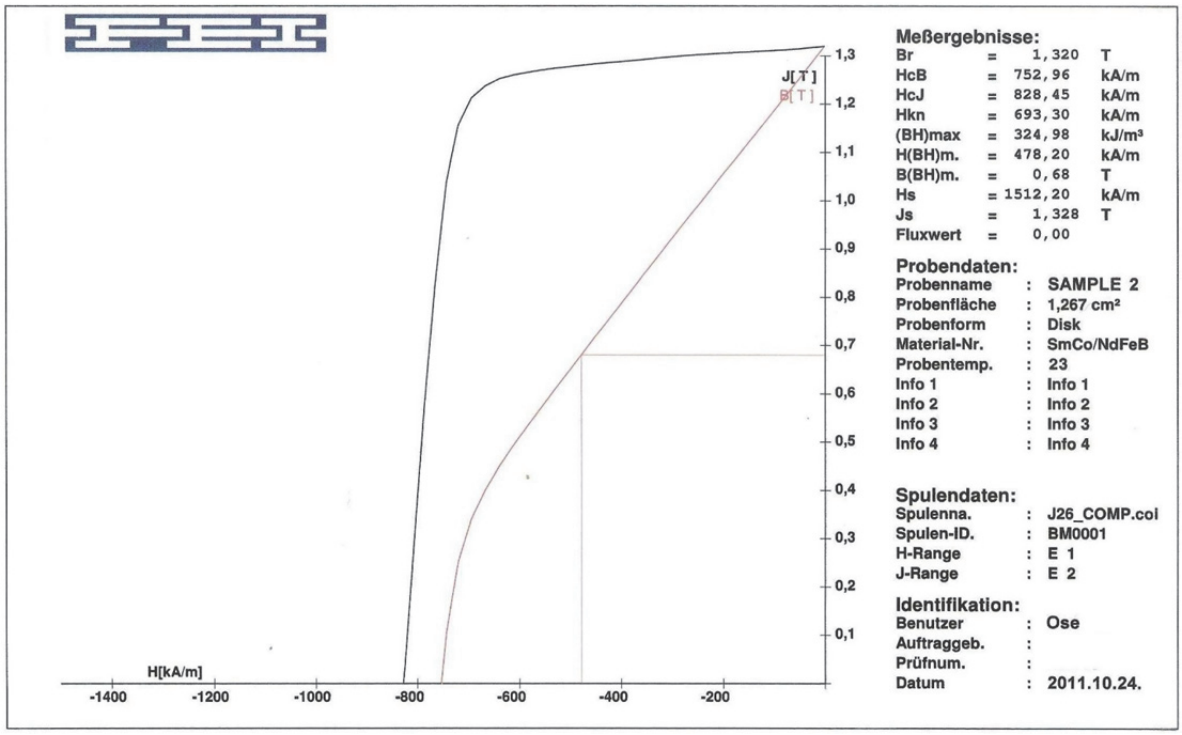

Fig. A.12 Test report for the second sample

Table A.1

Test results for NdFeB permanent magnets and catalogue data

Test number	Sample name	Test results (N42)			Catalogue data (N42)		
		B_r (T)	H_c (kA/m)	BH_{max} (kJ/m^3)	B_r (T)	H_c (kA/m)	BH_{max} (kJ/m^3)
1.	Sample 1	1.106	759.13	229.03	1.30–1.32	>875.4	318.3–334.2
2.	Sample 2	1.320	752.96	324.98			

Conclusions:

1. The magnetic properties — residual induction, coercive force and maximum product energy — vary for every magnet even from the same manufacturer and the same production set.
2. Usually the magnets have the magnetic properties in the range given in catalogues, but they may have values out of the given range (light red cells in table A.1).
3. In magnetic field modelling the properties are considered to be equal to all permanent magnets, but in reality it is not so, and thus the modelling results definitely will diverge from the real ones for some percentage.

Appendix 5

Example of CMC magnetic field calculation

One design variant of CMC is chosen to illustrate the main principles of magnetic field calculation in *QuickField* (*QF*). The problem is named "for example" (Fig. A.13). The *Magnetostatics* is chosen as problem type. For the model class the *Plane-parallel* is set. The axial length (L_z) is ten millimeters (10 mm), and the *Millimeters* are set as length units. The coordinate system is *Certesian*, and the precision is *Normal*. The geometry and data files by default are named the same ("for example") as the main/problem file.

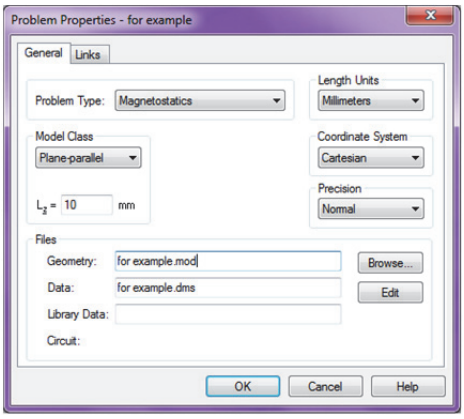

Fig. A.13 Dialog box of *Problem Properties*

This example CMC has the inner radius $R_1 = 10$ mm, the PMs' height $h_{PM} = 4$ mm, the air gap $\delta = 3$ mm, the outer radius $R_5 = 26$ mm, the magnetic coverage coefficient $\beta = 0.9$, pole pair number $p = 5$, and the PMs are made of strontium ferrite with coercive force $H_c = 225$ kA/m and residual induction $B_r = 0.38$ T.

For these variables the CMC drawing in *AutoCad* was made, file saved with extension .dxf. This drawing was imported in *QF*, and the geometric model looks as given in Fig. A.14. The *QF* automatically divides the drawing in vertexes, edges and blocks.

The labels are defined, after them the geometric objects are labelled accordingly. The yokes are labelled accordingly "Steel 3 In" (Fig. A.15) and "Steel 3 Out" (Fig. A.16), and for these labels are given the magnetization curve $B = f(H)$ (see subchapter 1.3.2., Fig. 1.18).

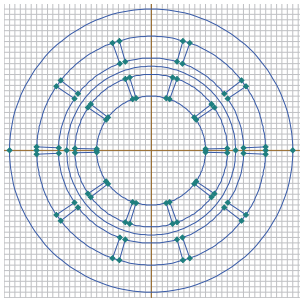

Fig. A.14 Geometric model of CMC in *QF*

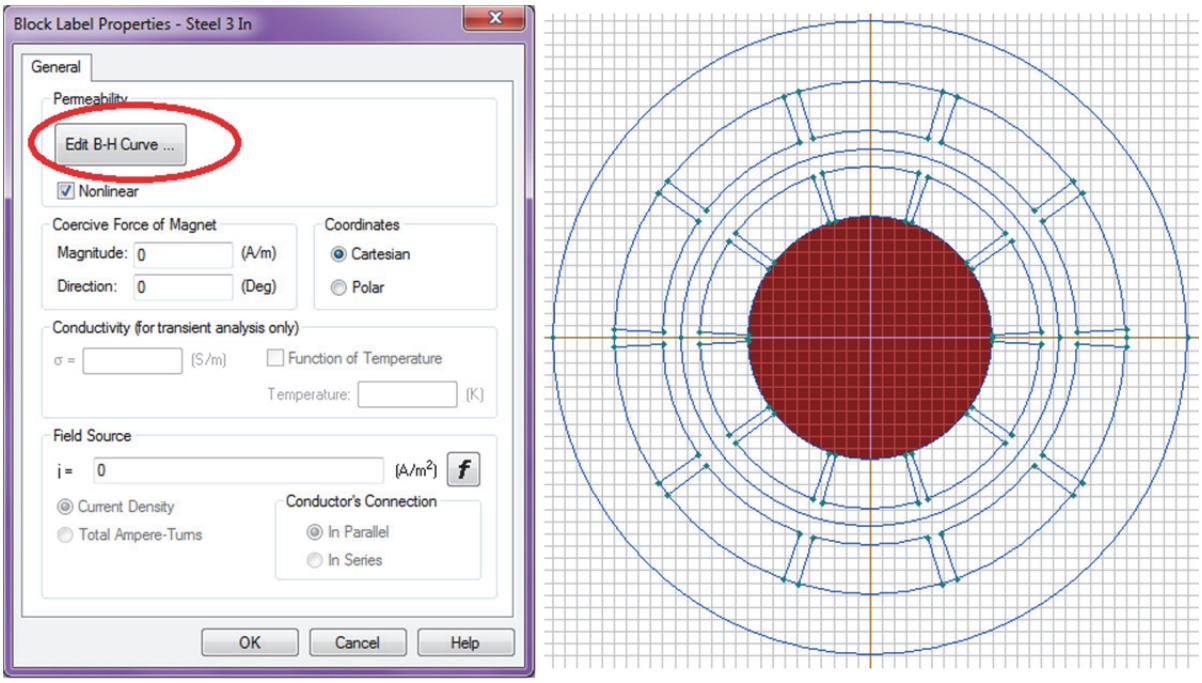

Fig. A.15 Labelling the inner yoke as “Steel 3 In”

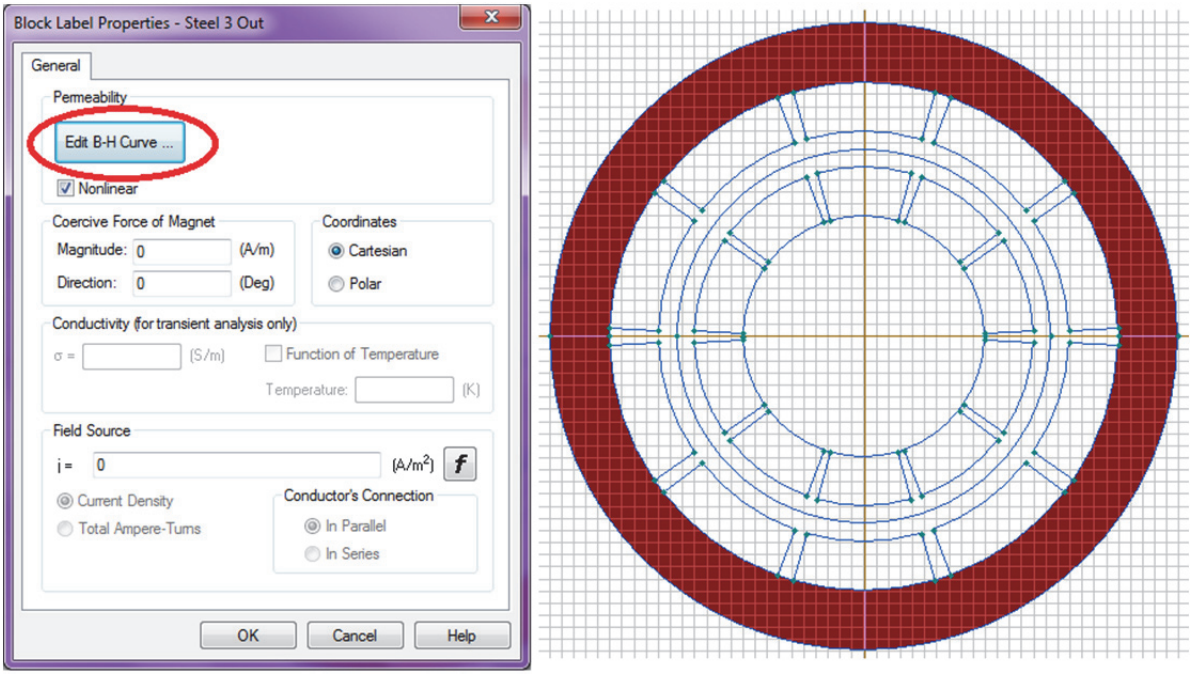

Fig. A.16 Labelling the outer yoke as “Steel 3 Out”

Between the inner and outer half coupling there is air with relative permeability $\mu_* = 1$. As the mechanical torque is calculated in the surface at circle by middle air gap radius, and this circle is drawn in, then for the air gap also two parts are labelled (Fig. A.17, A.18).

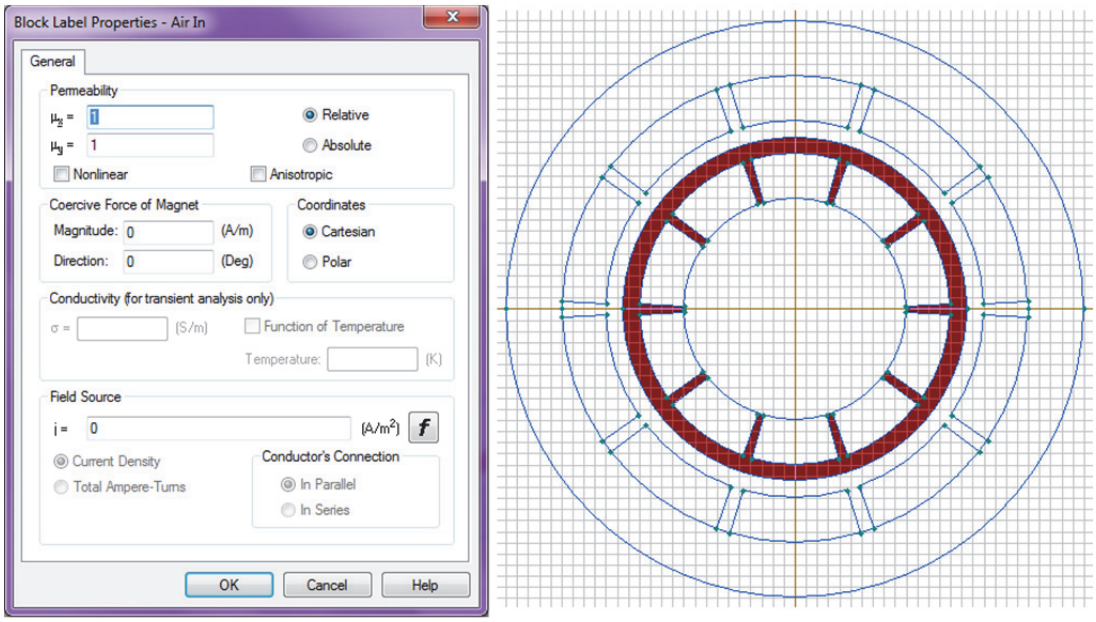

Fig. A.17 Labelling the inner part of air gap "Air In"

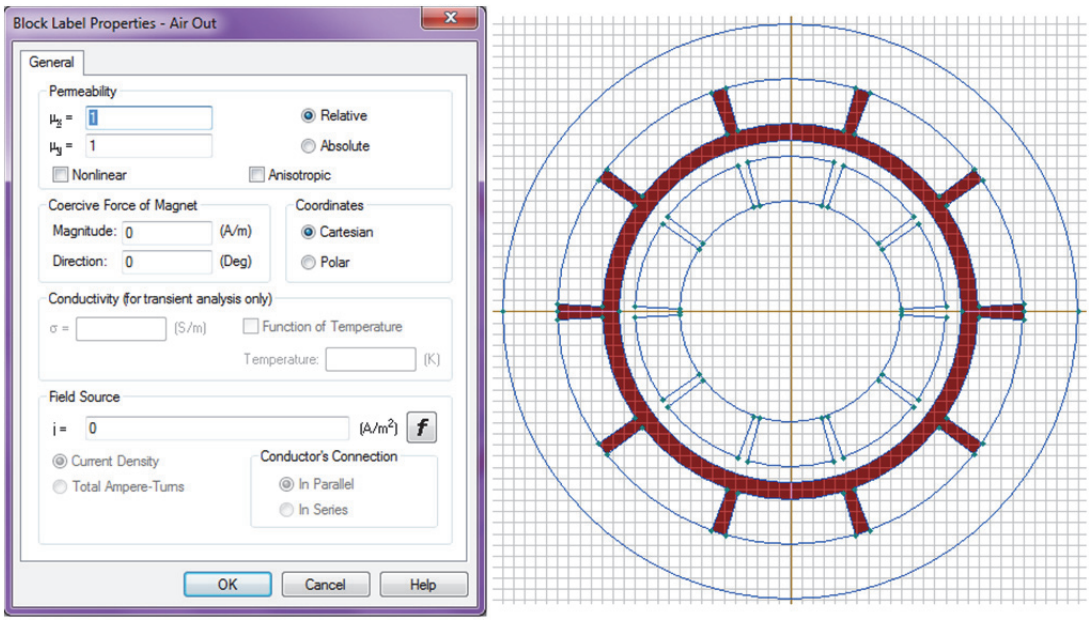

Fig. A.18 Labelling the outer part of air gap "Air Out"

The permanent magnets are also divided in inner and outer ones at the labelling (Fig. A.19, A.20), because of the necessity to simulate the turnings by an angle, and in this research the inner half coupling magnets are turned by an angle. From the given coercive force H_c and residual induction B_r the relative permeability is calculated (see chapter 1.2., (1.2)) for strontium ferrite ($\mu_* = 1.344$). With the permeability the PM material property is only described. To describe the magnetic field source the edges are used instead of "Coercive Force of Magnet" option in "Block Label Properties".

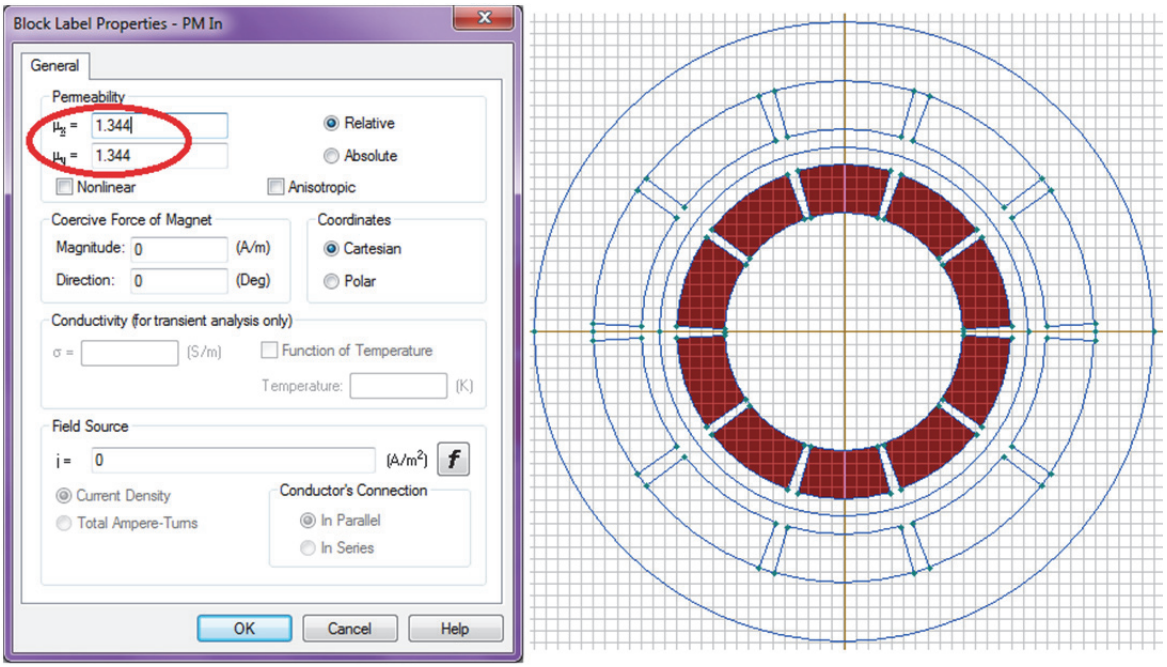

Fig. A.19 Labelling the PMs on inner half coupling “PM In”

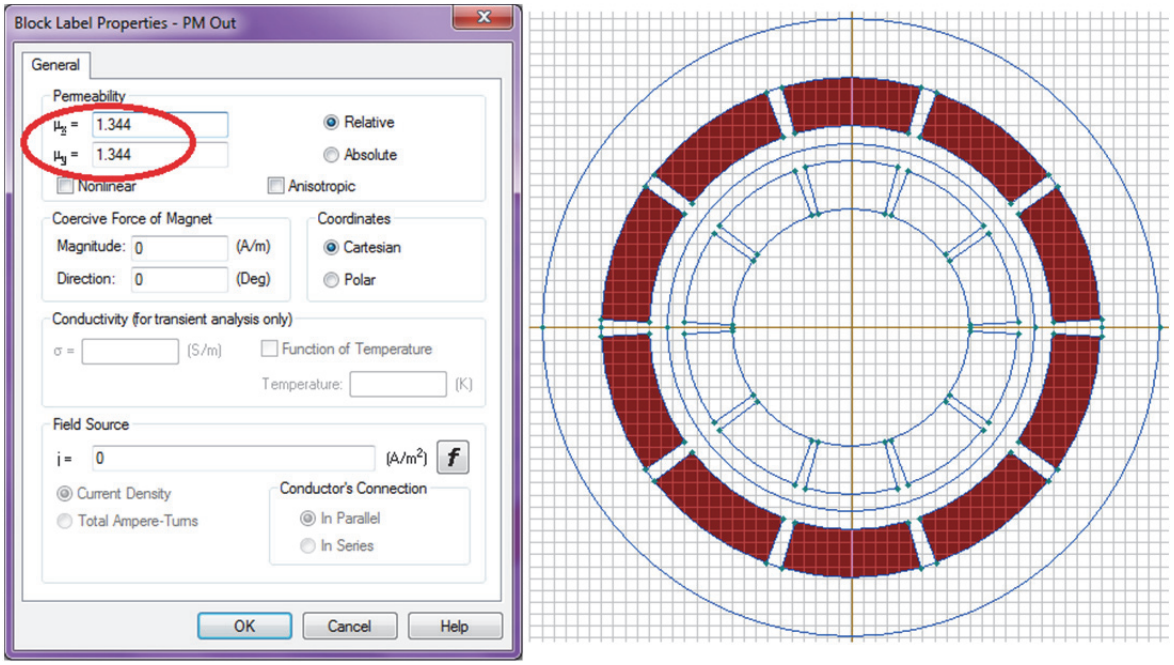

Fig. A.20 Labelling the PMs on outer half coupling “PM Out”

To define the magnetic field source the PMs’ edges are defined with the value of coercive force H_c = 225 kA/m (for strontium ferrite) as given in Fig. A.21 and A.22.

When the necessary objects are labelled and the labels are defined, the boundary conditions (see chapter 2.2) can be set. For the outer radius the Dirichlet condition/ magnetic potential $A = A_0$ is set: A_0 = 0 Wb/m (Fig. A.23).

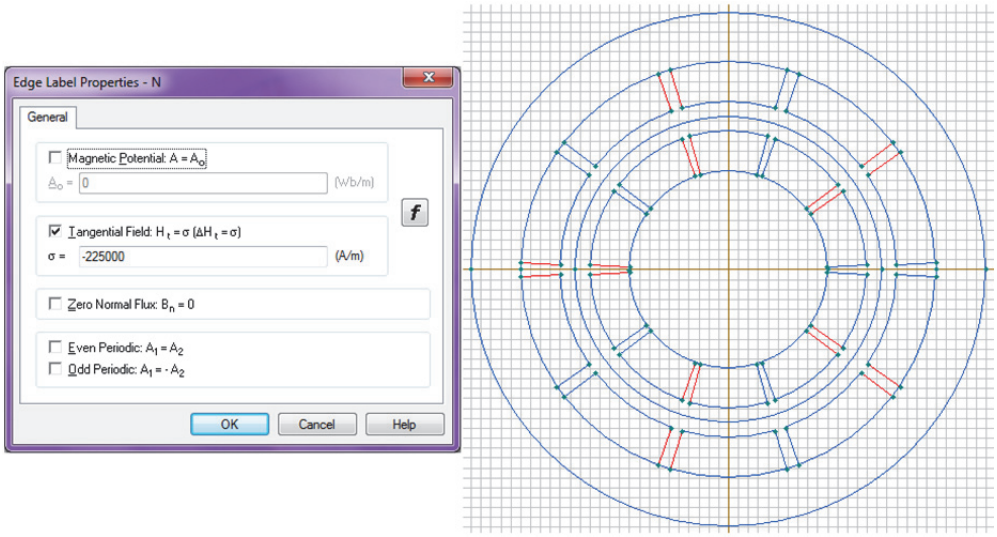

Fig. A.21 Labelling the PM north poles as “N”

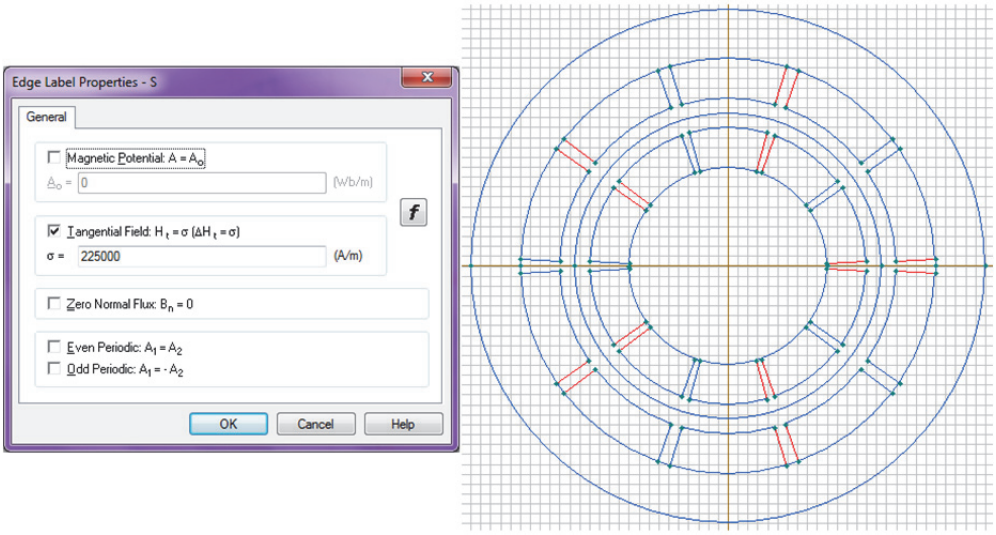

Fig. A.22 Labelling the PM south poles as “S”

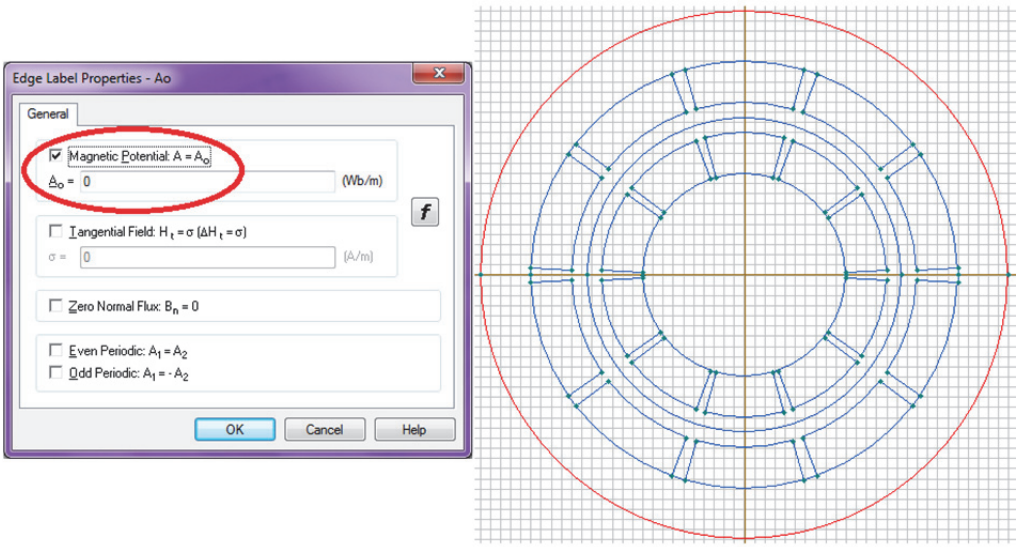

Fig. A.23 Labelling the outer radius as boundary

After the objects' labelling the mesh can be built (Fig. A.24).

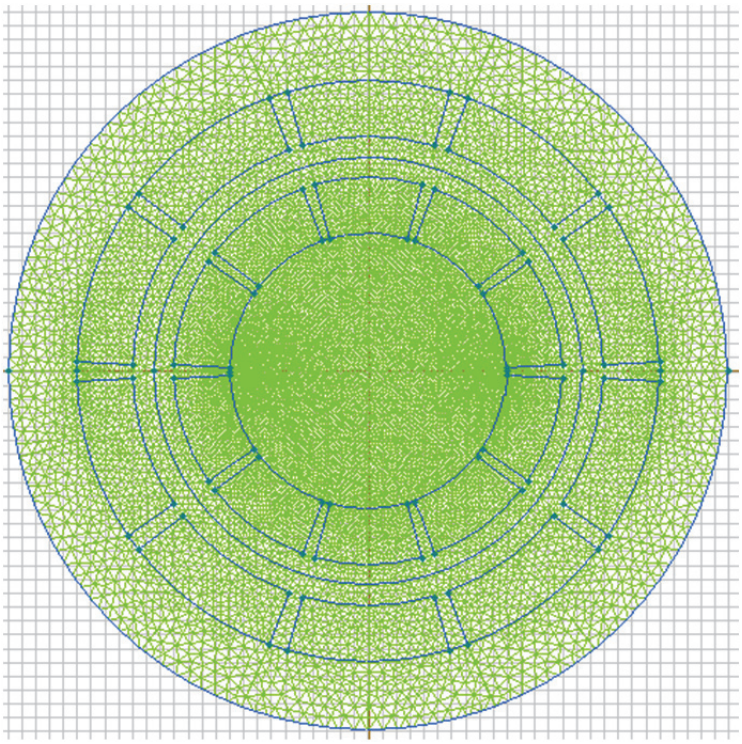

Fig. A.24 The built mesh

When the mesh is built, the problem can be solved — the magnetic field can be modelled, and by default the magnetic field is shown with lines as in Fig. A.25. But for more obvious field picture to see the places of magnetic saturation, it is expressed with flux density (Fig. A.26).

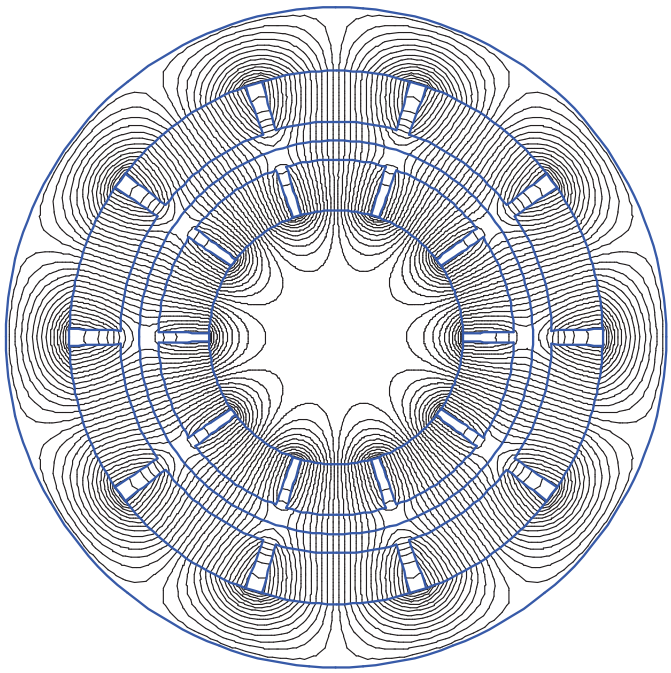

Fig. A.25 The magnetic field by magnetic field lines (scale is 0.0001 Wb)

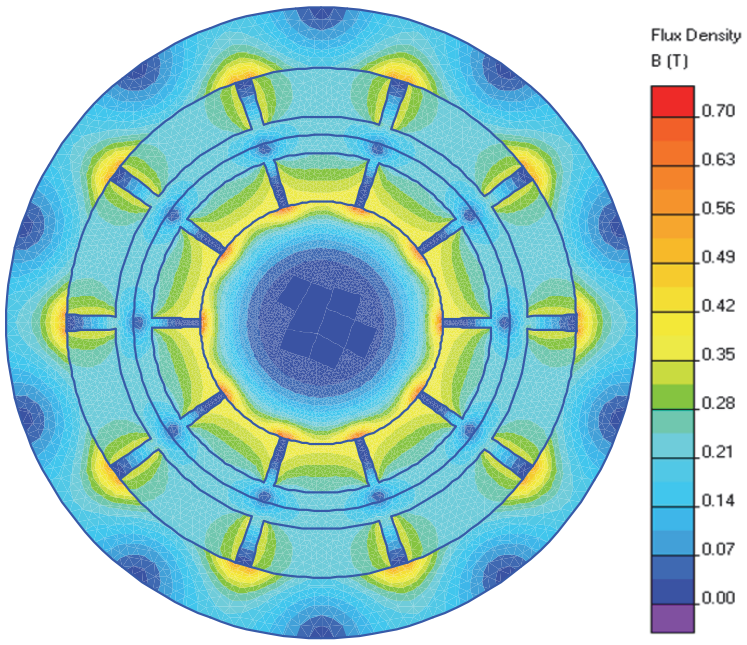

Fig. A.26 The magnetic field by flux density

The magnetic saturation is higher at the corners where the permanent magnets are placed on the steel. At these corners the magnetic flux density is monitored (in inner half coupling $B_{max\ in}$ (Fig. A.27), and in outer half coupling $B_{max\ out}$ (Fig. A.28)). To obtain the magnetic flux density value the "local values" tool is used at these corners, which are zoomed in. The obtained values are rounded to three decimal places. Thus such magnetic flux density values are obtained for this CMC with strontium ferrite magnets: $B_{max\ in} = 0.690$ T and $B_{max\ out} = 0.557$ T.

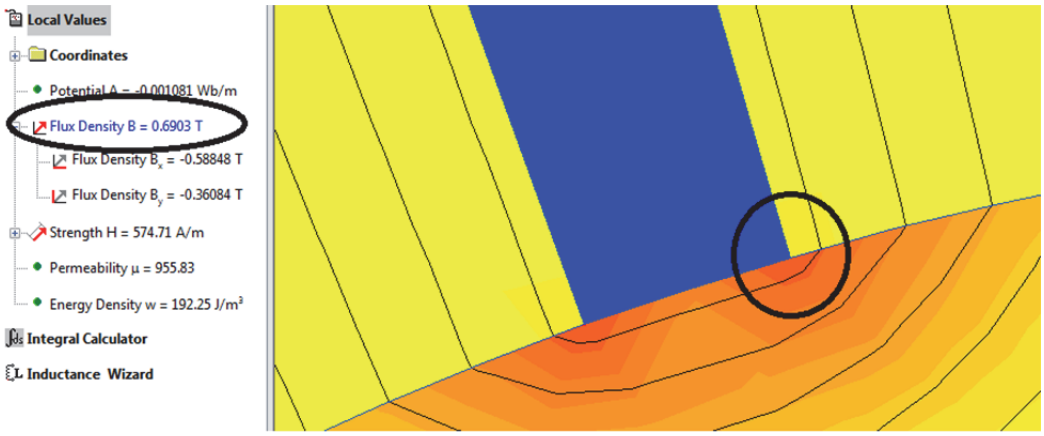

Fig. A.27 The maximum magnetic flux density in inner half coupling

After the acquisition of magnetic flux density values it is necessary to return to geometric model, mark the PMs and the steel in inner half coupling, then rotate them by 18 geometric degrees (°geom) (Fig. A.29). This angle is obtained by (1.3), for more information see chapter 1.4.

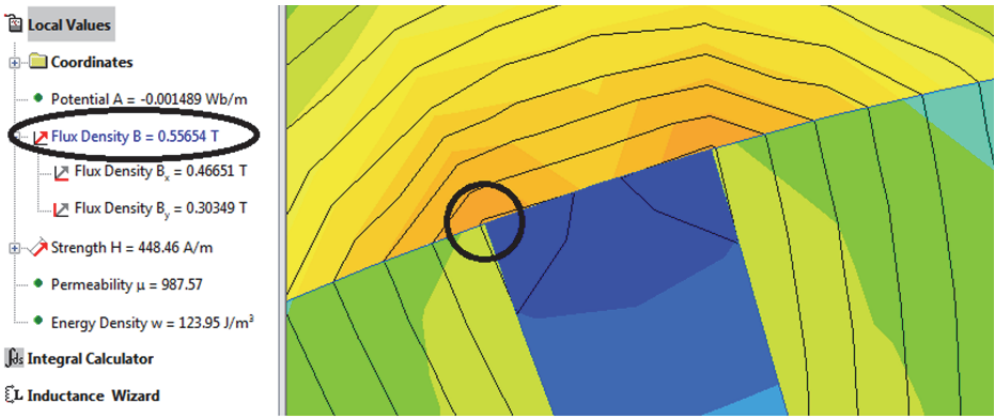

Fig. A.28 The maximum magnetic flux density in outer half coupling

At this position the CMC has its maximum value of mechanical torque. The torque value is calculated at the surface by middle radius of air gap (Fig. A.30) and it is acquired using the “integral calculator” tool (Fig. A.31).

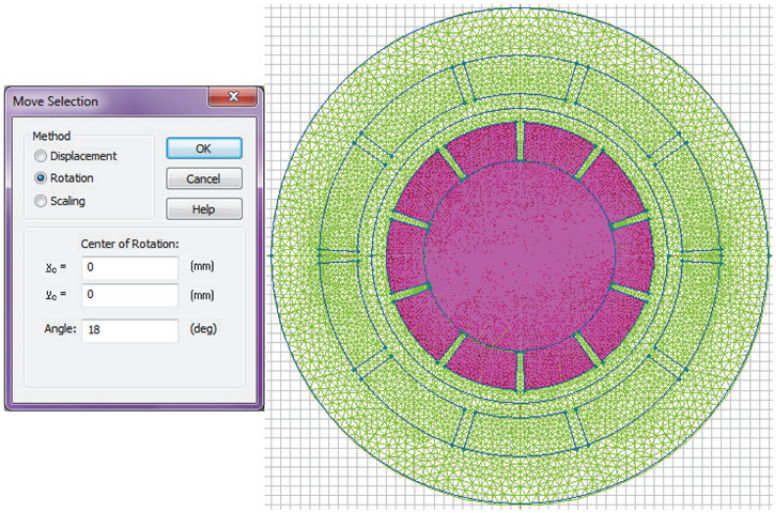

Fig. A.29 Turning the inner half coupling by 18 (°geom)

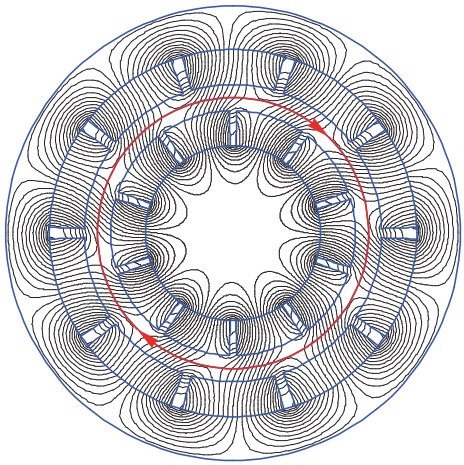

Fig. A.30 The contour (red line) for acquisition of mechanical torque

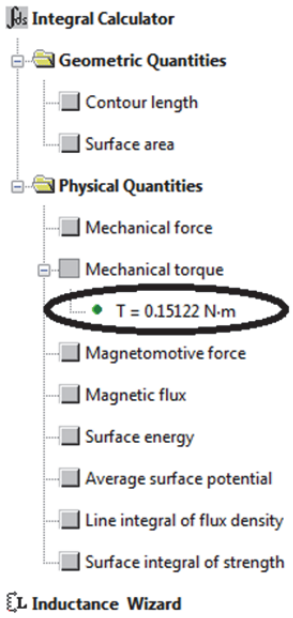

Fig. A.31 The value of mechanical torque

The values of mechanical torque are rounded to four decimal places, and in this case the torque is M_{max} = 0.1512 Nm.

This whole process from problem defining till acquisition of the necessary results is performed for all variants of experiment plan (more than a thousand).

Appendix 6

Elimination diagrams for M_{max}/V

The elimination diagrams show how the correlation (for values from formula with the simulation data; in per cent) changes at different numbers of parts N in the formula (the number of elementary functions plus one free element/ coefficient).

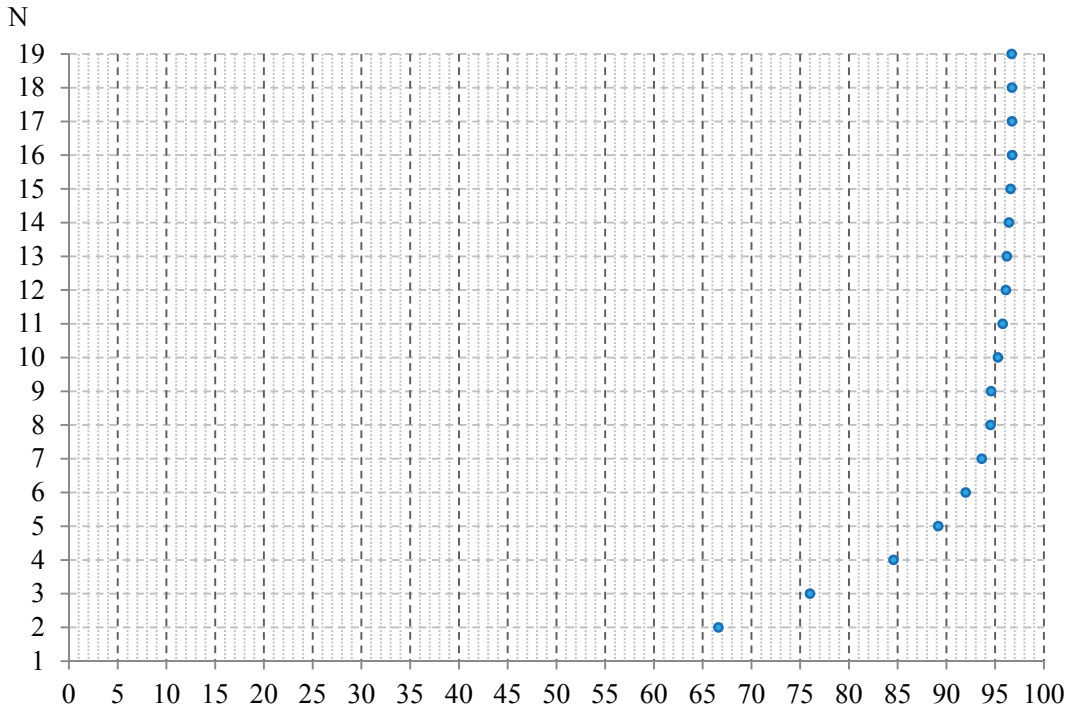

Fig. A.32 Correlation for NdFeB magnets ($\mu_* = 1.061$) with pole pair number range p = 1–4

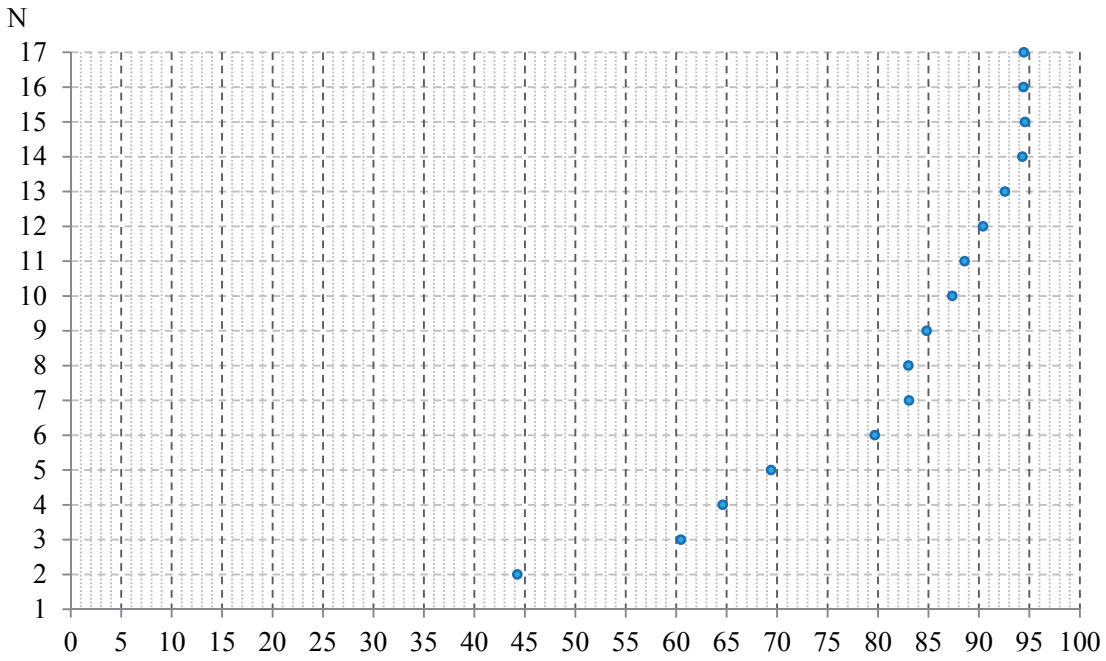

Fig. A.33 Correlation for NdFeB magnets ($\mu_* = 1.061$) with pole pair number range p = 5–6

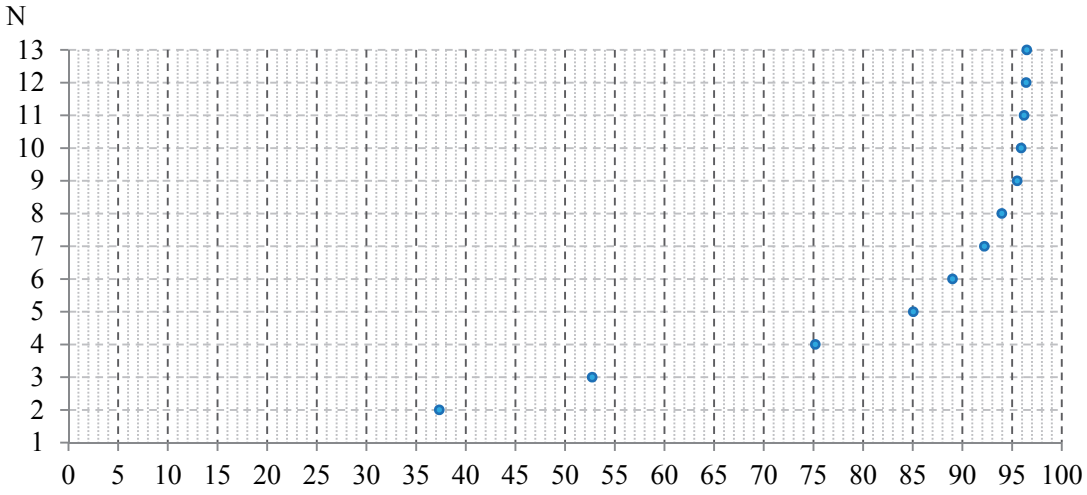

Fig. A.34 Correlation for NdFeB magnets ($\mu_* = 1.061$) with pole pair number range p = 7–9

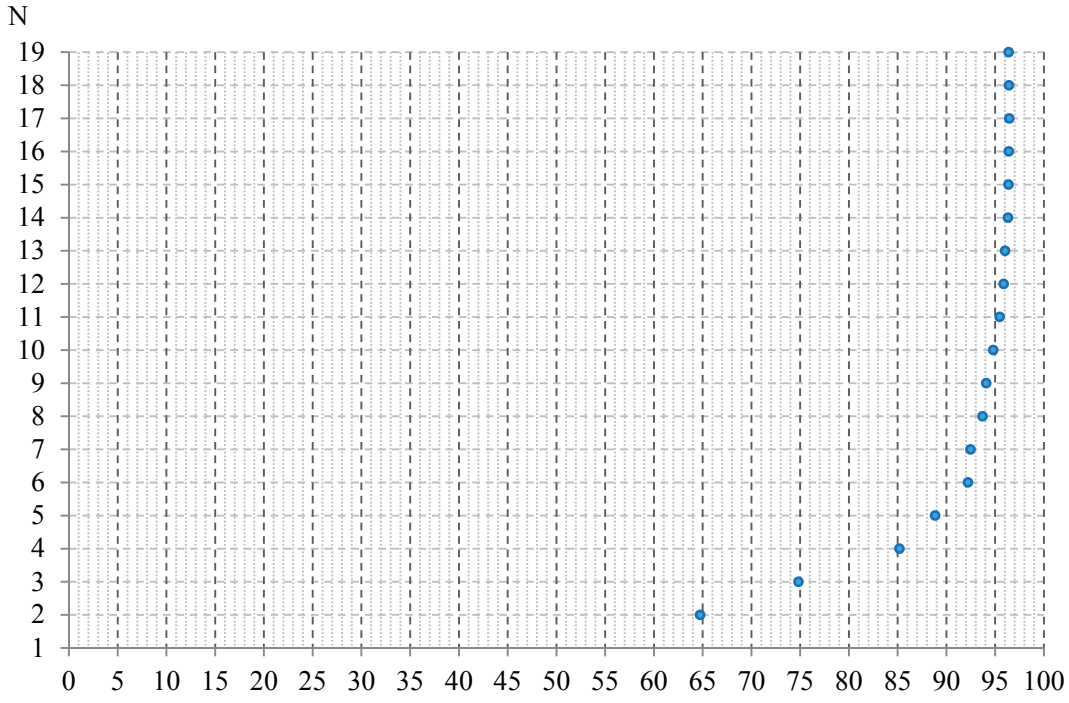

Fig. A.35 Correlation for SmCo magnets ($\mu_* = 1.094$) with pole pair number range p = 1–4

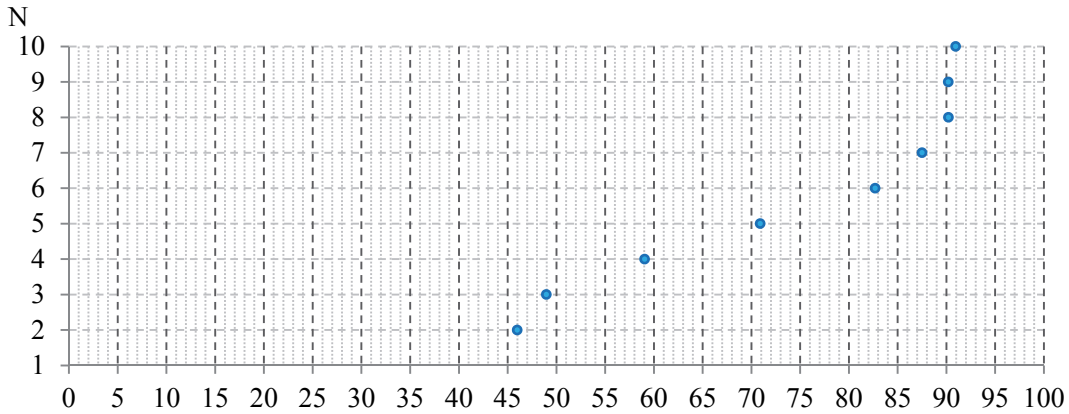

Fig. A.36 Correlation for SmCo magnets ($\mu_* = 1.094$) with pole pair number range p = 5–6

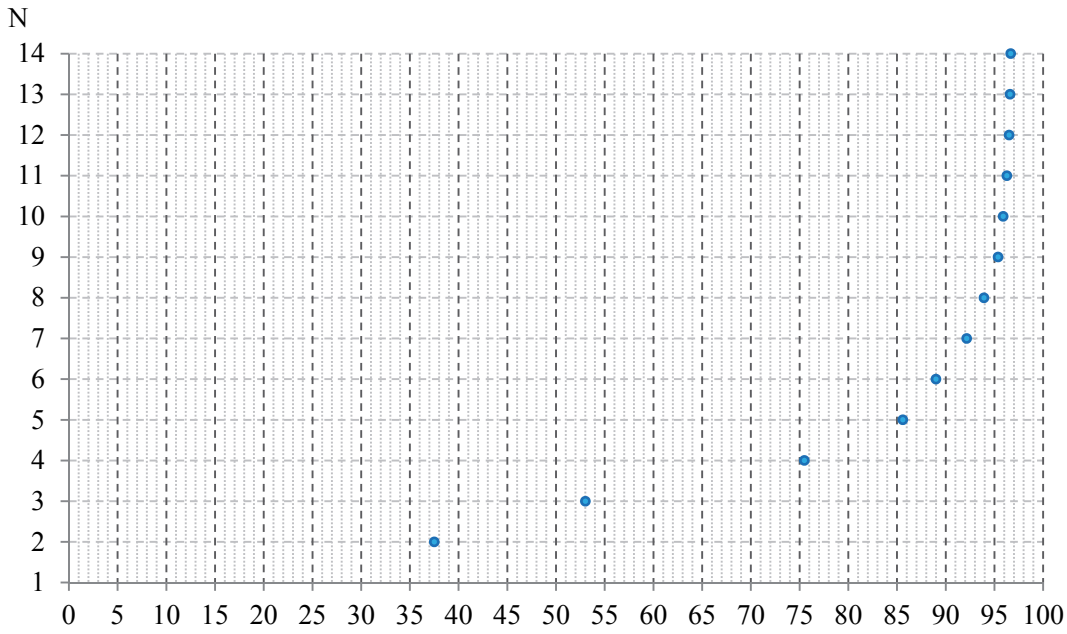

Fig. A.37 Correlation for SmCo magnets ($\mu_* = 1.094$) with pole pair number range $p = 7–9$

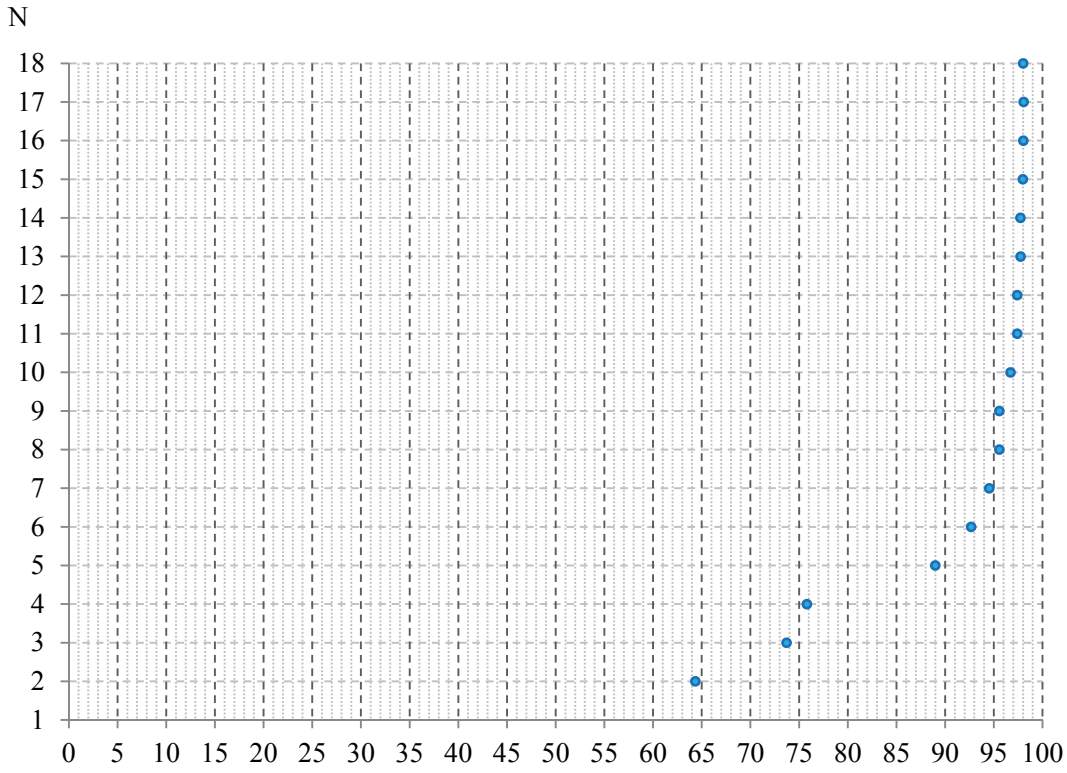

Fig. A.38 Correlation for Ba-ferrite magnets ($\mu_* = 1.114$) with pole pair number range $p = 1–2$

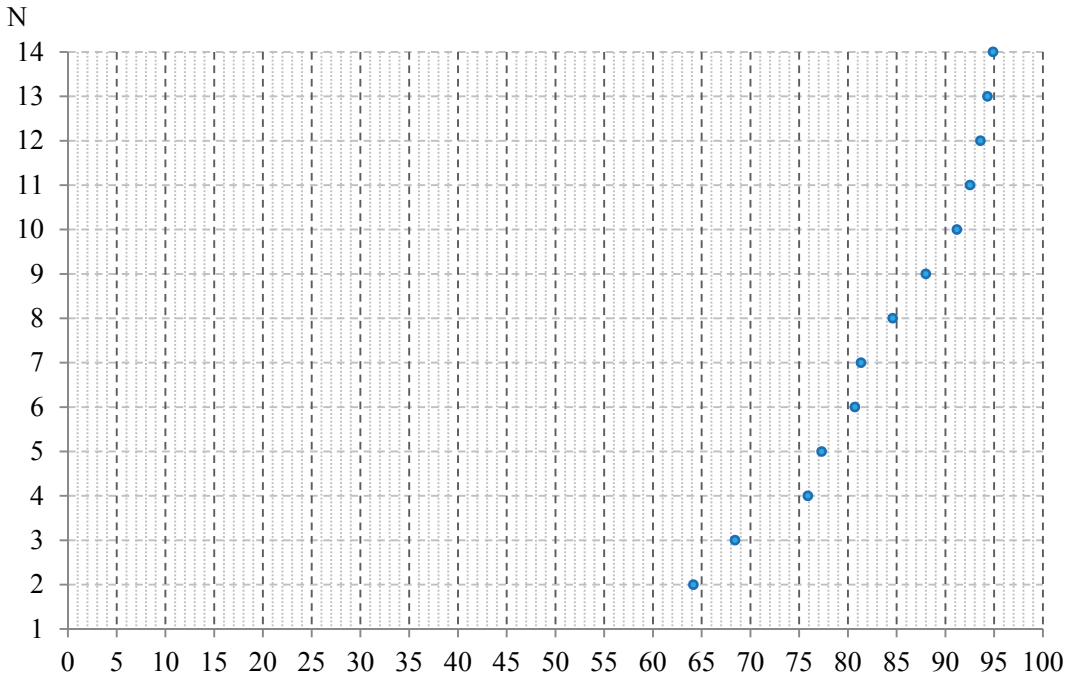

Fig. A.39 Correlation for Ba-ferrite magnets ($\mu_* = 1.114$) with pole pair number range $p = 3–5$

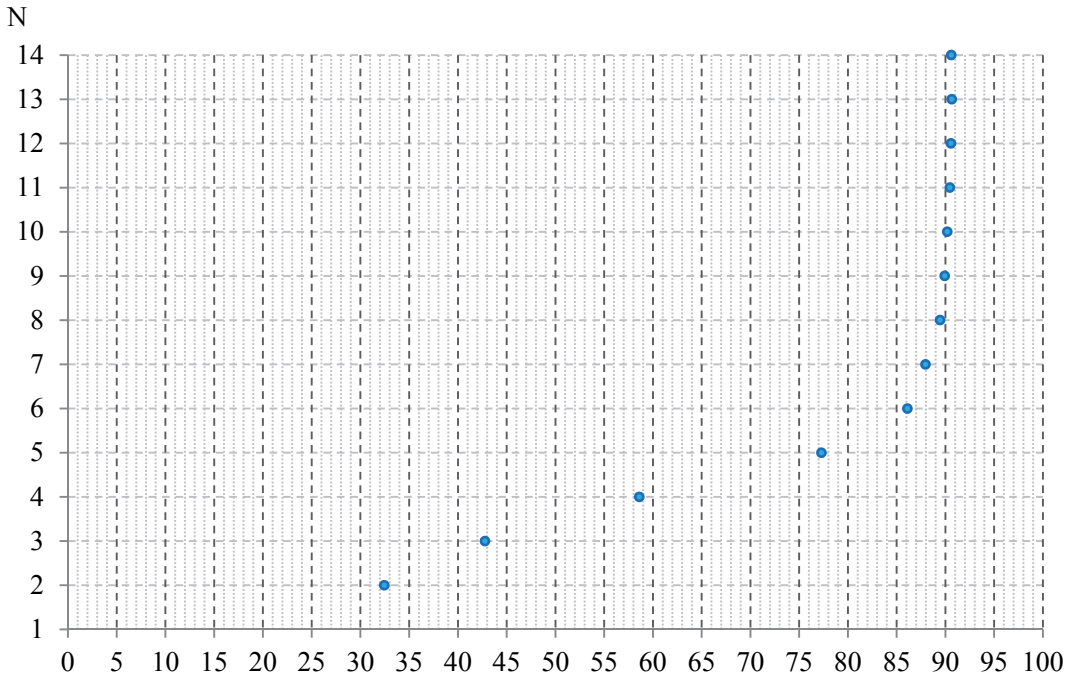

Fig. A.40 Correlation for Ba-ferrite magnets ($\mu_* = 1.114$) with pole pair number range $p = 6–9$

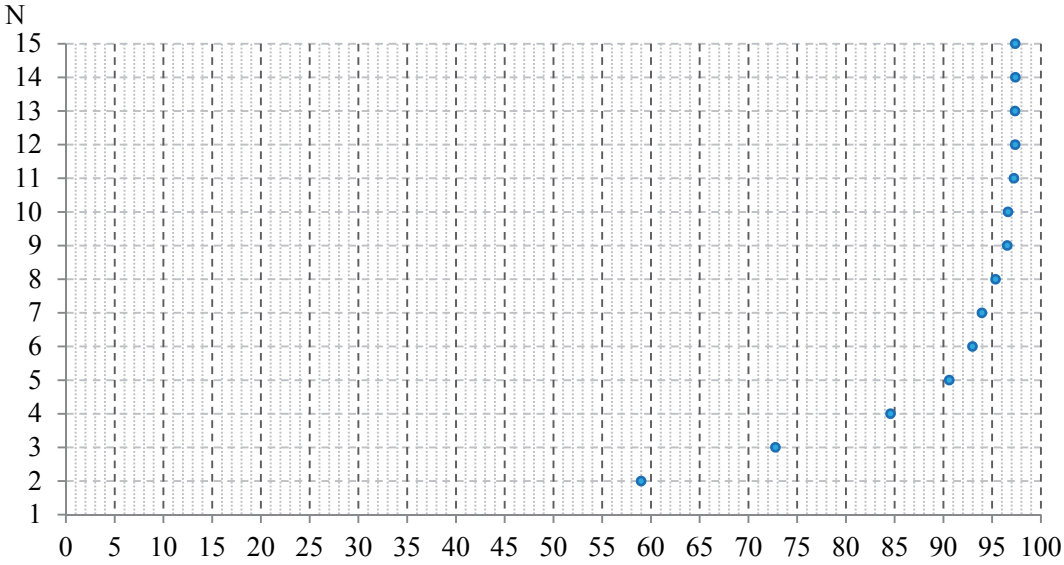

Fig. A.41 Correlation for Sr-ferrite magnets ($\mu_* = 1.344$) with pole pair number range $p = 1–2$

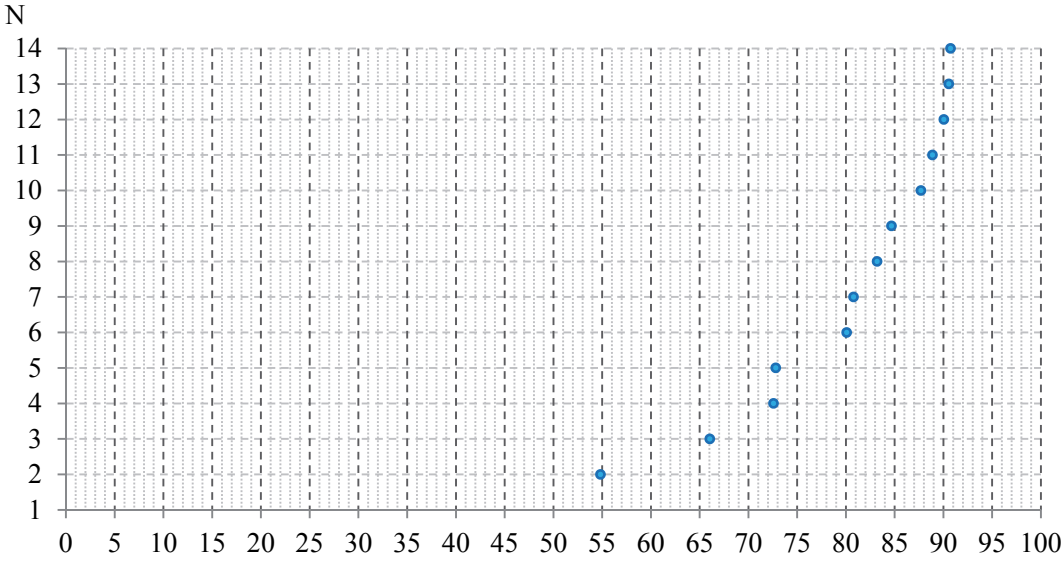

Fig. A.42 Correlation for Sr-ferrite magnets ($\mu_* = 1.344$) with pole pair number range $p = 3–6$

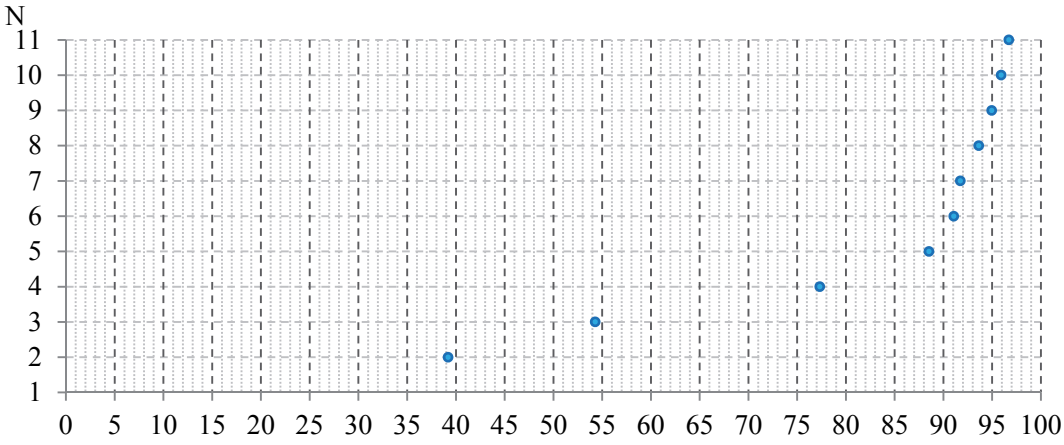

Fig. A.43 Correlation for Sr-ferrite magnets ($\mu_* = 1.344$) with pole pair number range $p = 7–9$

Appendix 7

Elimination diagrams for B_{max}

The elimination diagrams show how the correlation (for values from formula with the data calculated from magnetic field modeling; in per cent) changes at different numbers of parts N in the formula (the number of elementary functions plus one free element/ coefficient). These diagrams are for couplers with PMs made of NdFeB or SmCo.

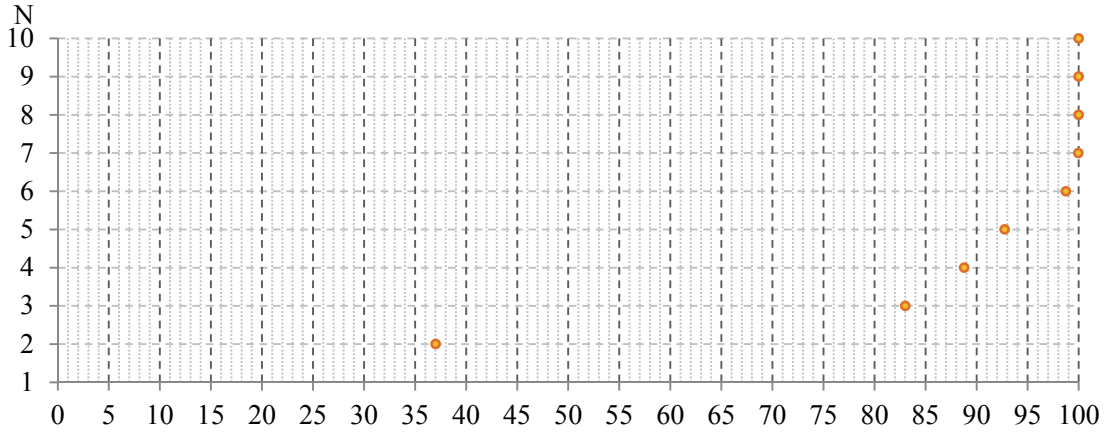

Fig. A.44 Correlation for $B_{max\ in}$ with pole pair number p = 1

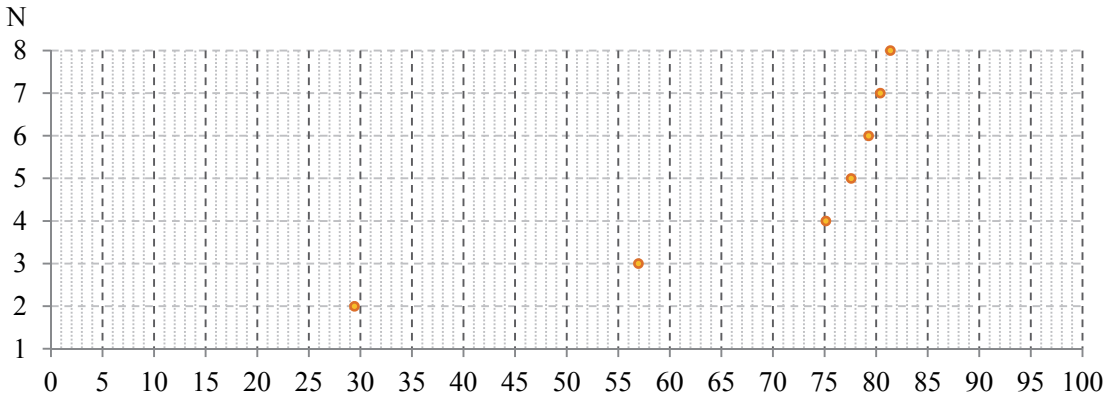

Fig. A.45 Correlation for $B_{max\ in}$ with pole pair number range p = 2–3

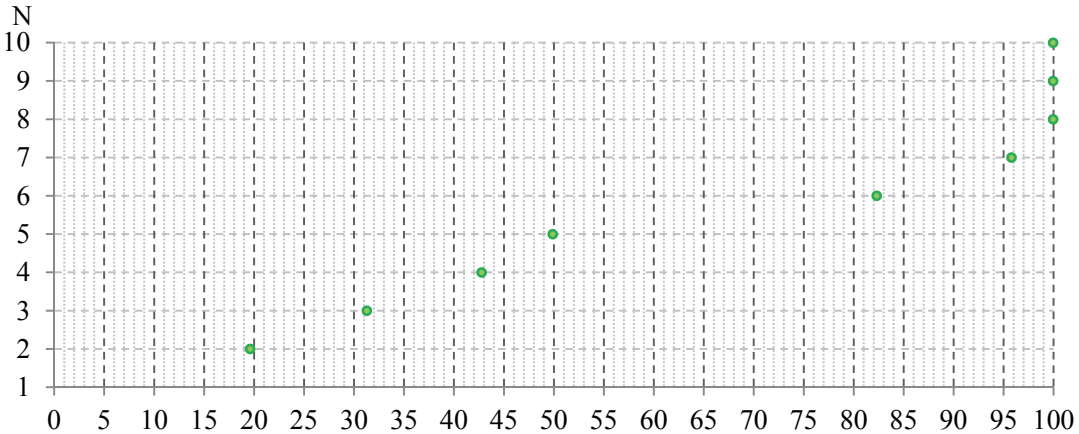

Fig. A.46 Correlation for $B_{max\ out}$ with pole pair number p = 1

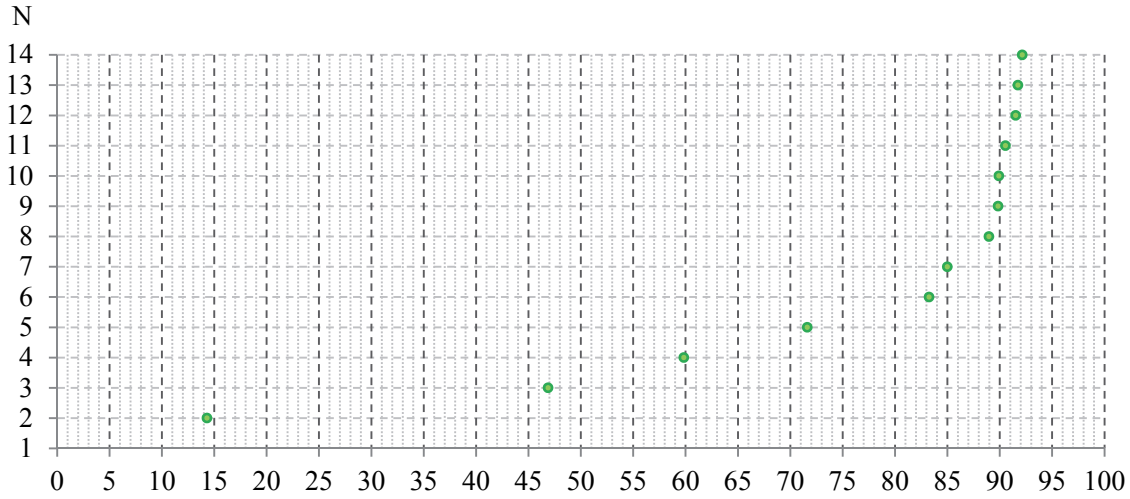

Fig. A.47 Correlation for $B_{max\ out}$ with pole pair number range p = 2–3

Appendix 8

Optimization and analysis in *SIMCA*

In one workspace two spreadsheets are set: one for rare-earth alloy material, second — simple ferrite material (Fig. A.48). In this figure the imported variables can also see. First is the number of experiment thus defining the primary ID. The respective variables are defined following: independent variables — „X variables", dependent variables — „Y variables".

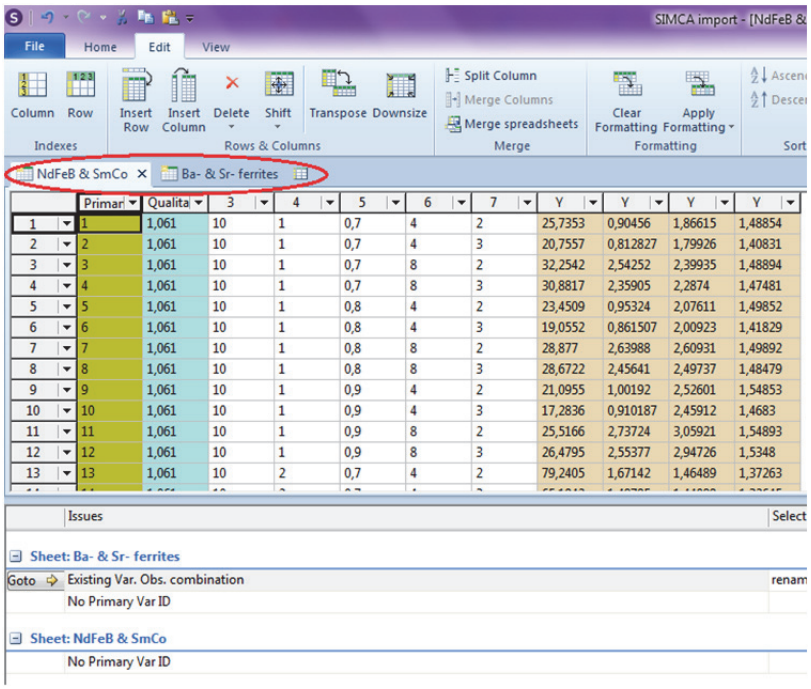

	Primar	Qualita	3	4	5	6	7	Y	Y	Y	Y
1	1	1,061	10	1	0,7	4	2	25,7353	0,90456	1,86615	1,48854
2	2	1,061	10	1	0,7	4	3	20,7557	0,812827	1,79926	1,40831
3	3	1,061	10	1	0,7	8	2	32,2542	2,54252	2,39935	1,48894
4	4	1,061	10	1	0,7	8	3	30,8817	2,35905	2,2874	1,47481
5	5	1,061	10	1	0,8	4	2	23,4509	0,95324	2,07611	1,49852
6	6	1,061	10	1	0,8	4	3	19,0552	0,861507	2,00923	1,41829
7	7	1,061	10	1	0,8	8	2	28,877	2,63988	2,60931	1,49892
8	8	1,061	10	1	0,8	8	3	28,6722	2,45641	2,49737	1,48479
9	9	1,061	10	1	0,9	4	2	21,0955	1,00192	2,52601	1,54853
10	10	1,061	10	1	0,9	4	3	17,2836	0,910187	2,45912	1,4683
11	11	1,061	10	1	0,9	8	2	25,5166	2,73724	3,05921	1,54893
12	12	1,061	10	1	0,9	8	3	26,4795	2,55377	2,94726	1,5348
13	13	1,061	10	2	0,7	4	2	79,2405	1,67142	1,46489	1,37263

Fig. A.48 Two spreadsheets in one workspace

The summary information is available (Fig. A.49). The 6 independent variables and the 4 dependent variable make together 10 variables in each spreadsheet. The number of experiments/observations (648) is also given.

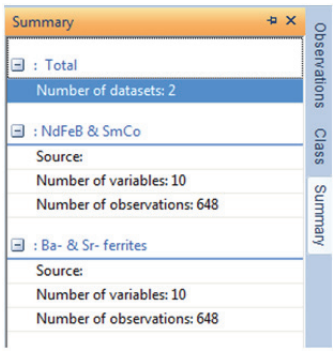

Fig. A.49 Summary for spreadsheets

The further analysis examples are given for the case of PMs made of rare-earth alloy.

The scatter plot of the first variable "Var_1" (μ_*) is given in Fig. A.50. The Var_1 is defined as a qualitative variable, thus two values as 1 (with $\mu_* = 1.061$) and 2 ($\mu_* = 1.094$) according at the first half and second half of data set are placed.

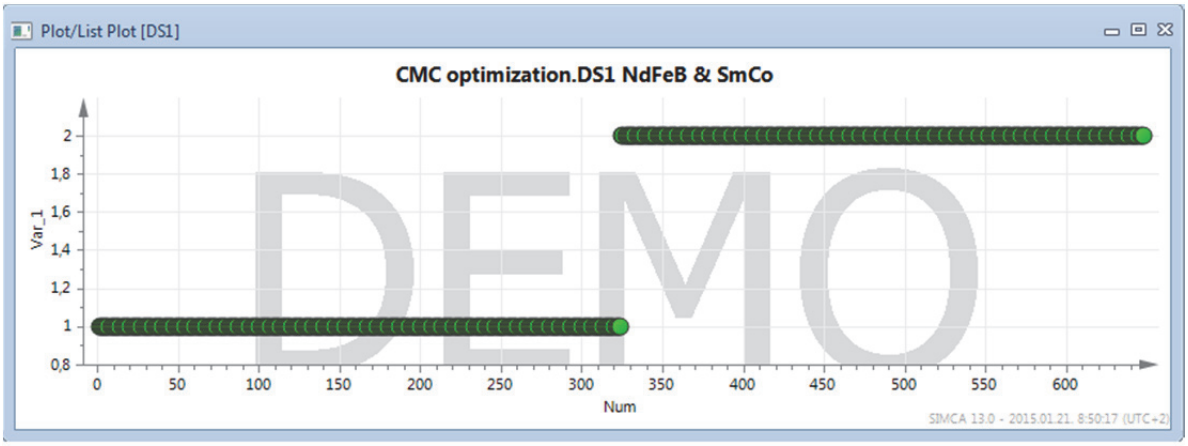

Fig. A.50 Scatter plot for Var_1 (μ_*)

The scatter plots of all the rest independent variables — from Var_2 till Var_6 — are given in according figures from Fig. A.51 till Fig. A.55. These variables are defined as quantitative and the real values are also given in the plots.

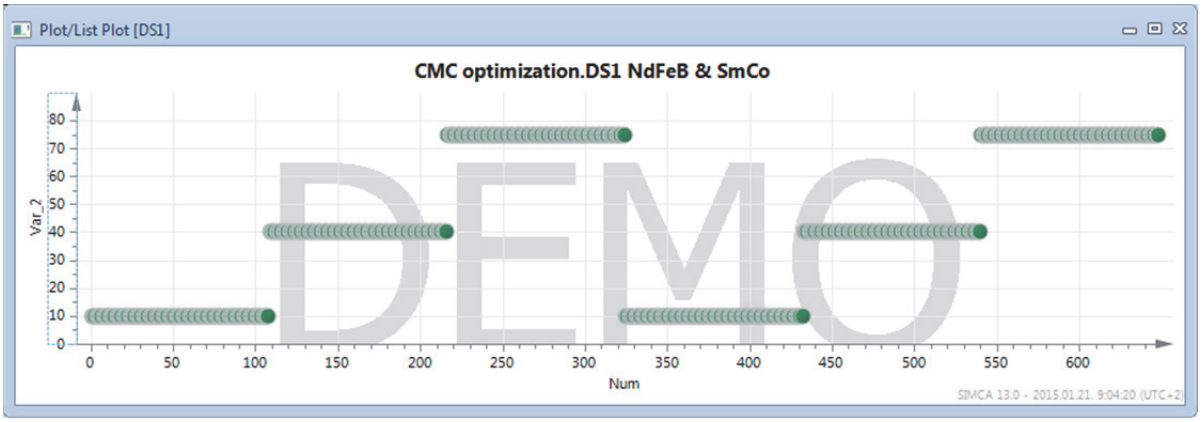

Fig. A.51 Scatter plot for Var_2 (l)

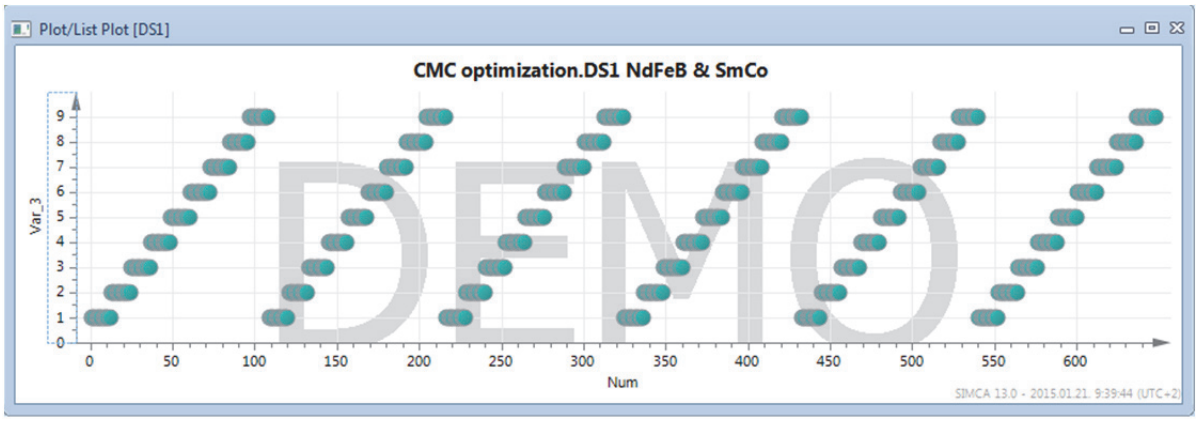

Fig. A.52 Scatter plot for Var_3 (p)

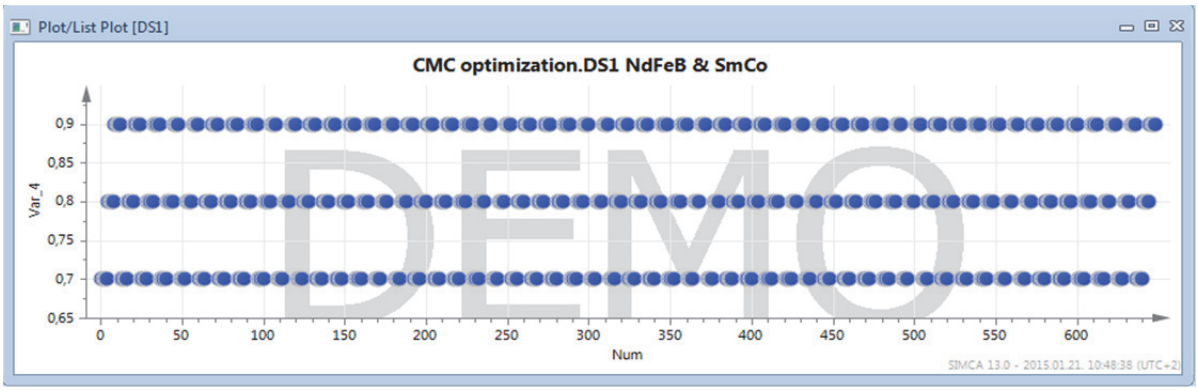

Fig. A.53 Scatter plot for Var_4 (β)

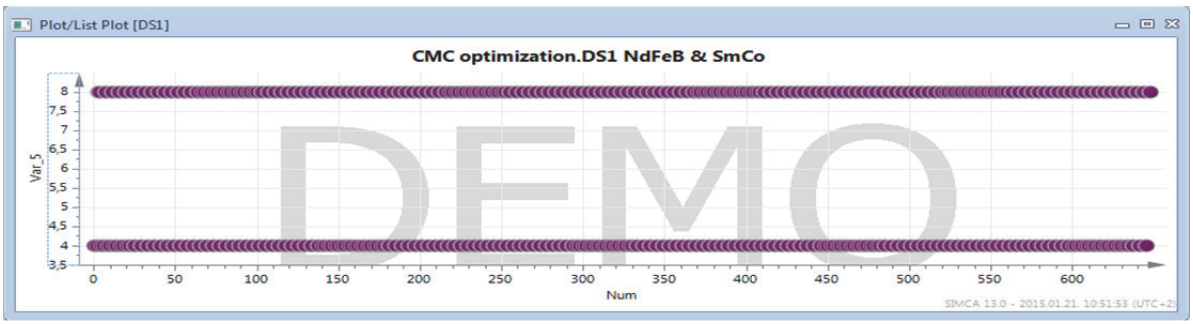

Fig. A.54 Scatter plot for Var_5 (h_{PM})

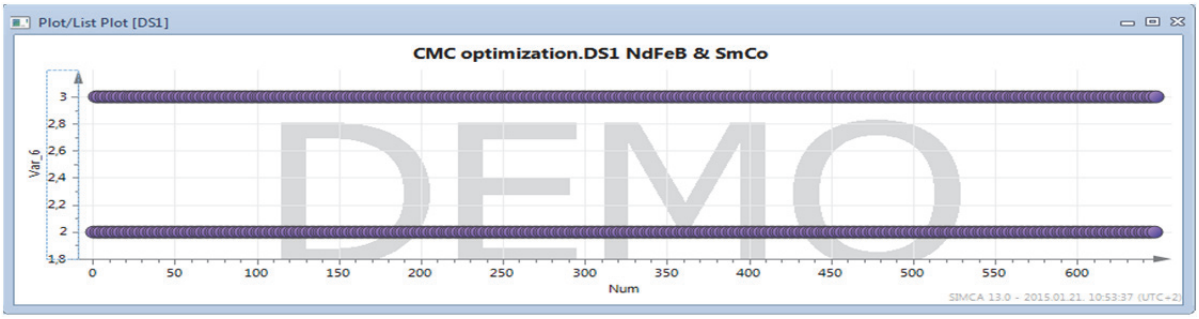

Fig. A.55 Scatter plot for Var_6 (δ)

For two dependent variables M_{max}/V and M_{max} the scatter plots are also given according in Fig. A.56 and A.57.

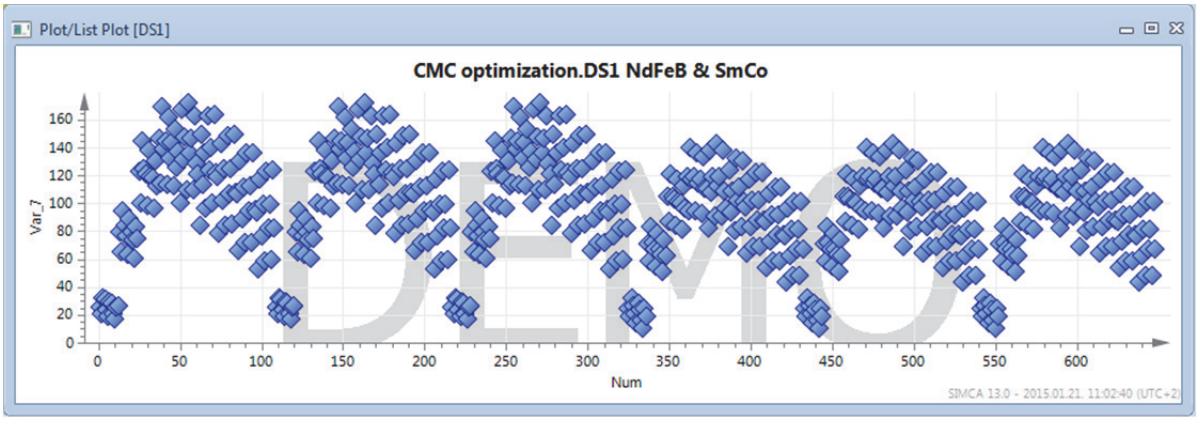

Fig. A.56 Scatter plot for Var_7 (M_{max}/V)

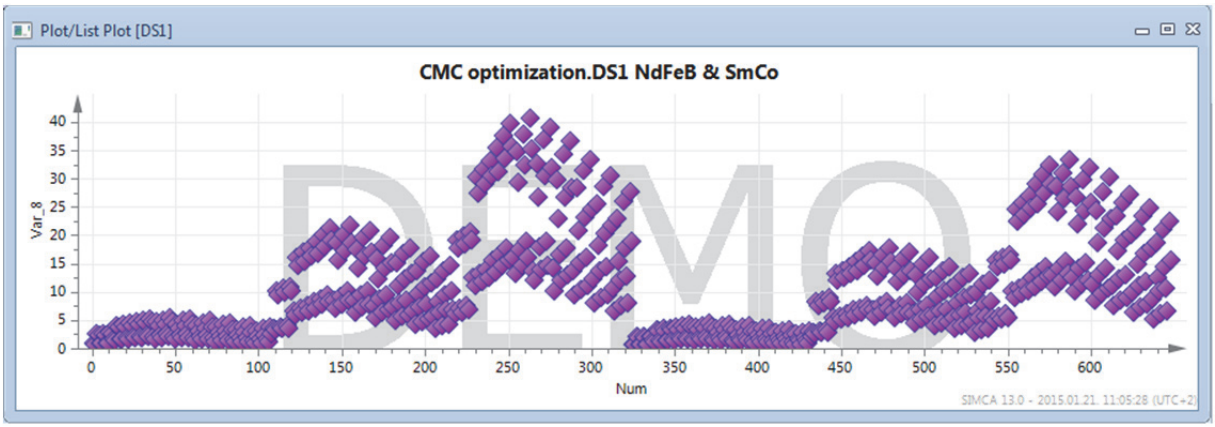

Fig. A.57 Scatter plot for Var_8 (M_{max})

From Fig. A.56 can be seen that optimum point should be in the data part where the PMS are made of NdFeB. The situation is similar with the Var_8 (M_{max}) in Fig. A.57 where the optimum point maximizing M_{max} is also in the NdFeB magnets' case. The NdFeB material is taken into account and from that data set dome points are overviewed closer, taking the top three points (Fig. A.58). Some data corresponding to these points are given in table A.2.

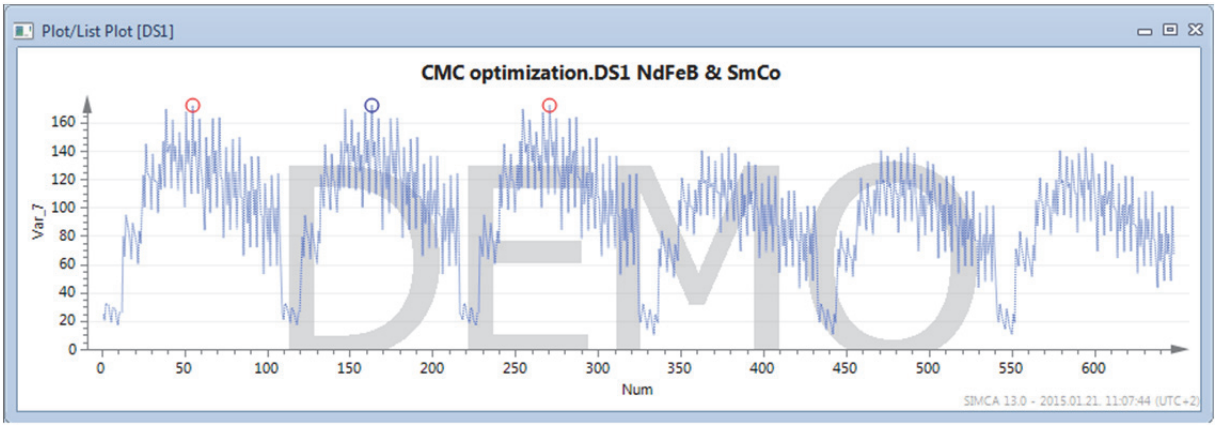

Fig. A.58 A plot for Var_7 (M_{max}/V)

Table A.2

Data for three potential optimum points

Point	Experiment ID	M_{max}/V (Nm/m^3)	M_{max} (Nm)	l (mm)	B_{max} (T)	
					Inner half coupling	Outer half coupling
1.	55	172.27	4.93	10	$B \leq 1.7$ & thus also <1.8	
2.	163	172.27	19.72	40		
3.	271	172.27	36.97	75		

The rest independent variables (excluding the axial length l) are equal to each of these points. It can be seen that all these points are optimum points when the M_{max}/V is maximized with respect to all independent variables.

The next step is the subsystem (design of these three points) optimization by M_{max} with respect to axial length l as the only varying variable in this situation. The conclusion is that the optimum is, of course, at the highest value of axial length l. The optimum point is found and all the values of every variable are given in the chapter 4.4.

The analysis of one more design parameter (pole pair number p) is given that influence the characteristics M_{max}/V (Fig. 59) and M_{max} (Fig. A.60).

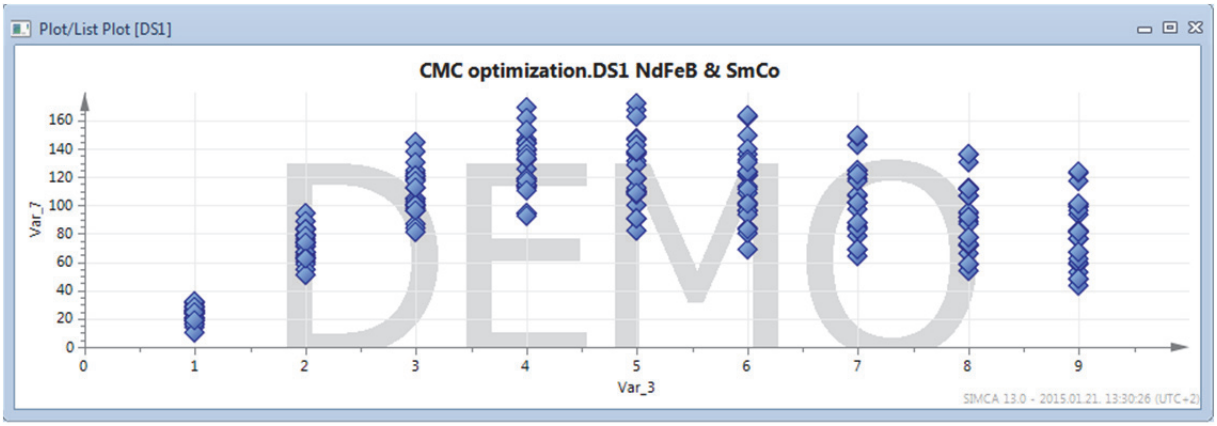

Fig. A.59 M_{max}/V by p

From Fig. A.59 can be seen that the highest values of M_{max}/V will be in range p = 4–6. But for the M_{max} the highest values are in the range p = 3–5.

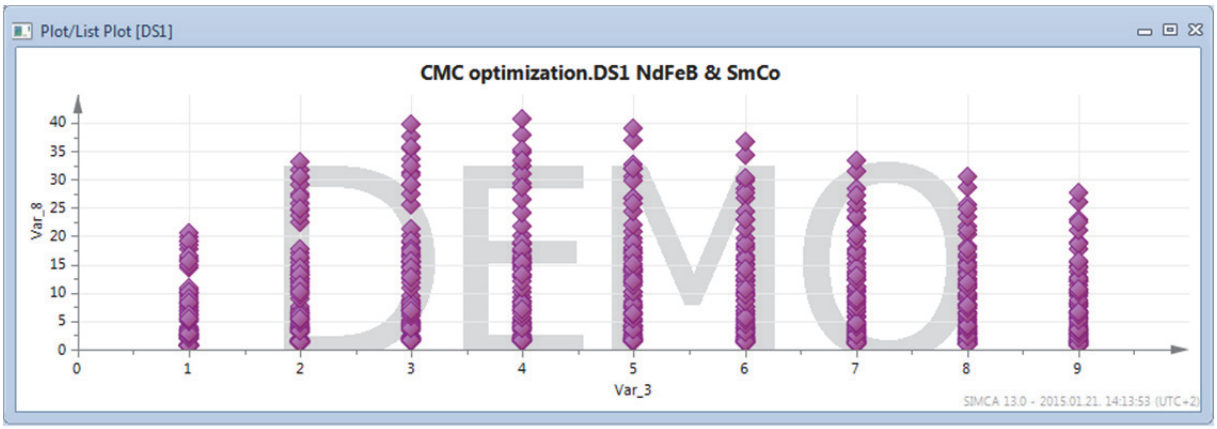

Fig. A.60 M_{max} by p

The taken optimum values for both magnet material types were in the limited range, but for $B_{max\ in}$ some examples are given (Fig. A.61) that are close to the limit B_{max}≤1.8 T and even exceeding it for about one and a half times. The highest values of $B_{max\ out}$ are also given (Fig. A.62), but the limit is not reached.

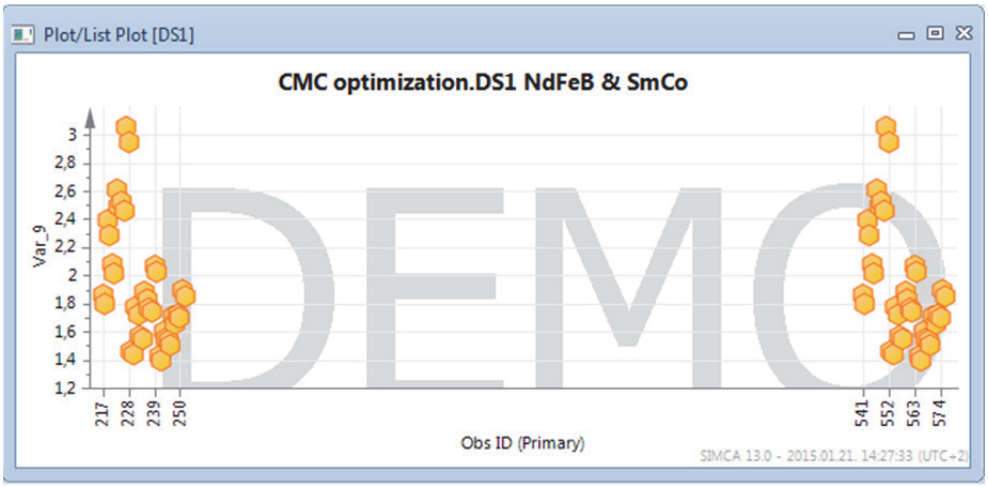

Fig. A.61 $B_{max\ in}$ for some numbers of experiments

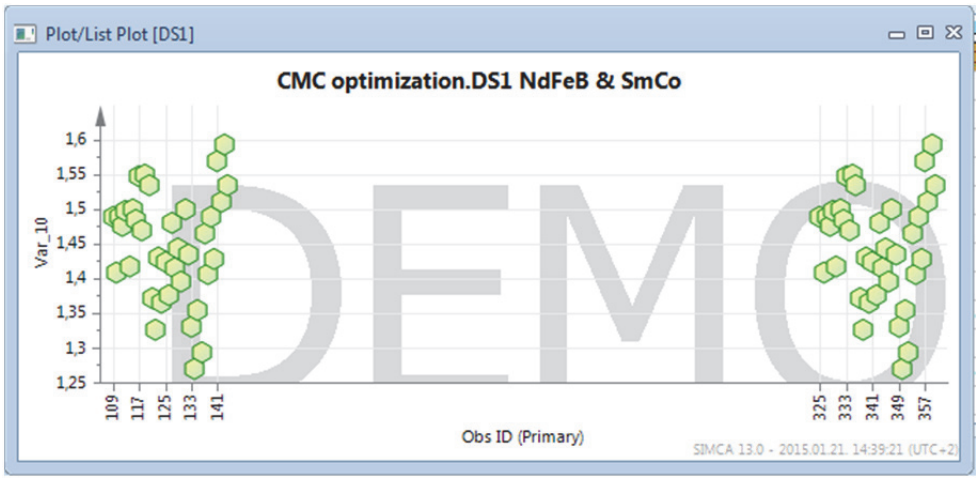

Fig. A.62 $B_{max\ out}$ for some numbers of experiments

BIBLIOGRAPHY

[1] Alston, C. L., Mengersen, K. L., Pettitte, A. N. Case Studies in Bayesian Statistical Modelling and Analysis. — Hoboken: John Wiley & Sons, 2012. — 499 p.

[2] American Iron and Steel Institute, homepage: http://www.steel.org (04.06.2014.)

[3] American Society for Testing and Materials, "ASTM International" homepage: http://www.astm.org (04.06.2014.)

[4] Austerlitz, H. Data Aquisition Techniques Using PCs. 2nd Edition. — Orlando: Academic Press, 2002. – 429 p.

[5] AWWA Staff. Water Transmission And Distribution (3rd Edition). — Denver: American Water Works Association, 2003. — 554 p.

[6] Bachus, L., Custodio, A. Know and Understand Centrifugal Pumps. — Kidlington: Elsevier Science & Technology, 2003. — 266 p.

[7] Bai, X., Wen, Y., Yang, J. and others. A magnetoelectric energy harvester with the magnetic coupling to enhance the output performance. *Journal of Applied Physics*, April 2012. — Volume 111, Issue 7. P.: 07A938–07A938-3.

[8] Bloch, H. P. Pump Wisdom: Problem Solving for Operators and Specialists. — Hoboken: Wiley, 2011. — 226 p.

[9] British Stainless Steel Association, homepage: http://www.bssa.org.uk (04.06.2014.)

[10] Bruce, D. W., O'Hare, D., Walton, R. I. Porous Materials. — Hoboken: Wiley, 2010. — 352 p.

[11] Buschok, K. H. J., de Boer, F. R. Physics of Magnetism and Magnetic Materials. Secaucus: Kluwer Academic Publishers, 2003. 191 p.

[12] Catalogue: AK Steel, Preliminary Product Data Bulletin, DI-MAX® M-10X Non-oriented Electrical Steels, 2014. — 8 p.

[13] Catalogue: AK Steel, Product Data Bulletin, Carlite® Grain Oriented Electrical Steels, 2012. — 27 p.

[14] Catalogue: Cogent, Surahammars Bruks AB, Non-oriented electrical steel, 2011. — 12 p.

[15] Catalogue: IBS Magnet, Dauermagnete — Werkstoffe und Systeme, N. 14 , 2012. — 44 p.

[16] Catalogue: KTR, Company catalogue 2014, 2014. — 328 p.

[17] Catalogue: Magnetfabrik Bonn. Permanent Magnet Manual, 1990. — 62 p.

[18] Childs, P. Mechanical Design Engineering Handbook. — Kidlington: Butterworth-Heinemann (Elsevier), 2014. — 800 p.

[19] Christensen, L. B., Johnson, R. B., Turner, L. A. Research Methods, Design and Analysis. 12th Edition. — New Jersey:Pearson Education, 2013. 509 p.

[20] Cleveland, C. J., Morris, C. Dictionary of Energy. — Jordan Hill: Elsevier Science & Technology, 2005. — 520 p.

[21] Committee on Materials Science and Engineering. Materials Science and Engineering for the 1990s: Maintaining Competitiveness in the Age of Materials. — Washington: National Academies Press, 1989. — 322 p.

[22] Comparison of different internationally used steel grades: http://www.steel-grades.com (04.06.2014.)

[23] Dantzig, G. B., Thapa, M. N. Linear Programming: Introduction. In series "Operations Research". — New York: Springer, 1997. — 473 p.

[24] Dargush, G. F., Soom, A., Serpe, C. I. Thermomechanical finite element analysis to describe the engagement and wear of electromagnetic clutches. *Tribology Series*, 2001. — Volume 39. P.: 141–149.

[25] Davis, J. R. Gear Materials, Properties and Manufacture. – Materials Park: ASM International, 2005. – 348 p.

[26] De Klerk, E. Aspects of Semidefinite Programming: Interior Point Algorithms and Selected Applications. In series "Applied Optimization", Vol. 65 — Dordrecht: Kluwer Academic Publishers, 2002. — 305 p.

[27] Dirba, J., Ketners, K. Elektriskās mašīnas (2. izdevums). — Rīga: RTU Izdevniecība, 2009. — 534 lpp.

[28] Dirba, J., Levin, N., Orlova, S, Pugachov, V. Brushless synchronous motors for appliances and power tools. *Proceedings of the 6th International Conference on ECT*: *Electrical and Control Technologies*, 5–6 May, 2011. — Kaunas, Lithuania. P.: 222.–225.

[29] Dronov, V. P., Burenin, V. V., Gaevik, D. T. Electric pumps with magnetic clutch. *Chemical and Petroleum Engineering*, 1978. — Volume 14, Issue 4. P.: 385–388.

[30] Dzemida, G., Saltenis, V., Zhilinskas, A. Stochastic and Global Optimization. In series "Nonconvex Optimization and Its Application", Vol. 59 — Dordrecht: Kluwer Academic Publishers, 2002. — 250 p.

[31] Eggers, R. Industrial High Pressure Applications: Processes, Equipment and Safety. — Somerset: Wiley-VCH, 2012. — 424 p.

[32] Eiras, J. R. Computer Science, Technology and Applications: Data Collection and Storage. — Huntington: Nova Science Publishers, 2011. – 124 p.

[33] European Union Standard EN 10088-1: Stainless Steels — Part 1: List of Stainless Steels, 2012.

[34] European Union Standard EN 10088-2: Stainless Steels — Part 2: Technical delivery conditions for sheet/plate and strip of corrosion resisting steel for general purpose, 2005.

[35] Fraser, R. C., Goeting, N. L. M. Research methods in general practice. – Southampton: Duphar, 1991. – 86 p.

[36] Freund, R. J., Wilson, W. J. Regression Analysis: Statistical Modelling of a Response Variable. 2nd Edition. — Boston: Academic Press (Elsevier), 2006. — 480 p.

[37] Garche, J. Encyclopaedia of Electrochemical Power Sources. — Amsterdam: Elsevier Science, 2010. — 4538 p.

[38] Gelman, A., Hill, J. Data Analysis Using Regression and Multilevel/ Hierarchical Models. — New York: Cambridge University Press, 2007. — 625 p.

[39] Govaert, G. Data Analysis. — Oxford: Wiley ISTE, 2010. — 343 p.

[40] Guntupalli, A. B., Djerafi, T., Wu, K. Ultra-compact millimetre-wave substrate integrated waveguide crossover structure utilizing simultaneous electric and magnetic coupling. *Proceedings of IEEE MTT-S: International Microwave Symposium Digest*, 17–22 June, 2012, Montreal, Canada. P.: 1–3.

[41] Gupta, C. K. Chemical Metallurgy: Principles and Practice. Darmstadt: John Wiley & Sons, 2006. 831 p.

[42] Gupta, C. K., Krishnamurthy, N. Extractive Metallurgy of Rare Earths. Boca Raton: CRC Press, 2004. 504 p.

[43] Gustafsson, B., Kreiss, H.-O., Oliger, J. Time Dependent Problems and Difference Methods. 2nd Edition. In series: "Pure and applied mathematics". — Hoboken: John Wiley & Sons, 2013. — 529 p.

[44] Hair, J. F., Black, W. C., Babin, B. J., Anderson, R. E. Multivariate Data Analysis. 7th Edition. — New Jersey: Pearson Prentice Hall, 2009. — 816 p.

[45] Herbst, J. F., Croat, J. J. Neodymium-iron-boron permanent magnets. *Journal of Magnetisms and Magnetic Materials*, November 1991. — Volume 100, Issue 1–3. P.: 57–78.

[46] Hertel, L., Hofmann, W. Magnetic Couplings in a Bearingless Reluctance Machine. *Proceedings of ICEM: International Conference on Electrical Machines*, 28–30 August, 2000. — Espoo, Finland. P.: 1776–1780.

[47] Hiroshi, K., Osamu, Y., Miki, H. Manufacture of Permanent Magnet: JPS54152198 (A). Japan — 30.11.1979.

[48] Hollands, L. Topological Strings and Quantum Curves. — Amsterdam: Amsterdam University Press, 2009. — 310 p.

[49] Hong, J., Lancaster, M. J. Microstrip Filters for RF/Microwave Applications. 2nd Edition. — Hoboken: Wiley, 2010. — 658 p.

[50] Hornreich, R. M., Shtrikman, S. Optimal Design of Synchronous Torque Couplers. *IEEE Transactions on Magnetics*, September, 1978. — Volume 14, Issue 5. P.: 800–802.

[51] Jēkabsons, G. Heiristiskas metodes daudzdimensiju regresijas modeļu būvēšanā. — Rīga: RTU, 2008. — 186 lpp.

[52] Jenkins, A. M. 6th Chapter – Reasearch Methodologies and MIS Research. — Amsterdam: Elsevier Science Publishers, 1985. — P.: 97–103.

[53] Jiles, D. Introduction to Magnetism and Magnetic Materials. Boca Raton: Chapman and Hall/CRC, 1997. 568 p.

[54] Kaede, K., Watanuki, K. Gait generation and change of direction for the underactuated three-legged robot. *Journal of Mechanical Science and Technology*, 2010. — Volume 24, Issue 12. P.: 55–58.

[55] Kan, M., Zhou, J., Li, Y. and other. Using carbon chains to mediate magnetic coupling in zigzag graphene nanoribbons. *Applied Physics Letters*, April 2012. — Volume 100, Issue 17. P.: 173106–173106-4.

[56] Kimura, M., Ichihara, A., Kusaka, M., Kaizu, K. Joint properties and their improvement of AISI 310S austenitic stainless steel thin walled circular pipe friction welded joint. *Materials and Design*, June 2012. — Volume 38. P.: 38–46.

[57] Klyatis, L. M. Accelerated Reliability and Durability Testing Technology. — Wiley Series in Systems Engineering and Management: Accelerated Reliability and Durability Testing Technology. — Hoboken: Wiley, 2011. — 434 p.

[58] Koon, N. (The United States of America as represented by the Secretary of the Navy.) Hard magnetic alloys of a transition metal and lanthanide: US4402770. The USA — 23.10.1981.

[59] Krasil'nikov, A. Ya. Selecting a magnetic clutch for a sealed pump. *Chemical and Petroleum Engineering*, 2001. — Volume 37, Issue 1–2. P.: 98–102.

[60] Krasil'nikov, A. Ya. Standard designs for magnetic systems and clutches. *Chemical and Petroleum Engineering*, 2002. — Volume 38, Issue 7–8. P.: 410–414.

[61] Krasil'nikov, A. Ya., Krasil'nikov, A. A. Analysis of the repulsive force of highly coercive permanent magnets in surface magnetic clutches and plane magnetic systems. *Chemical and Petroleum Engineering*, 2011. — Volume 47, Issue 5–6. P.: 309–314.

[62] Krasil'nikov, A. Ya., Krasil'nikov, A. A. Attractive forces of highly coercive permanent magnets in end magnetic clutches and plane magnetic systems. *Russian Engineering Research*, 2010. — Volume 30, Issue 6. P.: 543–546.

[63] Krasil'nikov, A. Ya., Krasil'nikov, A. A. Calculating the torque in an end magnetic clutch. *Chemical and Petroleum Engineering*, 2005. — Volume 41, Issue 7–8. P.: 383–387.

[64] Krasil'nikov, A. Ya., Krasil'nikov, A. A. Calculating vapour attraction for high-coercivity permanent magnets in planar magnetic systems and end clutches. *Chemical and Petroleum Engineering*, 2009. — Volume 45, Issue 11–12. P.: 696–701.

[65] Krasil'nikov, A. Ya., Krasil'nikov, A. A. Calculation of losses in current-conducting screen in sealed machines and devices due to lose packing of magnets in half-clutches of magnetic clutch. *Chemical and Petroleum Engineering*, 2011. — Volume 47, Issue 5–6. P.: 392–397.

[66] Krasil'nikov, A. Ya., Krasil'nikov, A. A. Calculation of the torque of a cylindrical magnetic clutch. *Chemical and Petroleum Engineering*, 2009. — Volume 45, Issue 3–4. P.: 120–125.

[67] Krasil'nikov, A. Ya., Krasil'nikov, A. A. High-coercivity permanent magnets in magnetic clutches. *Chemical and Petroleum Engineering*, 2006. — Volume 42, Issue 9–10. P.: 582–585.

[68] Krasil'nikov, A. Ya., Krasil'nikov, A. A. Highly coercive permanent magnets in Standard magnetic clutches. *Russian Engineering Research*, 2009. — Volume 29, Issue 4. P.: 342–344.

[69] Krasil'nikov, A. Ya., Krasil'nikov, A. A. Influence of layout of sealed pumps having a magnetic clutch on displacement angle of half-clutches and power loss in conducting screen. *Chemical and Petroleum Engineering*, 2009. — Volume 45, Issue 5–6. P.: 293–297.

[70] Krasil'nikov, A. Ya., Krasil'nikov, A. A. Influence of type of high-coercivity permanent magnet on characteristics of end magnetic clutch. *Chemical and Petroleum Engineering*, 2011. — Volume 47, Issue 3–4. P.: 186–192.

[71] Krasil'nikov, A. Ya., Krasil'nikov, A. A. Influence of type of high-coercivity permanent magnet on characteristic of magnetic clutch. *Chemical and Petroleum Engineering*, 2010. — Volume 46, Issue 7–8. P.: 479–484.

[72] Krasil'nikov, A. Ya., Krasil'nikov, A. A. Torque determination for a cylindrical magnetic clutch. *Russian Engineering Research*, 2009. — Volume 29, Issue 6. P.: 544–547.

[73] Krauss, G. Steels: Processing, Structure and Performance. — Materials Park: ASM International, 2005. — 634 p.

[74] Krawczyk, A., Wiak, S., Lopez-Fernandez, X. M. Electromagnetic Fields in Mechatronics, Electrical and Electronic Engineering. — Amsterdam: IOS Press, 2006. — 556 p.

[75] Kukjane, L., Brakanskis, U., Dirba, J. Visual Basic for application program for the automatic analysis of brushless DC motor magnetic field. *Proceedings of the 6th International Conference on ECT*: *Electrical and Control Technologies*, 5–6 May, 2011. — Kaunas, Lithuania. P.: 231.–234.

[76] Lai, J. K. L., Lo, K. H., Shek, C. H. Stainless Steels: An Introduction and Their Recent Developments. — Sharjah: Bentham Science Publishers, 2012. — 174 p.

[77] Latvijas Zinātņu akadēmijas Terminoloģijas komisija, Akadēmiskā terminu datubāze *AkadTerm*. Internet — http://termini.lza.lv/term.php (06.05.2014.)

[78] Lavrinovicha, L., Dobriyan, R., Onzevs, O. Metamodels for optimum design of outer-rotor synchronous reluctance motor. *Scientific Journal of Riga Technical University*, *Electrical*, *Control and Communication Engineering*, 2014. — Volume 5. P.: 34.–39.

[79] Levins, N., Kamoliņš, E., Vītoliņa, S. Bezkontaktu elektriskās mašīnas. — Rīga: RTU Izdevniecība, 2011. — 276 lpp.

[80] Lexcellent, C. Shape-Memory Alloys Handbook. — Somerset: Wiley-ISTE, 2013. — 398 p.

[81] Livington, J. D. Rising Force: The Magic of Magnetic Levitation. Cumberland (USA): Harvard University Press, 2011. 286 p.

[82] Longman, Dictionary of Contemporary English. — Essex: Pearson Education Limited, 2003. — 1950 p.

[83] Lueth, E., Ruiz-Arranz, M. Gravity Model of Workers' Remittances. — International Monetary Fund, 2007. — 20 p.

[84] Magnetic coupler working principle. Internet — http://www.wisegeek.com/what-is-a-magnetic-coupler.htm (05.03.2014.)

[85] Magnetic couplings' producer *Dexter magnetic technologies*. Internet — http://www.dextermag.com (08.04.2014.)

[86] Magnetic couplings' producer *Environment, Bioenergetics and Biotechnology Competence Centre*. Internet — http://www.vbbkc.lv (04.04.2014.)

[87] Magnetic couplings' producer *Magnetic Technologies*. Internet — http://www.magnetictech.com (08.04.2014.)

[88] Magnetic couplings' producer *Magnomatics*. Internet — http://www.magnomatics.com (08.04.2014.)

[89] Magnetic couplings' producer *Metau Engineering*. Internet — http://www.magnetic-coupling.it (08.04.2014.)

[90] Magnetic couplings' producer *Sintex*. Internet — http://www.sintex.com (08.04.2014.)

[91] Manual: Brockhaus Messtechnik, Hystograph, 2006. — 104 p.

[92] Markov, D. V., Sobolev, G. V., Frolov, Yu. I. Features of magnetic-clutch sealed chemical pumps. *Chemical and Petroleum Engineering*, 1994. — Volume 36, Issue 9–10. P.: 552–557.

[93] Matsuura, J. Managing Intelectual Assets in the Digital Age. — Norwood: Artech House, 2003. — 246 p.

[94] Matsuura, Y., Sagava, M., Fujimura, S. (Sumitomo Special Metals.) Process of producing permanent magnet materials: US4597938. The USA — 15.09.1983.

[95] Mechanical Engineers' Handbook: Materials & Mechanical Design. 3rd Edition. — Hoboken: John Wiley & Sons, 2006. 1341 p.

[96] Merwerth, J., Oswald, A., Horz, M., Herzog, H.-G. Developing a Brushless Permanent Magnet Synchronous Drive for an X-ray Microscope Condenser in Ultra High Vacuum. *Proceedings of ICEMD: IEEE International Conference on Electric Machines and Drives*, 15 May, 2005. — San Antonio, USA. P.: 1710–1714.

[97] Mobley, R. K. Maintenance Fundamentals (2nd Edition). — Saint Louis: Elsevier Science & Technology, 2004. — 426 p.

[98] Mu, C., Yu, J., Zhao, W., Liu, J. Study on Power Control of Electric Power Steering System. *Proceedings of ICCTP: Critical Issues in Transportation Systems Planning, Development and Management*, 5–9 August, 2009. — Harbin, China. P.: 3327–3332.

[99] National Research Consil (U. S.) Staff and others. Opportunities in High Magnetic Field Science. — Washington: National Academies Press, 2005. — 188 p.

[100] National Science Foundation Staff and others. Proceedings of the International Conference on Scientific Information: Two Volumes. — Washington: National Academies Press, 1959. — 1662 p.

[101] Nocedal, J., Wright, S. J., Birge, J. Numerical Optimization. In series "Operations Research".— New York: Springer-Verlag, 1999. — 656 p.

[102] Nozieres, J. P., De La Bathie, R. P., Lelievre, M. Process for the preparation of permanent magnets based on neodymium-iron-boron: US5356489. The USA — 12.12.1991.

[103] Nuemaier, R. Hermetic Pumps: The Latest Innovations and Industrial Applications of Sealless Pumps. — Houston: Gulf Professional Publishing, 1997. — 594 p.

[104] Nunney, M. J. Light and Heavy Vehicle Technology. Fourth Edition. — London: Routledge (Taylor&Francis Group), 2007. — 672 p.

[105] Ompusunggu, A. P., Sas, P., Van Brussel, H. Modeling and simulation of the engagement dynamics of a wet friction clutch system subjected to degradation: An application to condition monitoring and prognostics. *Mechatronics*, September 2013. — Volume 23, Issue 6. P.: 700–712.

[106] Onwubolu, G. Mechatronics: Principles and Applications. — Jordan Hill: Butterworth-Heinemann, 2005. — 666 p.

[107] Onževs, O. Mehānisku svārstību sistēmu optimizācijas un identifikācijas aprēķinu automatizācija. Disertācija. — Rīga: RTU, 1997. — 164 lpp.

[108] Optimal Computing products, homepage: http://www.optimalcomputing.be/xtreme-description.php (09.01.2015.)

[109] Ose, B., Pugachov, V. The influence of pole pair number and magnets' width on mechanical torque of magnetic coupler with rounded permanent magnets. *Scientific Journal of Riga Technical University*, *Power and Electrical Engineering*, 2011. — Volume 29, Issue 4. P.: 63.–66.

[110] Ose, B., Pugachov, V., Orlova, S. The influence of PM's construction parameters in magnetic coupler on its mechanical torque. *Proceedings of the 6th International Conference on ECT*: *Electrical and Control Technologies*, 4–6 May, 2011. — Kaunas, Lithuania. P.: 226–230.

[111] Ose, B., Pugachov, V., Orlova, S., Vanags, J. The influence of permanent magnets' width and number on the mechanical torque of a magnetic coupler with rectangular permanent magnets. *Proceedings of the IEEE ISIE*: *International Symposium on Industrial Electronics*, 27–30 June, 2011. — Gdansk, Poland. P.: 761.–765.

[112] Ose-Zala, B., Pugachov, V. Possibilities to reduce cogging torque of PMSG with non-overlapping concentrated windings. Submitted and accepted in *Elektronika ir elektrotechnika*.

[113] Ose-Zala, B., Pugachov, V. The Comparison of Active and Reactive Magnetic Couplers. *IEEE Proceedings of the 8th International Conference on PQ*: *Electric Power Quality and Supply Reliability*, 11–13 June, 2012. — Tartu, Estonia. P.: 25.–28.

[114] Ose-Zala, B., Pugachov, V., Levin, N. Start-Up Torques of Permanent magnet Synchronous Generator With Non-Overlapping Concentrated Windings. *IEEE Proceedings of the 9th International Conference on PQ*: *Electric Power Quality and Supply Reliability*, 11–13 June, 2014. — Rakvere, Estonia. P.: 195.–198.

[115] Panel on Bureau of Transportations Statistics International Trade Traffic. Measuring International Trade on U. S. Highways. — Washington: National Academy Press, 2005. — 62 p.

[116] Pardalos, P. M., Du, D.-Z., Birge, J. Stochastic Global Optimization. In series "Optimization and Its Application", Vol. 1 — New York: Springer, 2008. — 268 p.

[117] Permanent magnets' manufacturer *K&J Magnetics*, homepage: http://www.kjmagnetics.com/ (15.05.2014.)

[118] Phillips, G. M. Interpolation and Approximation by Polynomials. — New York: Springer-Verlag, 2003. — 326 p.

[119] Phillips, P. P., Stawarski, C. A. Data Collection: Planning for and Collection All Types of Data. — Hoboken: John Wiley & Sons, 2008. — 192 p.

[120] Pisanti, O., Esposito, S. Neutron Physics for Nuclear Reactors: Unpublished writings by Enrico Fermi. — River Edge: World Scientific Publishing Co., 2010. – 702 p.

[121] Powell, M. J. D. Approximation Theory and Methods. — Cambridge: Cambridge University Press, 1981. — 339 p.

[122] Powell, M. J. D. On the convergence of trust region algorithms for unconstrained minimization without derivatives. *Computational Optimization and Applications*, October 2012. — Volume 55, Issue 2. Pp.: 527–555.

[123] Powell, M. J. D. UOBYQA: Unconstrained optimization by quadratic approximation. *Mathematical Programming*, May 2002. — Volume 92, Issue 3. Pp.: 555–582.

[124] Product: NMath, homepage: http://www.centerspace.net/products/nmath/ (09.01.2015.)

[125] Product: OptiStruct, homepage: http://www.altairhyperworks.com/Product,19,OptiStruct.aspx (09.01.2015.)

[126] Product: PottersWheel, homepage: http://www.potterswheel.de (09.01.2015.)

[127] Product: SIMCA, homepage: http://www.umetrics.com (09.01.2015.)

[128] Product: SmartDO, homepage: http://www.smartdo.co/Software/index_e.htm (09.01.2015.)

[129] Product: solidThinking Evolve, homepage: http://www.solidthinking.com (09.01.2015.)

[130] Product: VisSim, homepage: http://www.vissim.com (09.01.2015.)

[131] Product: What's*Best*, homepage: http://www.lindo.com (09.01.2015.)

[132] Product: WORHP, homepage: http://www.worhp.de (09.01.2015.)

[133] Pugacevs, V., Ose-Zala, B., Zicans, J., Merijs Meri, R. Reactive magnetic coupler: EP2733835A2. The European Patent Office (France) — 21.05.2013.

[134] Pugačevs, V., Ose-Zaļā, B., Zicāns, J., Merijs Meri, R. Reaktīvais magnētiskais sajūgs: LV14857. Latvia — 16.11.2012.

[135] Pyrhonen, J., Jokinen, T., Hrabovcova, V. Design of Rotating Electrical Machines. 2nd Edition. — Somerset: John Wiley & Sons, 2013. 614 p.

[136] Ramalingam, K. K. Handbook of Mechanical Engineering Terms. — Delhi: New Age International, 2009. — 366 p.

[137] Sagawa, M., Fujimura, S., Togawa, N., Yamamoto, H., Matsuura, Y. New material for permanent magnets on a base of Nd and Fe. *Journal of Applied Physics*, 15 March, 1984. Vol. 55, Is. 6. Pp. 2083–2087.

[138] Salon, S. J., Chari, M. V. K. Numerical Methods in Electromagnetisms. In series "Electromagnetism". — New York: Academic Press, 2000. — 782 p.

[139] Sanford, R. L., Cooter, I. L. basic Magnetic Quantities and the Measurement of the Magnetic Properties of Materials. *National Bureau of Standards*, 21 May, 1962. — Monograph 47. 37 p.

[140] Shain, J. C., Gay, D. E. (General Motors Corporation.) Encapsulated oxidation-resistant iron-neodymium-boron permanent magnet particles: US5395695. The USA — 19.08.1993.

[141] Shain, J. C., Gay, D. E.. (General Motors Corporation.) Encapsulated oxidation-resistant iron-neodymium-boron permanent magnet: US5272008. The USA — 16.03.1992.

[142] Sharma, S. Applied Nonlinear Programming — Delhi: New Age International, 2006. — 90 p.

[143] Shin, Y. H., Kim, S. C., Kim, M. S. Use of electromagnetic clutch water pumps in vehicle engine cooling systems to reduce fuel consumption. *Energy*, 1 August 2013. — Volume 57. P.: 624–633.

[144] Sinha, S. M. Mathematical Programming: Theory and Methods. — New Delhi: Elsevier Science & Technology, 2006. — 589 p.

[145] Skomski, R. Simple Models of Magnetism. Oxford: Oxford University Press, 2008. 366 p.

[146] Snyman, J. A. Practical Mathematical Optimization. In series "Applied optimization", Vol. 97 — New York: Springer, 2005. — 257 p.

[147] Software *QuickFiled* for electromagnetic, thermal and stress analysis, homepage: http://www.quickfield.com (04.06.2014.)

[148] Spina, D. Statistical Methods in Research. *Methods in Molecular Biology*, 2011. — Volume 746. — P.: 443–472.

[149] Spurgeon, P. Fire Service Hydraulics and Pump Operations. — Tulsa: PennWell, 2012. — 244 p.

[150] Stainless steels' producer *aalco*, homepage: http://www.aalco.co.uk (04.06.2014.)

[151] Steel. A Handbook for Materials Research and Engineering. Volume 1: Fundamentals. — Dusseldorf: Springer — Verlag Stahleisen, 1992. 737 p.

[152] Steel. A Handbook for Materials Research and Engineering. Volume 2: Applications. — Dusseldorf: Springer — Verlag Stahleisen, 1993. 839 p.

[153] Strnat, K. J. Method of producing permanent magnets of rare earth metals containing Co or mixtures of Co, Fe and Mn: US3424578. The USA — 05.06.1967.

[154] Strnat, K. J., Strnat, R. M. V. Rare earth-cobalt permanent magnets. *Journal of Magnetisms and Magnetic Materials*, November 1991. — Volume 100, Issue 1–3. P.: 38–56.

[155] Sung-Hun, L., Hyeong-Joon, A., Changkun, P. Study on Fault Current Limiting Characteristics of an SFCL Using Magnetic Coupling of Two Coils with Mechanical Switch Driven by Electromagnetic Repulsion Force. *IEEE Transactions on Applied Superconductivity*, June 2014. — Volume 24, Issue 3.

[156] Thompson, J. R. Empirical Model Building: Data, Models and Reality. 2nd Edition. — Hoboken: John Wiley & Sons, 2011. — 460 p.

[157] Vorob'yeva, T. M., etc. Electromagnetic Clutches and Couplings. — London: Pergamon Press Ltd., 1965. — 224 p.

[158] Walliman, N. Research Methods: The Basics. — Abigdon: Routledge (Taylor & Francis Group), 2010. — 208 p.

[159] Wang, Ch., Xu, Sh. Simulation and experimental study on electromagnetic field in magnetic particle clutch. *Proceedings of ICCSE: 6th International Conference on Computer Science & Education*, 3–5 August, 2011. — Singapore, Singapore. P.: 437–440.

[160] Wang, Ch., Xu, Sh. Study on Performance of Vehicle Magnetic Powder Clutch with Permanent Magnet. *Proceedings of ICIC: IEEE International Conference on Information and Computing*, 25–27 April, 2011. — Phuket Island, Thailand. P.: 208–211.

[161] Webb, A. Statistical Pattern Recognition. 2nd Edition — Chichester: John Wiley & Sons, 2007. — 496 p.

[162] Wickelmaier, F. An introduction to MDS. — Aalborg: Aalborg University, 2003. — 26 p.

[163] Yamanaka, Y., Watanabe, K., Honshima, M., Kikuchi, H. (Shin-Etsu Chemical Co.) Rare earth-containing permanent magnets: US3982971. The USA — 20.02.1975.

[164] Yang, X.-S. Introduction to Mathematical Optimization: From Linear Programming to Metaheuristics. — Cambridge: Cambridge International Science Publishing, 2008. — 160 p.

[165] Zhu, F., Hong, W., Chen, J. X., Wu, K. Quarter-Wavelength Stepped-Impedance Resonator Filter with Mixed Electric and Magnetic Coupling. *IEEE Microwave and Wireless Components Letters*, February 2014. — Volume 24, Issue 2. P.: 90–92.

[166] Ziedris, A. Elektrisko mašīnu elektromagnētiskie aprēķini. Rīga: RTU, 2001. 71 p.

[167] Zinn, S., Semiatin, S. L. Elements of Induction Heating: Design, Control, and Applications. — Materials Park: ASM International, 1988. – 342 p.

[168] Zviedris, A. Datorrealizācijas matemātiskās metodes. Lekciju konspekts. — Rīga: RTU, 2004. — 78 lpp.

[169] Zviedris, A. Elektromagnētisko ierīču magnētisko sistēmu optimizācija. Lekciju konspekts. — Rīga: RTU, 2004. — 46 lpp.

[170] Анализ и синтез в динамике механических систем. *Вопросы динамики и прочности*, 1991. Вып.: 53. 165 с.

[171] Аудзе, П. П. , Эглайс, В. О. Новый подход к планирований многофакторных экспериментов. *Вопросы динамики и прочности*. 1977. Вып.: 35. Ст.: 104–107.

[172] Башта, Т. М., Руднев. С. С., Некрасов. Б. Б. Гидравлика, гидромашины и гидроприводы. — Москва: Машиностроение, 1982. — 424 с.

[173] Бут, Д. А. Бесконтактные электрические машины. — Москва: Высшая школа, 1990. — 416 с.

[174] Васильцов, Э. А., Невелич, В. В. Герметичные электронасосы. — Ленинград: Машиностроение, 1968. — 260 с.

[175] Вольдек, А. И., Попов. В. В. Электрические машины. Машины переменного тока. — Санктпетербург: Питер, 2007. — 350 с.

[176] Ганзбург, Л. Б., Федотов, А. И. Проектирование электромагнитных и магнитных механизмов: справочник. — Ленинград: Машиностроение, 1980. — 364 с.

[177] Гольдберг, О. Д., Свириденко, И. С. Проектирование электрических машин. — Москва: Высшая школа, 2006. — 430 с.

[178] Добротворский, В. В., Красильников, А. Я., Сухоростов, Л. Н. Герметичное оборудование с магнитными муфтами. *Химическое и нефтяное машиностроение*, 1994. — №6. С.: 39.

[179] Каволелис, А.-П. К. Механизмы и устройства для передачи вращения, виброзащиты и стабилизации на основе центробежных сил. — Вильнюс: Мокслас, 1983. — 188 с.

[180] Клевец, Н. И., Смирнов, В. С., Чохели, М. А. Расчет радиальной магнитной муфты. *Тезисный доклад с XV Международной конференции по постоянным магнитам*, 19–23 Сентября, 2005. — Суздаль, Россия.

[181] Клубникин, П. Ф. Быстродействующие индукционные муфты в системах автоматического регулирования. — Москва: Машгиз, 1962. — 220 с.

[182] Красильников, А. Я. Особенности использования магнитной муфты в конструкциях герметичных машин. — Екатеринбург: УГТУ-УПИ, 2007. — 144 с.

[183] Красильников, А. Я., Красильников, А. А. Магнитные системы и муфты на постаянных магнитах для герметичного оборудования. *Химическое и нефтегазовое машиностроение*, 2003. — №4. С.: 28–29.

[184] Поляков, В. С., Барбаш, И. Д. Муфты. Конструкции и расчет. Издание 4-е. — Ленинград: Машиностроение, 1973. — 336 с.

[185] Попов, В. С., Подлевский, Н. И., Чернышев, А. И., Абдрахманова, Т. Б. Особенности разработки и использования герметизированных электродвигателей с магнитными муфтами в нефтегазовом насосном оборудовании нового поколения. *Электронные и электромеханические системы и устройства* — Томск: НЦП Полюс, 2000. С.: 75–77.

[186] Преображенский, А. А. Теория магнетизма, магнитные материалы и элементы. — Москва: Высшая школа, 1972. — 633 с.

[187] Сергеев, П. С., Виноградов, Н. В., Горяинов, Ф. А. Проектирование электрических машин. — Москва: Энергия, 1969. — 633 с.

[188] Шабашов, А. П., Николаев, Е. А. Магнитная муфта: 218580. СССР — 17.05.1968.

[189] Шаров, В. С. Элекптомагнитные муфты скольжения. — Москва: Госэнергоиздата, 1958. — 104 с.

[190] Эглайс, В. О. Аппроксимация табличных данных многомерным уравнинием регрессий. *Вопросы динамики и прочности*. 1981. Вып.: 39. Ст.: 120–125.